ENGINEERING

OF

HYBRID ORGANIC ELECTROCHEMICAL TRANSISTORS (OECT) AS EMERGING MEDICAL DIAGNOSTICS

A Dissertation Submitted for the award of the degree of

DOCTOR OF PHILOSOPHY

By

INDRANI MEDHI

Roll No. 156153005

Centre for Nanotechnology

Indian Institute of Technology Guwahati

Guwahati – 781039

June 2023

Dedicated to My Parents & Family…

INDIAN INSTITUTE OF TECHNOLOGY
GUWAHATI
Centre for Nanotechnology

STATEMENT

I do hereby declare that the work contained in the thesis entitled "**Engineering of Hybrid Organic Electrochemical Transistors (OECT) As Emerging Medical Diagnostics**" is the result of investigations carried out by me at the Centre for Nanotechnology, Indian Institute of Technology Guwahati, Assam, India under the supervision of Prof. Parameswar Krishnan Iyer, Professor, Department of Chemistry and Officiating Director of Indian Institute of Technology Guwahati, Assam, India.

In keeping with the general practice of reporting scientific observations, due acknowledgements have been made wherever the work described is based on the findings of other investigators. I further declare that this work has not been submitted in part or full elsewhere for the award of any degree.

June, 2023
IIT Guwahati

Indrani Medhi
Indrani Medhi

INDIAN INSTITUTE OF TECHNOLOGY
GUWAHATI
Centre for Nanotechnology

CERTIFICATE

This is to certify that the work contained in the thesis entitled "**Engineering of Hybrid Organic Electrochemical Transistors (OECT) As Emerging Medical Diagnostics**" by Indrani Medhi, a PhD research scholar of Centre for Nanotechnology, Indian Institute of Technology Guwahati, for the award of the degree of Doctor of Philosophy, has been carried out under my supervision. I further certify that this work has not been submitted elsewhere in part or full for the award of any degree.

June, 2023
IIT Guwahati

Prof. Parameswar Krishnan Iyer
Thesis Supervisor
Officiating Director
Department of Chemistry
Indian Institute of Technology Guwahati
Guwahati – 781039
Assam, India.

Acknowledgement

It is my immense pleasure to convey my sincere gratitude to many people for their time and effort; who supported me in this incredible research journey. I thank all who in one way or another contributed in the completion of this thesis. I humbly acknowledge their contributions.

My heartfelt thanks and gratitude to my loving, supportive and caring family which includes my mother Professor Chitrani Medhi, my father Late Professor Okhil Kumar Medhi, my husband Mr. Hridesh Kumar Shrotriya, my sister Ragini Medhi, my father-in-law Late Mr. Umashankar Shrotriya and my mother-in-law Mrs. Uma Devi for being the wind beneath my wings. They consistently encouraged, motivated and prayed for me. Their untiring support, care and unconditional love are the backbone of my entire PhD journey. They have my deepest love for their unfailing encouragement and support in every endeavour I pursue.

I whole-heartedly express my deepest gratitude to my supervisor, Professor Parameswar Krishnan Iyer for providing me the opportunity to start this wonderful research journey, valuable training for my presentation skills and insistence on perfection that has helped in this dissertation to come out in shape. Besides, I am deeply grateful for his continuous support, comments at every stage of my writing and guidance during my entire PhD journey. I would like to acknowledge my fellow colleagues at Centre for Nanotechnology, Department of Chemistry, Department of Chemical Engineering, Department of Civil Engineering, Department of Design & Centre for Environment, Indian Institute of Technology Guwahati whose challenges and productive critics have provided new perspective to the work.

I am highly obliged to my DC members Professor Pranab Goswami, Dr. Partho Sarathi Gooh Pattader and Dr. Nageswara Rao Peela for their incessant monitoring of my research progress and keeping me on track. I appreciate their precious advice in refining my research work time to time throughout my PhD journey. I am indebted to Professor Arun Chattopadhyay and Professor Siddhartha Sankar Ghosh for their continuous support and co-operation.

I would like to extend my gratitude to the staff of Centre for Nanotechnology and Central Instruments Facility (CIF) for their timely help and co-operation. I am blessed to have met Upashi Goswami, Emlin Elsa Abraham, Gayatri Natu, Niranjan Meher, Namami Goswami, Ujjowal Barman, Shweta Singh, Saswati Das, Thomas T. Daniel and Ramesh Babu Yathirajula for their friendship, constant encouragement, helping in removing obstacles in my path, boosting my self-confidence and for their faith in me. I am deeply grateful to Nimmakayala V. V. Subbarao, P. Gopikrishna, Sameer Hussain, Akhtar Hussain Malik, Anamika Kalita, Radhakrishna Ratha for being supportive seniors and sharing their glasswares when I had none.

I take this opportunity to thank Gautam Barman, Kaustubh Acharyya, Sandhan Sarma, Martin Mazumdar, Triveni Sangam, Debadrita Bhattacharya, Stela Ksh, Milan Hazarika, Paran Jyoti Dutta and Ayon Kumar Paul for treating me like a friend than a mere student and creating a lively atmosphere whenever we met. I owe my sincere thanks to Priyanka Dutta, Avishek Banik, Jitendra Kumar, Shaad Ansari, Reena Dey, Debashree Debasmita, Menan Elsy, Devirupa Saha, Surjendu Maity, Laxmi Raman Adil and Subrata Mondal for their warm back up and support. A special mention to my labmates Suresh Vasimalla, Jupitara Das, T. Bhim Raju, Himani Kalita, Debasish Barman, Debika Barman, Rajdikshit Gogoi, Priyam Ghosh, Retwik Parui, Tamal Pal, Mst Nasima Khatun, Paromita Bhattacharjee, M. Anita Chanu, Muzzaffer Ahmad, Tapashi Sarmah for keeping a healthy atmosphere in the lab.

Lastly, this thesis is exclusively dedicated to my late father Professor Okhil Kumar Medhi who took the lead to heaven before the completion of this work. He was an eminent scientist in the field of Bio-inorganic Chemistry, a renowned academician of Assam and Former Vice Chancellor of Gauhati University. He is my first guru, first guide, pillar of strength and guiding hand through the entirety of my life. Like many others, he is my inspiration, strength, courage, resolution, commitment and dedication in everything I do.

"You touched my life in many different ways and continue to inspire me with your ideals and ideas to this day."

It is through the ideas, memories and stories of him that he shall continue living among us. We continue to battle with the overwhelming emotions of this irreparable loss that is but permanent. There are so much and so many emotions in there, deep inside the heart, intertwined with memories that it becomes extremely difficult to find an expression for them.

"You are our calm of shade in the scorching heat Papa…!!"

Miss you Papa.

Indrani Medhi

Abstract

The increasing prevalence of chronic diseases and the increasing emphasis of health institutions on early diagnosis and treatment lead to increased diagnostic and surgical procedures. The prevalence of chronic diseases such as diabetes, cancer and other infectious diseases is increasing due to sedentary lifestyles and other factors. Chronic diseases and the treatment of patients suffering from these diseases put enormous pressure on the health systems of different countries. This has led to a global financial burden in treating these diseases. A patient's hospitalization costs are significantly higher, and longer hospitalizations are associated with a greater financial burden. The increase in hospital care and surgical and diagnostic procedures is driving the demand for medical equipment, including capital equipment and consumer goods, in developed and emerging economies. This is compounded by the increasing investments of the major R&D market players in the development of technologically advanced devices to meet the growing demand for innovative devices. Growing R&D investments by medical technology companies will boost the medical device industry during the forecast period. Moreover, due to the outbreak of the COVID-19 pandemic and the growing health concerns of the population, the market demand for these devices has increased. The customer base of the devices was also increased by the introduction of improved models with new functions and reduced prices by market participants. This provides a huge growth opportunity for new entrants and incumbents to focus on this segment and launch new biomedical devices to meet the growing demand.

Synopsis

The content of this thesis entitled **"*ENGINEERING OF HYBRID ORGANIC ELECTROCHEMICAL TRANSISTORS (OECT) AS EMERGING MEDICAL DIAGNOSTICS*"** has been divided into 7 chapters as summarized below:

Chapter 1. INTRODUCTION

Bioelectronic devices, such as high-resolution neural recording of the brain and 24-hour blood monitoring of metabolites and disease markers, produce complex data that must be analyzed to determine their biological significance. Ions dissolved in the water environment play an important role in plants, animals and humans. Ions regulate biological processes at the single-cell scale, enable the propagation of electronic signals, and maintain the proper balance between extracellular and intracellular fluids, which are important for many processes such as nerve impulses, hydration, muscle function, and pH regulation. Quantification of in situ ion concentrations in aquatic environments is thus of great interest in several emerging fields, including biomedical diagnostics, environmental monitoring, health products, water and food testing and monitoring, agriculture, and security.

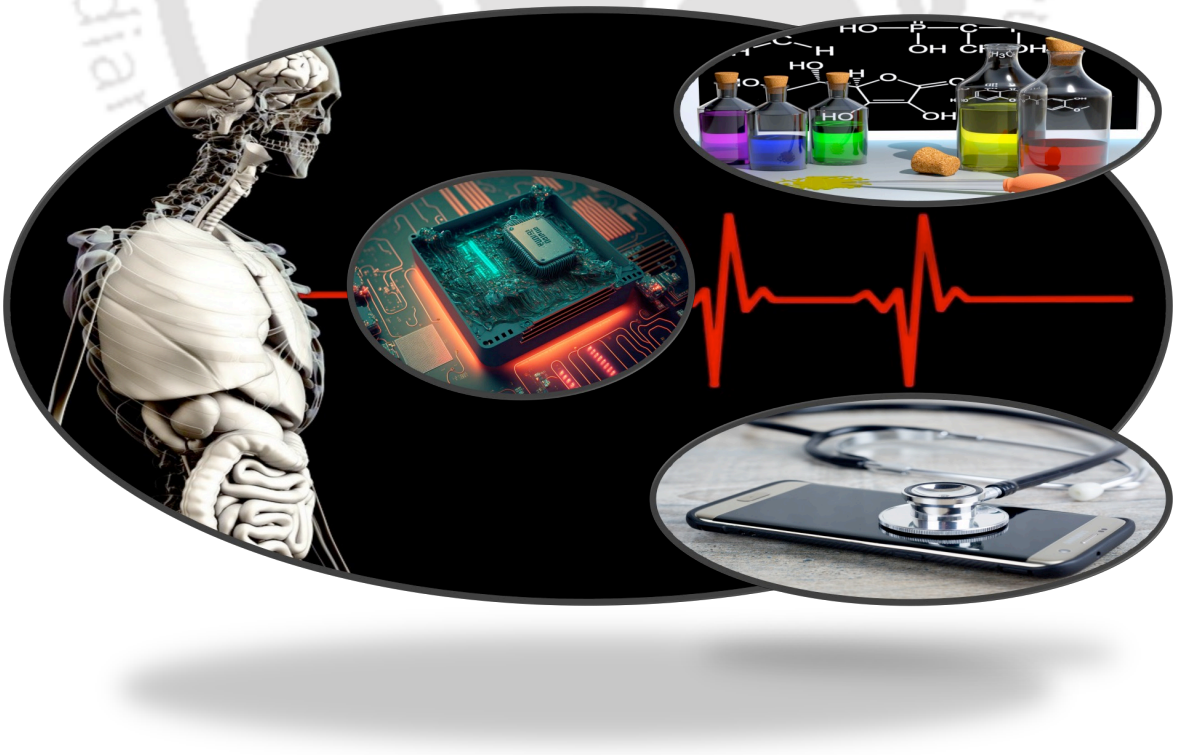

Figure S1. Bioelectronics progressing towards advanced medical care.

Chapter 2. An engineered organic electrochemical transistor (OECT) platform with a high ammonia-sensitive mesoporous membrane

Organic electrochemical transistors (OECTs) exploit the ability of organic semiconductors to conduct ions in addition to electronic charge and are of great interest in sensor and biosensor applications because they can operate in liquid environments. In addition, they have a simple geometry, typically a planar monolayer structure consisting of a channel and a gate contact near the channel. PEDOT: PSS provides an attractive platform for the development of organic electronics, i.e., thermoelectric converters, photovoltaic devices, supercapacitors and sensors, etc. It has excellent solution processing ability and miscibility with functional films, usually by drop-casting and spin-coating and spray coating to demonstrate high and adjustable conductivity. In addition, it has excellent chemical and electrochemical stability, good optical transparency and good biocompatibility. Rather than a mere case study, the choice of ammonia as a pollutant gas is based on solid scientific evidence that comprehensive monitoring of ammonia concentrations and fluxes is key to reducing risks to human health and vegetation. For realistic monitoring of outdoor ammonia (NH_3) concentrations in urban environments, chemically resistant gas sensors (CGS) should offer sensitivity well below the ppm scale, hopefully at the ppb level.

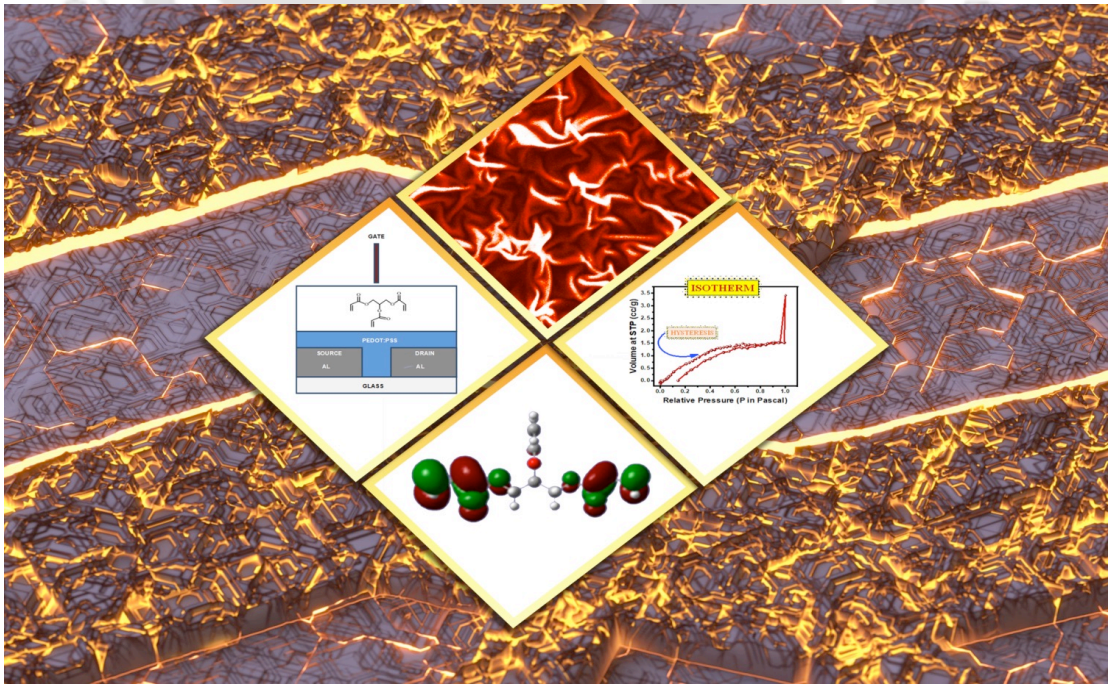

Figure S2. Developed Hybrid OECT selectively detects ammonia at room temperature.

Chapter 3. Clinical Ammonia Detection as a potential biomarker for Chronic Liver Disease

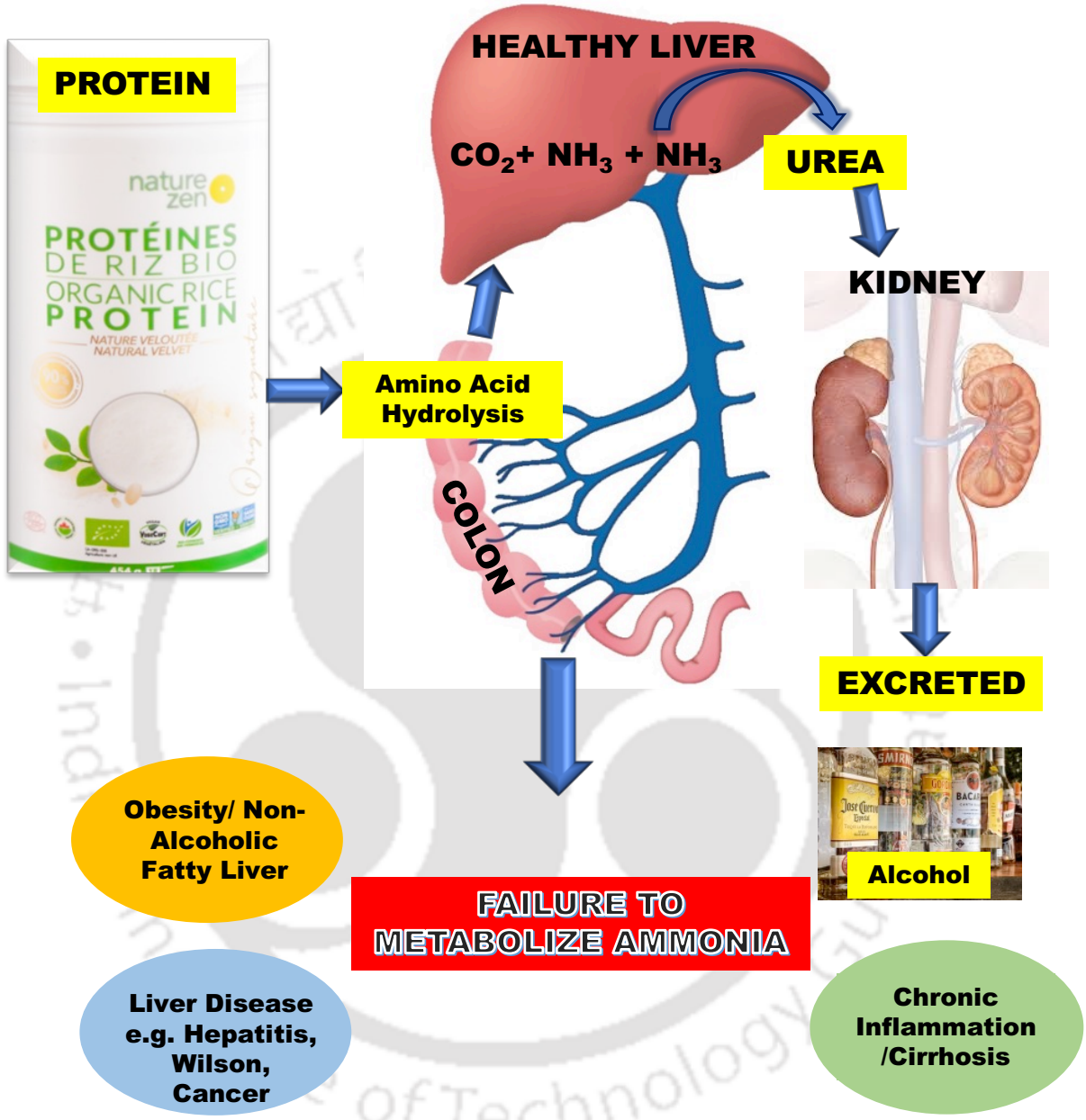

Figure S3. Schematic Representation of Hybrid OECT to clinically detect ammonia under physiological conditions.

Direct exposure to NH_3 poses a serious health risk due to multi-organ dysfunction. Therefore, long-term exposure to high concentrations of ammonia in the human body is usually related to the development of fatal diseases such as chronic kidney disease (CKD), peptic ulcer and even epidemic diseases and COVID-19 (SARS - CoV - 2) due to

weakened immune response. Ammonia is normally formed in muscle and peripheral tissues and transported to the liver to be converted to urea by the urea cycle. The most important signal of acute and chronic liver damage is elevated ammonia, a life-threatening metabolic condition. There is still a need to develop a non-invasive, real-time, accurate and rapid screening device to detect ammonia levels for better monitoring of such diseases. In this context, low ammonia concentration, location and abundance of disturbances/interferences are considered to be the main challenges in monitoring certain diseases. An Organic Electrochemical Transistor (OECT)-based device demonstrates accurate and selective detection of ammonia. The detection data and results obtained with the OECT device were found to be highly selective for the detection of ammonia over other analytes and interfering substances, making it very useful in clinical applications.

Chapter 4. Ammonia as Early Diagnostic Tool via elevated metabolite in Cancer Microenvironment

Hepatocellular carcinoma (HCC) is highly malignant and is usually diagnosed at an advanced stage, accounting for more than 80% of primary liver cancers. Detecting HCC at an early stage is not easy, although enormous efforts have been made to find new biomarkers. Many studies have been devoted to finding serum biomarkers for the diagnosis of HCC from the perspective of metabolites. The role of ammonia in cancer cells has yet to be determined. At physiological pH, ammonia exists as ammonium ions (NH_4^+). Ammonia is mainly removed in the form of urea formed in the liver. Therefore, the concentration of ammonia in the blood must remain very low, because even a slightly elevated concentration (hyperammonemia) is toxic to the central nervous system (CNS). In addition, hyperammonemia (increased ammonia levels) can cause serious consequences for human health. During treatment, it is necessary to measure the level of ammonia several times very accurately. To date, a limited number of cost-effective methods are available for the rapid, inexpensive, and accurate estimation of ammonia at room temperature. Combining metabolomics and biochemical methods can discover new biomarkers for the early diagnosis of HCC and rapidly implement them in clinical diagnosis. Thus, PEDOT: PSS-based PHD was used as an effective biosensor for HCC detection.

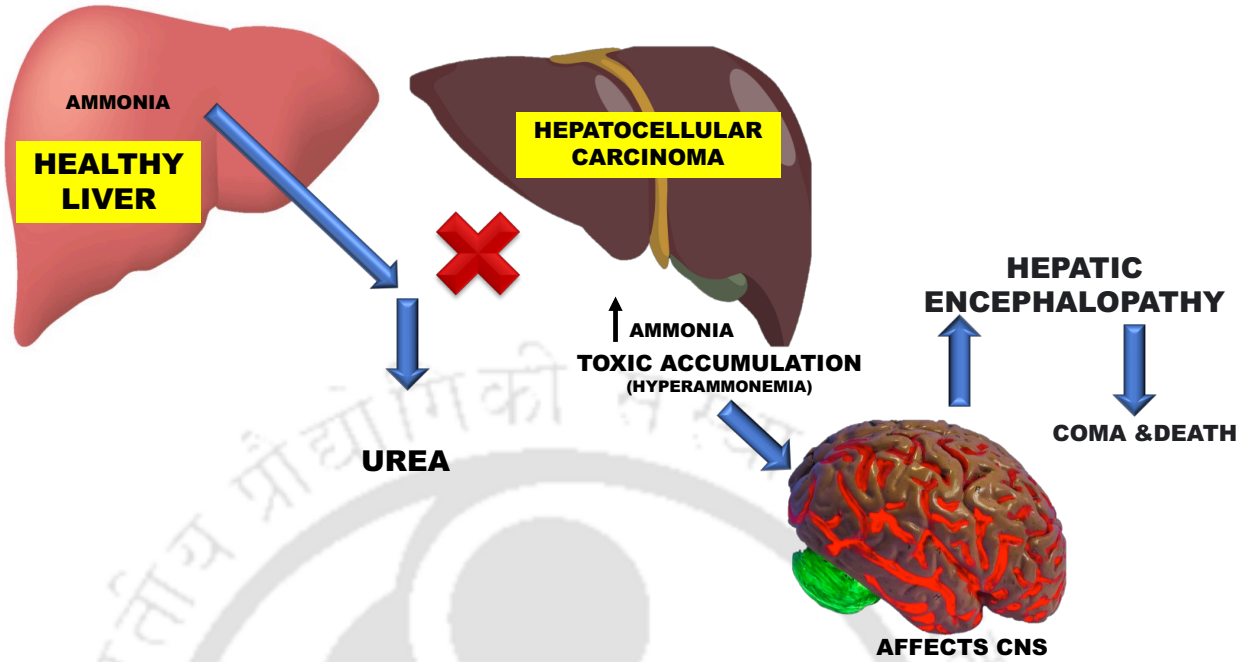

Figure S4. Graphical Representation of Detecting Hepatocellular Carcinoma using ammonia as a Diagnostic Tool.

Chapter 5. Polyhydroxyl Derivative (PHD) conjugated folic acid as an efficient Biomedical Platform for identifying folate-receptor cancer cells

A major challenge in today's cancer treatment is to achieve a satisfactory balance between the destruction of cancerous tissues and the destruction of healthy tissues, including damage to the immune system and highly proliferative cells. Thus, the detection of cancer cells at a sufficiently early, or controllable, stage is essential for possible therapy. As such, newly developed nanotechnology techniques bring hope to the world of oncology research. Nanotechnology is currently being tested and used, but there is a need to improve current technologies and develop new ones to detect, prevent and treat cancer. When we look at the tumour microenvironment, passive targeting is a well-known process. In recent years, folate receptors (FRs) have been used as a strategic target in cancer detection and diagnosis. The high affinity between FA and FR suggests the use of FA as a biosensing element in the construction of electrochemical sensors. This interaction causes the inhibition of electron transfer across the insulating cell membrane and the associated change in current.

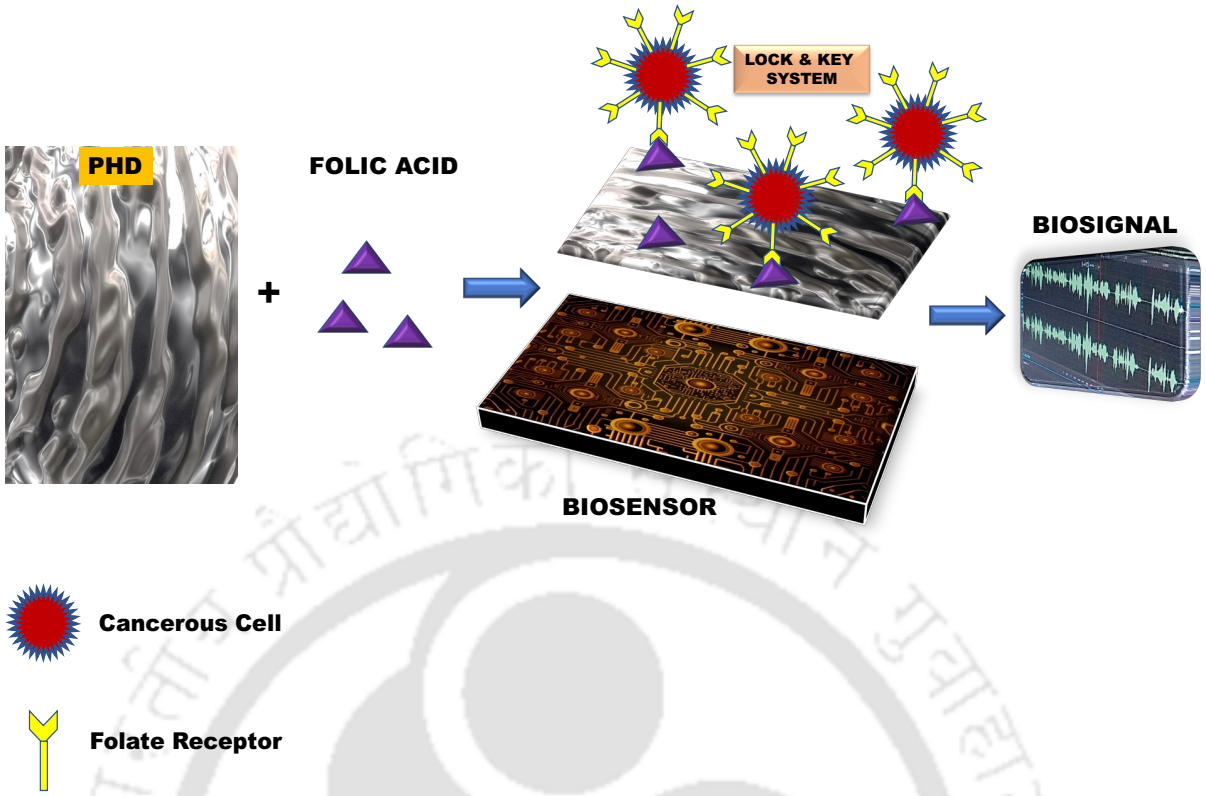

Figure S5. Pictorial Representation of targeting Folate Receptor in Cancerous Cells.

Chapter 6. Photo-electronic room temperature detection of Ammonia using reusable luminescent porous networks

Ammonia (NH_3) emissions are a growing problem worldwide due to their toxicity and reactivity. Exposure to NH_3 has serious consequences for human health. Inhalation, ingestion or direct exposure to NH_3 causes many side effects such as inflammation, tissue damage and many other scars, as it reacts with water to form ammonium ions. Due to its pungent odour, NH_3 is detectable in the range of 5-53 ppm and causes extreme irritation at concentrations above 80 ppm. We have introduced a UV-based two-electrode ammonia detection system that is stable at room temperature. In its current state, ammonia can be detected in gaseous form. In the absence of ultraviolet radiation, traces of current can be observed in the controlled system. In the presence of UV radiation, the magnitude of the current changes. The presence of ammonia causes a change in amperage. Such a current reading is still observed in the presence of UV radiation.

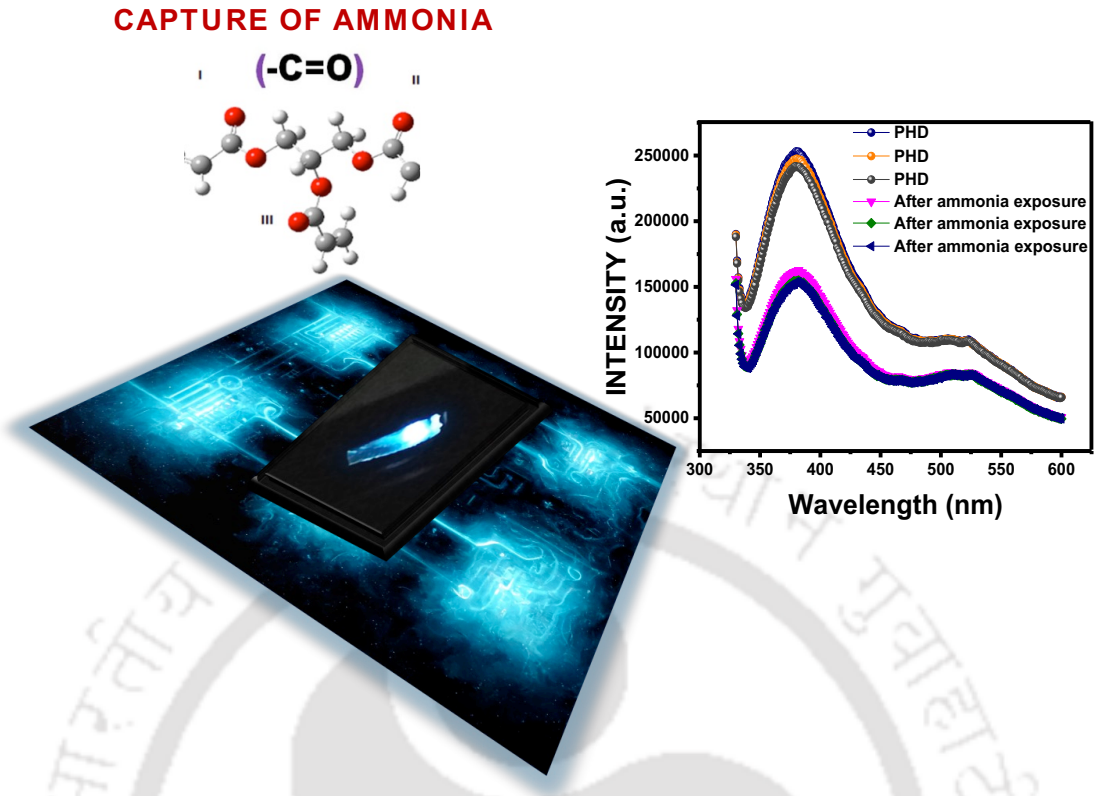

Figure S6. Graphical Representation of Photo-electronic Detection of gaseous ammonia.

Chapter 7. Theoretical Insights and Computational Analysis in Understanding the Role of Hydrogen Bonding in a Polyhydroxyl Derivative for ammonia sensing

Computational studies focusing on the mechanistic investigation of PHD sensitivity to NH_3 were performed using DFT and TD-DFT methods. Three donor sites, the -C=O group of the PHD, are prone to form hydrogen bonds with NH_3, but not with the other three -C-O-C groups. The theoretically calculated interaction capacity of NH_3 with PHD can be used to determine the H-bond strength or to perform chemisorption. NH_3 molecules form stable clusters and the presence of NH_3-NH_3 interaction between them at an optimal distance was tested. We then observe efficient NH_3 aggregation as an extended H-bond network. PHD bonded with one NH_3 molecule can help polarize the attached NH_3 molecule to attract incoming NH_3 molecules, facilitating cavity condensation.

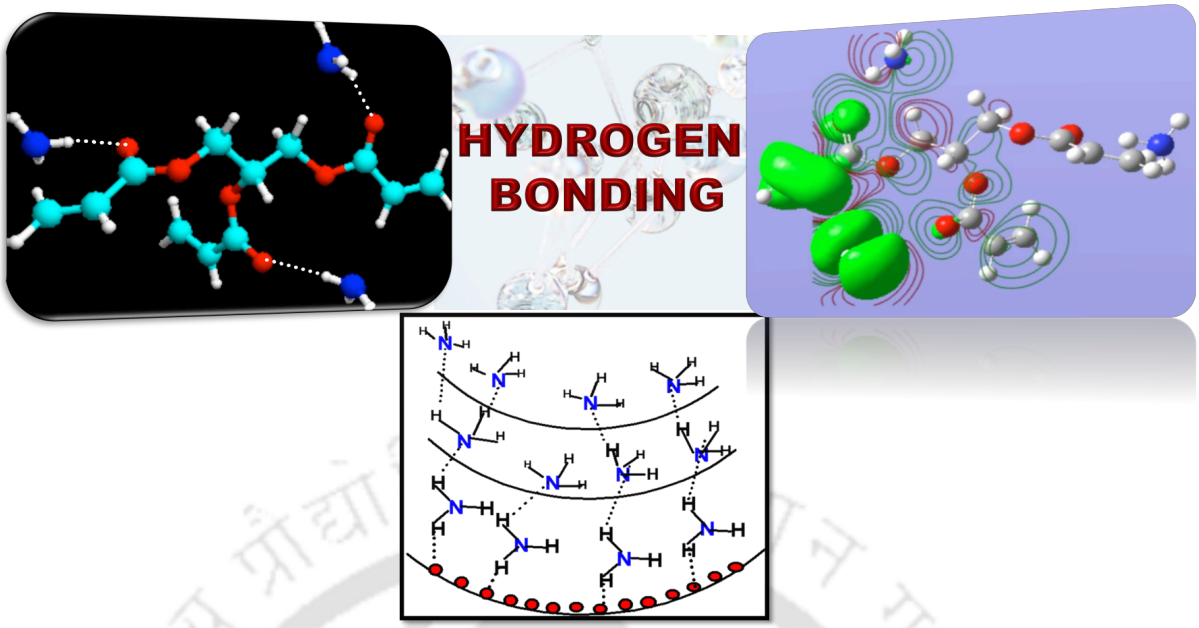

Figure S7. Formation of strong hydrogen bonds resulting in chemisorption of ammonia.

THESIS OVERVIEW AND FUTURE PROSPECTS

In conclusion, a portable and economical hybrid OECT prototype for the in-situ detection of ammonia in both the solution phase and vapour phase was established in a realistic environment. Ammonia detection has received enormous attention due to its significant impact on the environment and human health. Ammonia is highly toxic and corrosive, which easily spreads into the environment because it is widely used in fertilizers, cooling systems, dyes, pharmaceuticals, synthetic fibres, plastics, etc. The lower limit of human odour perception of ammonia is about 50 ppm. But even below this limit, it irritates the respiratory system, skin and eyes. The long-term (8h) permitted ammonia concentration for workers is 25 ppm. Ammonia emissions also affect the growth and productivity of vegetation and crops around the plant. Crops wither due to excess ammonia gas. In addition to these reported applications of ammonia detection, interest in ammonia detection is high due to its possible association with chronic diseases such as asthma, severe respiratory infections, and lung diseases associated with its presence as an environmental pollutant. In addition, detailed studies are needed to design individualized intervention strategies for human health exposure to ammonia, and highly sensitive detection technology for environmental monitoring is needed, including features such as cost-effectiveness, high selectivity, lightness, compactness, and mass production. The

high demand for analytical equipment requires the development of intelligent technologies that enable faster and more efficient detection of the desired analytes.

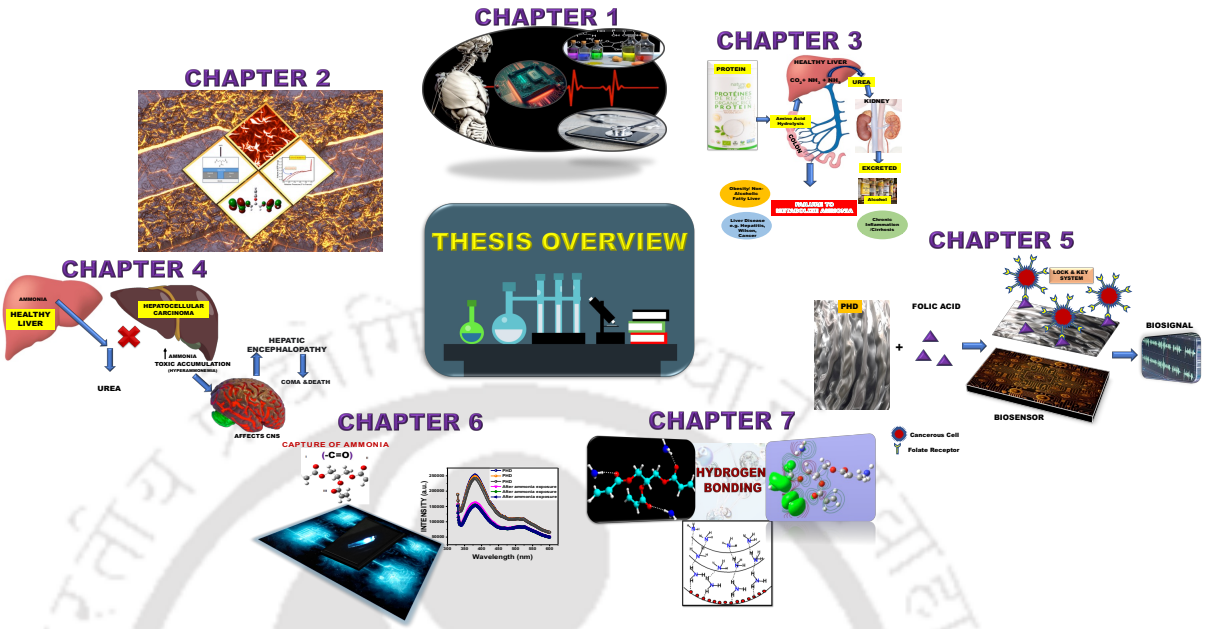

The increase in hospitalizations and the increase in surgical and diagnostic procedures are driving the demand for medical equipment, including capital equipment and consumables, in developed and emerging economies. OECT is a multidisciplinary field and is expected to adapt to other emerging technologies. This will lead to a revolution in the medical diagnostic market. The global medical devices market size was estimated to be USD 488.98 billion in 2021. The market is expected to grow from USD 495.46 billion in 2022 to USD 718.92 billion by 2029, with a CAGR of 5.5% during the forecast period. The global COVID-19 pandemic has been unprecedented and staggering, with demand for medical equipment lower than expected in all regions compared to pre-pandemic levels. Based on our analysis, the global market fell by -1.4% in 2020 compared to 2019. The increase in chronic diseases and the increasing emphasis of health institutions on early diagnosis and treatment lead to an increase in the number of diagnostic patients and surgical procedures.

Contents

LIST OF FIGURES

LIST OF TABLES

Chapter – 1

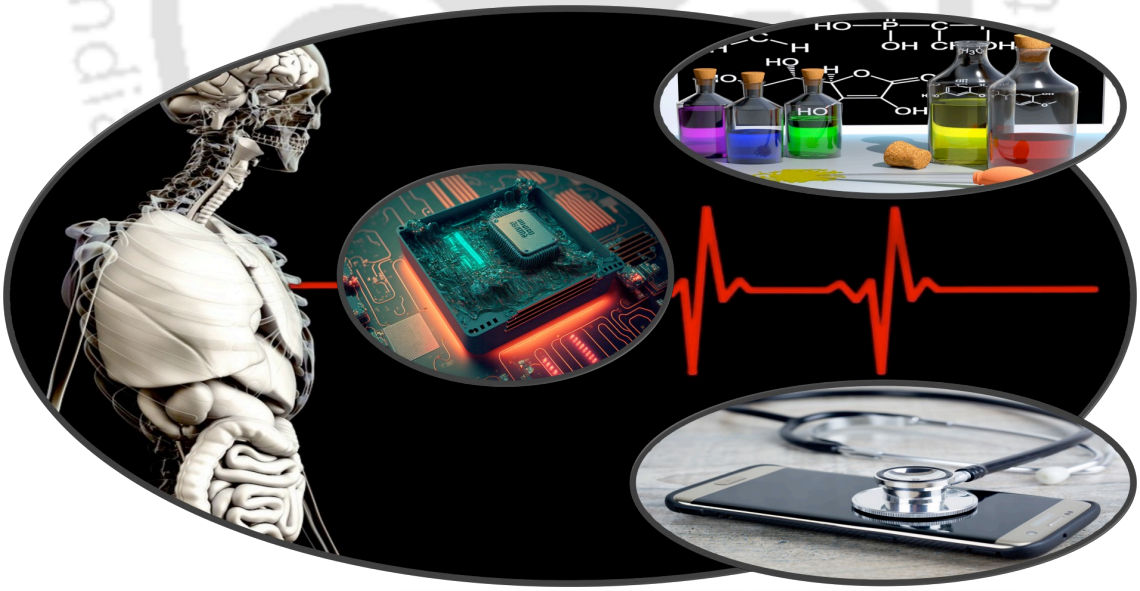

1.1 INTRODUCTION

The first specific goal of bioelectronics is the development of the next generation of advanced medical care. Minimal invasiveness is required for health devices, but it is necessary to maintain functionality and high performance. Activities aimed at implementing biologically inspired working principles require systems whose architecture differs from traditional systems. Before we can fully exploit the advantages of bioelectronics in practical devices, several scientific and technical challenges must be overcome. To begin with, we currently have only a limited understanding of electronic-biological interfaces, so it is important to obtain a theoretical model of complex systems containing water and ions. We also need a better understanding of the interaction of molecular rules when we include multiple functions of soft materials, such as charge transport. Bioelectronics is a rapidly developing field at the intersection of physics, chemistry, and life sciences, which aims to create new medical interventions, biosensors, monitoring devices, etc., by reading or writing biological signals directly with traditional semiconductor-based electronics. In biology, electric currents are primarily driven by the flow of ions (the smallest of which is the proton), rather than electrons, which are charge carriers in semiconductors and metals. The physics of both ion flows and electron flows are individually very well understood - albeit from completely different perspectives and scientific communities.

Bioelectronics is a new and interdisciplinary field, so it is expected to adapt to other emerging fields, such as microfluidics for drug delivery and the study of induced pluripotent stem cells for regenerative medicine. From a technical perspective, one of the biggest challenges in bioelectronics is data analysis, because it generates large amounts of new types of data. Recently developed methods for processing massive amounts of data and machine learning technologies are needed to analyse the vast amount of data generated from the biosensors being deployed in this emerging field. Potential applications of bioelectronic devices, such as high-resolution neural recording of the brain and 24-hour monitoring of blood levels of metabolites and disease markers, produce complex data that must be analysed to determine their biological significance. Dissolved ions in the water environment play an important role in plants, animals and humans. Ions regulate biological processes at the single-cell scale, enable the propagation of electronic signals, and maintain the proper balance between extracellular and intracellular fluids,

which are crucial for several processes such as nerve impulses, hydration, muscle function, and pH regulation. In situ, quantification of ion concentrations in aqueous environments is thus of considerable interest in several emerging fields, including biomedical diagnostics, environmental monitoring, health products, water and food testing and monitoring, agribusiness, and security.

A fundamental limitation of current transistor-based approaches is the trade-off between sensitivity, ion concentration range, and operating voltage. The coupling or "conversion" of ion and electron currents into the signals they carry is not trivial because of differences in their fundamental physics. Materials that support high number density and mobile ion currents in the solid state are few, with ion transport membranes such as Nafion and other polymer electrolytes being limited examples. Conductors that effectively carry the flow of both ions and electrons are even rarer. Therefore, delivery strategies have focused primarily on devices that combine two media/materials, each preferably hosting one carrier type, rather than a single medium supporting both, as evidenced by reviews of multiple device platforms. Suitable device architectures for creating this transformative interface between these two materials include bipolar ionic junctions, film-coated nanowires, proton field transistors, and perhaps the most mature and studied technology, organic electrochemical transistors (OECTs). OECTs were first demonstrated by White et al. in a device where the conductivity of the semiconducting polymer polypyrrole film was modulated by applying a gate voltage across the liquid electrolyte.[1,2,3] Organic electrochemical transistors (OECTs) are thin-film transistors that have shown great promise in a variety of applications such as biosensing, logic circuits, and neuromorphic designs. The device properties of OECTs are determined by the interaction between ionic and electronic charge carriers. This interaction distinguishes OECTs from traditional transistor technologies and necessitated the development of device models for the unique behaviour of OECTs.[4] They consist of a (semi-)conductive polymer channel between the source and drain electrodes in direct contact (i.e., no dielectric layer) with the surrounding electrolyte. When a suitable gate potential is applied, the conductivity (doping level) of the channel material changes due to ion migration and the accompanying hole injection. Local potential variations in biological tissue modulate the effective gate voltage of OECTs and thus the doping state in most of the channels. This modulation of the effective gate potential is usually converted/measured by recording the drain current of the

transistor. Because these devices operate at low voltage, this principle has been used in many biological sensor applications. [5]

Recently, there has been a huge demand for monitoring and control of air pollutants, one of the most common examples of serious environmental pollutants is ammonia (NH_3). Too much ammonia in ecosystems can cause nutrient imbalances and eutrophication. In terrestrial ecosystems, it causes a reduction in the diversity of plant species and habitats, and in aquatic ecosystems, algal blooms and hypoxia. In recent years, research into new and more efficient NH_3 gas sensors using nanostructured materials has received much attention due to various applications such as environmental monitoring, industrial process monitoring, automotive exhaust gas detection and medical diagnosis.[6] Room temperature operation, low detection limit and fast response time are highly desirable in many gas detection applications. However, available gas sensors suffer mostly from the high-temperature operation or external stimulus-response/recovery. Ammonium nitrate is found in many explosives and gradually decomposes to release small amounts of ammonia. Therefore, it is necessary to detect very low concentrations of ammonia to prevent fatal accidents.

The change in conductivity of metal oxides and conducting polymers was studied for ammonia detection in the ppb (parts per billion) range. Conventional solid-state and conducting polymer-based sensors have very low detection rates at room temperature. Commercially available conductive polymer sensors require high power consumption because they provide sufficient sensitivity only at high temperatures. Intensive research is underway to develop new sensor materials and devices for a wide range of applications, especially at room temperature. [7] Cost is always important in the marketing of biosensors, but a single-use policy is the most effective way to prevent infections in hospitals and can be expensive. Customization is particularly important in clinical applications, as it allows devices to be manufactured according to the needs of individual patients. Finally, mixed electronic and ion transport in conducting polymers also allows coupling to ions in the biological environment, enabling low-resistance contacts for efficient electrical recording and stimulation. Reliable detection of ammonia (NH_3) is highly required in many situations, such as air leak detection in environmental analysis, explosives and fertilizer industries, air conditioning compressors, breath analysis for

medical diagnoses, and animal shelters. In addition, the high toxicity of ammonia also justifies its rapid detection at very low concentrations.

Several chemosensors may be classified into different categories based on the sensor operating principle. Some typical sensors are based on optical measurements i.e., depending on colourimetric or fluorescence change, and also may be electrical, which is based on measurement of resistance, capacitance, impedance or other electrical signals, IR spectrometry, mass spectrometry, chromatography, surface acoustic wave etc. Chemosensors based on electrical signal modulation are much more straightforward and facile for device design, signal transduction and system integration, which combined can be made to be portable and small in size, thus suited for the real-time onsite operation. In these cases, electrochemical and electronic signals are mostly used in electrical mode chemosensors. So, an electrochemical sensor can transform the amperometric, potentiometric, or voltammetric effect of the analyte–electrode interactions into a measurable signal which can be used to identify as well as quantize the analytes present in the solution. The surface charge-transfer interaction with chemical analytes in chemosensors can directly indicate a signal arising from the change of electrical properties (resistive, conductivity, etc.) [8,9,10]

1.2. CHARACTERISTICS OF SOME SENSING MECHANISM

1.2.1. HYDROGEN BOND-BASED CHEMOSENSORS

Although the formation of hydrogen bonds is still one of the main strategies used for the development of anion optical sensors, the detectable changes of many systems are triggered by the deprotonation of sensors by basic anions such as fluoride or cyanide. Urea, thioureas, amides and sulfonamides are still the most commonly used binding motifs based on hydrogen bonds. For example, a urea-functionalised 4-amino-1,8-naphthalimide based fluorescent anion sensor has been reported by Lenehan [11] and co-workers. The properties of the urea and thioureas appended with this fluorophore have been extensively investigated in the past by Gunnlaugsson's group. [12]

A useful hydrogen bond donor group for the design of optical anion chemosensors is hydrazine. Azo-hydrazone tautomerism (akin to that of azo-dyes) is a well-known mechanism in which labile protons can be intramolecularly exchanged, leading to tautomers with different optical properties.[13] Chemosensor was reported by Trivedi and co-workers. [14] It has been indicated that in DMSO solution the red-shifted absorption

band after the addition of F-, AcO-, and to a less extent H_2PO_4 has been found. This was attributed to an intramolecular charge transfer process between the oxygen of the hydroxyl group on the quinoline ring and the electron-withdrawing phenyl ring, due to the formation of an H-bond complex between the hydroxyl groups of and the anionic species.

1.2.2. PHOTO-SWITCHABLE SENSORS

The design and development of photo-switchable receptors for selective recognition of anions have received considerable attention in recent years, not only in academic studies but also because of their application in diagnostics, imaging, and environmental science. Several examples of photo-switchable chemosensors have been recently proposed enable to detect highly basic anions such as F-, and CN-. In this context, Guo and co-workers reported the photo switchable systems consisting of dicyanovinyl-functionalized dithieenylethene, in which the dicyanovinyl group was able to respond to cyanide anion. [15,16]

1.2.3. CHEMO-DOSIMETERS

Chemo-dosimeters are compounds that react with a substrate selectively giving a colorimetric or fluorescence response allowing them to be used as a sensor. Among the most interesting systems recently proposed, Yi and co-workers described the chemo-dosimeter. In the presence of fluoride, a desilylation reaction occurred with the release of the free methylene blue and a fluorescence response in the near Infrared Region at 690 nm in DMSO/HEPES with very high selectivity. In this way, it is possible to distinguish between different sources of fluoride (organic and inorganic). [17]

1.2.4. OPTICAL METHOD (TUNABLE DIODE LASER ABSORPTION SPECTROSCOPY, TDLAS)

Gas sensors utilizing optical absorption have attracted immense attention as they can overcome obstacles that other gas sensors using contact-sensing techniques generally have, e.g., measurement error from the long-term memory effect. [18-25] Also, this technique is very appealing in commercialization due to its simplicity of operation and ability to achieve very high selectivity, fast analysis, and great sensitivity along with a relatively long-life time. Moreover, this method shows attractive properties in gas detection since it can be operated at a wide range of temperatures (from room temperature

to temperatures as high as 1500°C). Amongst gas sensors using optical absorption, the tunable diode laser absorption spectroscopy (TDLAS) has been well-developed for NH_3 gas detection. [26-45]

1.2.5. ELECTROCHEMICAL SENSORS

This method has been used for gas sensors due to its attractive aspects including lower power consumption as well as high sensitivity and relatively perfect selectivity. A typical electrochemical gas sensor consists of a sensing electrode (or working electrode), a counter electrode, a reference electrode, an electrolyte and a gas-permeable hydrophobic membrane (usually, PTFE or Teflon). [46-48] The solid-state electrolyte-based sensors normally use amperometric and potentiometric techniques and, on the other hand, the liquid-state electrolyte sensors, usually, employ voltammetric and potential step chronoamperometric methods. The NH_3 gas sensors using the potentiometric method, for example, adopt a sensing mechanism that the difference in the electrical potential between the sensing and counter electrodes is measured when NH_3 gas diffuses across the gas permeable membrane into the electrolyte solution, and the electrochemical reaction between the electrolyte and NH_3 gas molecules occurs at the sensing electrode. As a result of the electrochemical reaction, nitrogen, hydrogen ions and six electrons are produced through the oxidation of ammonia at the sensing electrode and, meanwhile water is formed at the counter electrode through the reaction between hydrogen ions generated from the sensing electrode and oxygen.[49-65]

1.3. AMMONIA GAS SENSING METHODS

There are a variety of sensing techniques existing for NH_3 detection, however, the most prevalent detecting methods can be classified into three major categories,

(a) the solid-state sensing methods (metal oxide-based sensors, and conducting polymer sensors), (b) the optical method (optical sensors utilizing tunable diode laser spectroscopy), and (c) other methods (electrochemical sensors, surface acoustic wave sensors, and field effect transistor sensors). [66-79]

DIFFERENT TYPES OF SENSOR MATERIALS

1.3.1. CONDUCTING POLYMER SENSORS (CPS)

From a traditional viewpoint, polymers are well-known as insulating materials. The CPs can be used as sensitive layers, particularly given their inexpensive synthesis, high

sensitivity and wide detection range of volatiles. In the process, when CPs are exposed to an analyte, many changes could occur including solvation effects on the polymer chain, modifications of the backbone conformation, and the attraction of dopant counter ions or transfer of electrons in the polymer. The change in electron mobility and the swelling of the polymer matrix can be converted into electrical and/or mechanical signals. Amongst the conducting polymers, polypyrrole (PPY), polyaniline (PANI), and poly(3,4-ethylenedioxythiophene) (**PEDOT) are** by far the most frequently used in the gas sensor field. [50-73] So, CPs with high sensitivity consisting of PANI, PPY and poly (3,4 ethylenedioxythiophene) (PEDOT) are used for various sensors such as gas sensors, temperature sensors, humidity sensors, strain sensors, and biosensors. Moreover, the combination of CPs and other sensing materials such as carbonaceous materials, metal oxides, metals, metal sulfide etc. produces different composites with higher sensing performance.

However, since the advent of conducting polymers, a great number of gas sensors have utilized conducting polymers due to their advantages, such as ease of fabrication and modification, stability, design flexibility, and tunability with other materials. There are conductometric, potentiometric, amperometric, colourimetric, and gravimetric modes of operation methods for conducting polymer-based sensors. [74-113]

1.3.2. POLYPYRROLE (PPY) BASED SENSORS

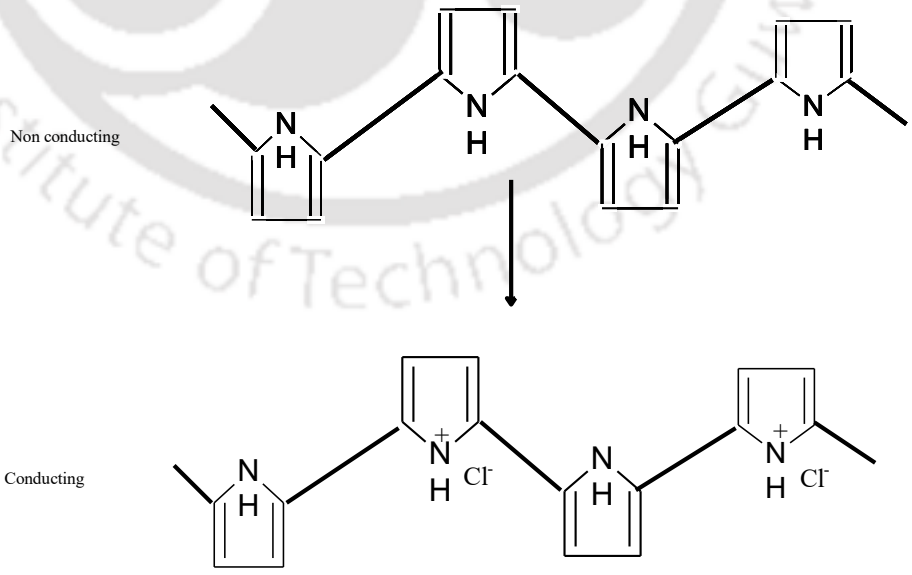

Figure 1.1. Chemical Structure of PPY.

PPY has received enormous attention due to its easy oxidation, conductive nature, water solubility and the commercial availability of pyrrole monomers (Fig. 1.1). PPY-based materials have various applications as electrocatalysts, anticorrosive, carbon dioxide capture, light emitting diodes, batteries, electrochemical capacitors and sensors. PPY exhibits excellent sensitivity to strain and temperature, and can also be used as a gas sensor material. [50-61]

PPY/Carbon nanotubes (CNT) composite

This nanohybrid composite has been reported from the electrochemical-assisted synthesis of PPY with sodium dodecyl sulfate (SDS) as a surfactant and supported with functionalized multi-walled CNTs (f-MWCNTs). It is used as a nitrite sensor in an aqueous medium. Upon incorporation of f-MWCNTs into the PPY/SDS matrix, PPY/SDS/f-MWCNT composite films exhibit lower impedance and higher capacitance than pure PPY/SDS films. The capacitance of the composites gradually increased with an increasing percentage of f-MWCNTs.[36]

PPY/Graphene(G) composite

PPY-functionalized graphene nanosheets (GNs) have much-enhanced sensitivity. This is due to the porous structure as well as the large effective area of PPY-functionalized graphene nanosheets (GNs) in a PPY-GNs-modified electrode. This hybrid sensor of an ultrathin PPY layer formed by chemical vapour deposition grown on GN has been demonstrated to give an excellent performance. It might be a result of a synergistic effect between the PPY layer and GN. It in turn serves as a high, fast and reversible response of NH_3 sensing with efficient selectivity at room temperature and also rather good stability, reproducibility and immunity to humidity have been shown. It is likely that on absorption of NH_3 on the PPY layer, the electron transfer from NH_3 to the PPY layer, and then to GN through the PPY layer occurs which perhaps might change the resistance of the PPY layer and GN enhancing the sensitivity. Moreover, the porous nature of the ultrathin PPY layer contributes an important influence on the sensor response, selectivity and immunity to humidity. [54-61]

PPY/Metal oxide composite

The voltammetric sensor of PPY/bismuth oxide (Bi_2O_3) nanocomposite for the electroanalysis of clofazimine has been found. It shows the highest sensitivity with a

detection limit of 0.97 μmol mL^{-1} and a quantification limit of 3.23 μmol mL^{-1}. This sensor also reveals exceptional reproducibility, satisfactory recovery and long-term stability. Another PPY/TiO2/GCE voltammetric sensor is found to be exhibited an exceptional electroanalytical performance compared to PPY/GCE, TiO_2/GCE and bare GCE sensors. [53-60]

PPY/metal nanocomposite

PPY nanosphere/Ag nanocomposite and PPY fiber/Ag nanocomposite are some of the PPY/metal nanocomposite materials. These are prepared by using template-free and template-assisted methods for NH_3 gas sensing. The PPY fiber/Ag nanocomposite sensor exhibits enhanced NH_3 gas sensing performance including sensitivity, response time and recovery time than the PPY nanosphere/Ag nanocomposite sensor. There are large differences in NH_3 gas saturation for these two sensors, herein PPY fiber/Ag nanocomposite sensor is not saturated even in the presence of 250 ppm NH_3 gas whereas the PPY nanosphere/Ag nanocomposite is saturated with 100 ppm NH_3 gas concentration. The sensitivity of Au-nanoparticle-decorated PPY nanowires towards arsenic is quite sensitive towards concentration and the detection limit of this sensor is reported to be 0.32 μmol L^{-1}. [55-56]

1.3.3. PANI BASED SENSORS

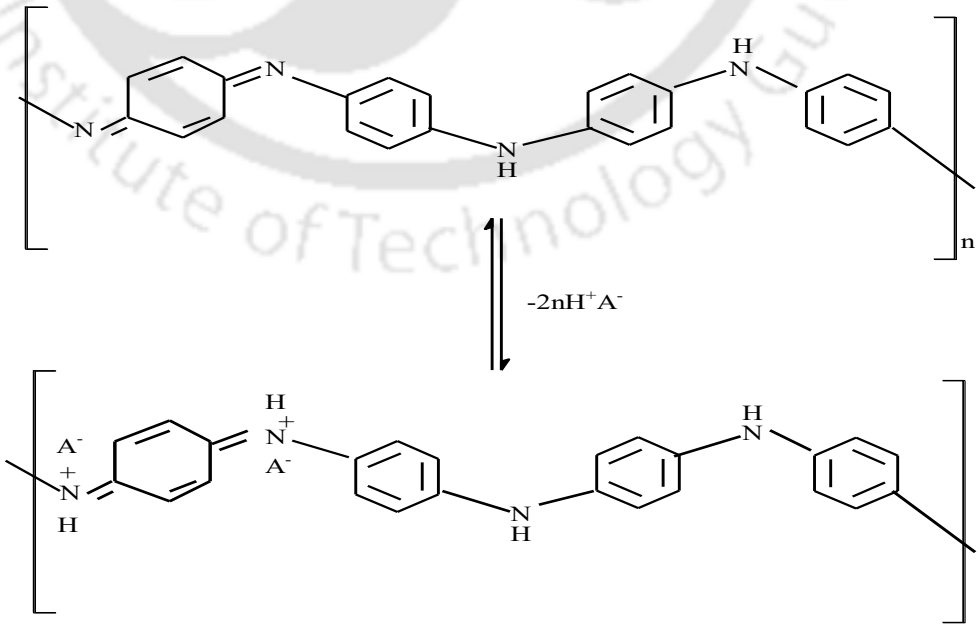

Figure 1.2. Chemical Structure of PANI.

PANI nanofiber-based sensors

PANI nanofibers for sensor applications have greater sensitivity and a faster response time due to a higher effective specific surface area and shorter penetration depth for target analyte molecules compared with conventional bulk materials. The diameter of PANI nanofibers is usually tailored via temperature-controlled polymerization. The conductivities of doped PANI nanofibers increase with a decrease in diameter. PANI nanofibers with smaller diameters exhibit a much faster response than larger-sized fibers or bulk PANIs due to their large surface area and high intrinsic conductivities. The NH_3 gas sensor based on the 4-toluenesulfonic acid (TSA) doped PANI nanofibers on interdigitated array electrodes represents rapid response time (10 s) and quick recovery time (100s) at 50 ppm NH_3 gas. As reported in the literature, the PANI nanofiber film also shows a better sensitivity (1.06), compared to a conventional PANI film (0.3) for 50 ppm NH_3 gas. The improved sensor response and sensitivity could be attributed to the fact that more NH_3 molecules are probably diffuse into their nanofiber film and react with the active site of PANI chains swiftly because of its large specific area resulting from the small diameter and the interconnected network of PANI nanofibers.

The sensing mechanism of PANI nanofiber to NH_3 through deprotonation rate relies on the concentration of NH_3, increasing the film resistance. In this process, as the sensing film is exposed to the air, the ammonium ions decompose into ammonia molecules and protons which restore the original doping level of PANI. Consequently, this decomposition leads to a decrease in the film resistance. [76-87]

PANI blend nanofiber sensors based on electrospun

The electrospun polyacrylonitrile/PANI blend nanofibers are reported to be quite sensitive towards NH_3 gas, and it is due to the semiconducting behaviour of this material that could respond quickly towards NH_3 gas. Poly (vinyl alcohol)/PANI nanofibers are another material prepared for use in NH_3 sensors. The large surface area, dimensions and quality of the nanofibers are essential parameters for a good response of the NH_3 gas sensor of these materials. The PANI/polyethylene oxide nanofibers doped with CSA have been used for the hydrogen sulfide (H_2S) gas sensor, and this material is found to exhibit good sensitivity, good recovery speed and superior performance in comparison to other PANI-based sensors. [58,61,64,76]

PANI composites for sensors

PANI and carbonaceous material composites for sensors such as carbon nanotubes (CNTs) and graphene oxide (GO) are ideal candidates for gas sensing due to their unique electrical, physical and chemical properties. [84-87] These materials are highly stable and considered to be active materials for gas sensing. It may be due to the large specific surface area, high surface-to-volume ratio and rich conjugation of π-electrons along the surface. Usually, PANI is quite a sensitive polymer among CPs towards various gases due to the existence of two distinct oxidation states. However, PANI undergoes a volumetric change during oxidation/reduction (doping/de-doping) resulting in it being mechanically unstable. The mechanical stability of PANI can be increased by adding suitable fillers such as CNTs or graphene. The incorporation of CNTs increased the robustness of PANI, flexibility and the number of active sites, as they effectively increase the intra- and inter-chain charge mobility along the polymer chain in the presence of electron donor or acceptor gases. As an example, sensors based on multi-walled CNT (MWCNT) and single-walled CNT-doped PANI composite thin films for hydrogen sensing show a higher response than pure PANI.

PANI/MWCNT composites.

PANI/MWCNT nanocomposites have been useful for the detection of trace-level NH_3 gas (up to 2 ppm NH_3). This composite material is highly sensitive as gas sensors and also the response as well as short recovery time have been demonstrated. The PANI/MWCNT-modified screen-printed carbon electrode (SPCE) based electrochemical sensor is used for the simultaneous detection of urea and pH. It shows a lower detection limit and higher selectivity than reported biosensors of 10 μmol L^{-1}. In other cases, carboxylic acid functionalized MWCNTs ((MWNTs-COOH)/PANI/ITO composite) can substantially decrease the oxidation potential of nifedipine (NIF) by about 170mV in comparison with bare indium tin oxide (ITO) and showed a synergistic effect on the electrochemical oxidation of NIF and a lower detection limit of NIF. The electrochemical performance variation of these films is also improved.[56]

PANI/metal oxide composite

Various inorganic semiconducting metal oxides such as undoped or doped titanium dioxide (TiO_2), tin (IV) oxide (SnO_2) and zinc oxide (ZnO) have been well-studied as

sensitive materials for gas detection. As such PANI is one of the CPs used in many sensing materials. The drawbacks of PANI (Fig. 1.2) as a sensing material are due to poor mechanical strength and no selectivity. So, PANI/inorganic nanocomposites have been proposed for gas sensing applications. Composites of PANI with metal oxides such as ZnO, TiO_2, iron (III) oxide (Fe_2O_3), SnO_2, tungsten oxide (WO_3), copper (II) oxide (CuO), cerium (IV) oxide (CeO_2) etc. exhibit excellent sensing properties. [87-89]

A PANI/TiO_2 composite with superficial deposition of PANI on TiO_2 has an average size of 25 nm and an aggregated granular porous morphology serves as a good sensing material. Likewise conducting PANI/niobium doped TiO_2 (Nb-TiO_2) nanocomposites with different weight percentages of Nb-TiO_2 nanoparticles have been found excellent material in terms of sensitivity and fast response to NH_3 gas at room temperature. [88]

PANI/Au

The Noble metal Au particles are used for glucose sensors. The Au particles were electro-deposited on PANI film under optimum growth conditions for maximum dispersion to achieve a highly sensitive glucose sensor. This composite material can achieve better electrocatalytic behaviour, anti-poisoning characteristics, advanced biocompatibility and a wide range of oxidation potential due to its maximum dispersion on a polymer matrix. [53,56(f)]

1.3.4. Poly (3,4-ethylenedioxythiophene) (PEDOT) based sensors

The electrodeposition of a PEDOT layer on a GCE in a solution containing 3,4-ethylenedioxythiophene (EDOT) and sodium citrate has been reported to be good sensing material. Also, with the introduction of nickel cations to the peptide-anchored PEDOT film Ni–O coordination bonds connected the carboxyl groups from the PEDOT film surface and the peptide group has been demonstrated. A DNA sensor was successfully fabricated based on peptide-anchored PEDOT film for the immobilization of a BRCA1 (a gene closely related to breast cancer) recognition probe. This biosensor with high sensitivity and favourable selectivity can efficiently detect BRCA1 in real complex samples. [93(g)]

poly(3,4-ethylenedioxythiophene): poly(styrene-sulfonate) (PEDOT: PSS) BASED SENSORS

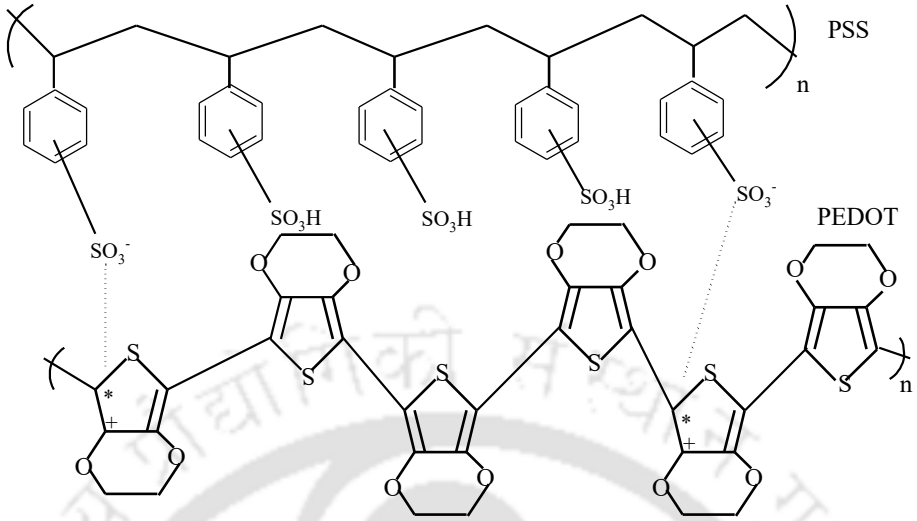

Figure 1.3. Chemical Structure of PEDOT: PSS.

PEDOT: PSS is an appealing sensing material because of its high conductivity and solubility in water and low redox potential. The doping of PEDOT with PSS improved the solubility and processability because PSS (through an insulator) can connect PEDOT to water (Fig. 1.3). PEDOT: PSS possesses an increased radiation transparent property compared to carbon black. Compared to other conductive materials, it seems to be less sensitive to oxidation and has an increased stability and degradation resistance. On the other hand, a mixture of PEDOT: PSS with water-soluble electrocatalytic materials or colloidal metal nanoparticles provides an excellent method for modulating the sensing properties.[93]

PEDOT: PSS/sulfide composite

In a PEDOT: PSS/sulfide composite material the molybdenum disulfide (MoS_2) based active region showed high responsivity towards low humidity levels, but while the PEDOT: PSS based portion is reported to be responded well to high humidity levels. A single humidity sensor based on PEDOT: PSS and MoS_2 as the active layers of two separate transducers acquire very high sensitivity and excellent response and recovery times of 0.5 s and 0.8 s, respectively. [93(i)]

PEDOT: PSS/metal composite

Incorporating silver nanowires (AgNWs) of optimized concentration into PEDOT: PSS film i.e., PEDOT: PSS/AgNW composite film as the active layer can significantly

improve the sensitivity of NH_3 sensors. The sensor achieved excellent sensing performance for detecting very low NH_3 concentrations below 500 ppb and considerable selectivity concerning water and common organic vapours. Usually, the sensor was integrated with a self-designed portable data acquisition system only for monitoring the freshness of pork. [93(j)]

PEDOT: PSS/metal oxide composite

ZnO nanorods (NRs)/PEDOT: PSS hybrid is an excellent material for sensors and the heterojunctions are highly efficient UV sensors that showed diode-like behaviour and sensitivity of 37.65 under UV (λ = 256 nm, 130W) illumination. The properties like response and sensitivity of the ZnO NR/polymer heterojunction device are reported to enhance by a factor of 10 and 8 compared with bare ZnO, NR arrays, the, respectively. The enhanced performance may be due to the effective charge separation guided by the built-in potential at the interface between the ZnO NRs and PEDOT: PSS. [93(k)]

PEDOT: PSS/carbonaceous materials composite

A reduced graphene oxide (rGO)-PEDOT: PSS/GCE sensor is another promising material as a sensor which maintains good stability, repeatability and reproducibility, with a high peak current and low working potential (electrocatalytic activity) during the electrochemical measurements. The electro-sprayed GO/PEDOT: PSS can enhance the current response due to a simple increase of the screen-printed carbon electrode (SPCE)surface area. It showed faster electron transfer kinetics than the unmodified SPCE. The sensing response of the resistive NH_3 gas sensor based on PEDOT: PSS and N-doped graphene quantum dots (N-GQDs) dopant has been reported. On addition of 50 wt.% N-GQDs in PEDOT-PSS sensing response towards NH_3 can increase from 30.13% to 212.32% at 1500 ppm. [93(l)]

The poly(3,4-ethylenedioxythiophene): poly(styrene-sulfonate) (PEDOT: PSS) film in water has been found useful for handling the strategies of swelling, disintegration, cracking and peeling-off of this conducting polymer another film of EDOT-*co*-EDOT: PSS (poly (EDOT-*co*-EDOT-AA): PSS) has been reported. There have been reports on further modification to prepare organic polymer–inorganic nanocomposites by

incorporating carbon nanomaterial, graphene, and a unique and versatile clay nanomaterial, halloysite. [93]

1.3.5. Poly (acrylic acid) (PAA)

The research on the improvement of developing more compatible materials for several sensor designing is never-ending. Moreover, the development of mono-dispersed cross-linked poly (acrylic acid) (PAA) droplets prepared by using the microfluidic method is found useful for detecting both Ca^{2+} and Mg^{2+} in human saliva and serum. [94(b)] This typical polyacrylic acid (PAA)/polyvinyl alcohol (PVA)-based quartz crystal microbalance (QCM) was fabricated by depositing composite PAA/PVA nanofibrous substrates onto QCM gold electrodes that can efficiently detect ammonia sensors up to 100 ppb. [94(c)]

1.4. OVERVIEW OF THE SURVEY AND OBJECTIVE

Developing Gas sensors have been a subject of interest for many years. It has been known that the semiconductor can be well affected by any reducing or oxidizing ambience, hence it is likely to exploit for any environmental contaminations and other chemical controlling strategies. It may be mentioned that several materials such as conducting polymers, metal oxides, and certain sensitive organic layers have been extensively found in the application of gas sensing. Eventually, there are several metal oxide-based gas sensors which are developed in many laboratories, and also some are commercially available for various applications. The major issues of sensors are due to the low selectivity as well as reduced lifetime, in some cases high operable temperature leading to inconveniences in the operation. It may be mentioned that organic compounds such as molecular crystals can be used as sensitive layers of gas sensors but still, the problem of repeatability and poor selectivity cannot be ignored. Rather than metal oxide-based sensors, there are certainly conducting polymers which are used as sensing material due to their unique electrical properties. Most of these polymers are easy to synthesize and also very convenient for operating at room temperature and have attracted the development of gas sensing.

The emission of ammonia (NH_3) has been a major concern as it is a major air pollutant that contributes to particulate matter and is also responsible for the eutrophication of ecosystems. Several functional materials have been used as NH_3 sensor elements,

including inorganic oxides, carbon nanotubes, conducting polymers, and composites.[93] In addition to these reported applications of ammonia detection, there is great interest in ammonia detection due to its possible association with chronic diseases such as asthma, severe respiratory infections, and lung disease associated with its presence as an environmental pollutant. Over the past decade, ammonia sensors with detection limits ranging from 200 ppm to 0.35 ppm have been reported based on technologies such as metal oxides, catalytic processes, organic polymer membranes, optical detection methods, and gas-coupled mass spectrometry chromatography (GCMS).[114]

A detailed study is further required for designing personalized intervention strategies for ammonia exposure to human health and environmental monitoring calls for a highly sensitive sensing technique along with other attributes such as cost effectiveness, high selectivity, light weight, compactness and mass production. Organic polymer-based field effect transistors (FETs) provide a highly suitable match but owing to either high cost, bulky with high-temperature requirements, high operating voltage, lack of high selectivity or having a limit of detection too high for non-occupational settings alternative electronic technologies are a need of the hour. Moreover, it has been found that the major concern of using n-type OFETs is the instability of radical anions under air. Hence, in some cases, the addition of functional groups of high electron affinity into p-type semiconducting materials i.e., the n-type and p-type hybridization gas sensing systems are found. So, further improvement is the most challenging aspect of biological systems.

Organic electrochemical transistors (OECTs) exploit the ability of organic semiconductors to conduct ions in addition to electronic charge and are of great interest in sensor and biosensor applications because they can operate in liquid environments. In addition, they have a simple geometry, typically a planar monolayer structure consisting of a channel and a gate contact near the channel. PEDOT: PSS provides an attractive platform for the development of organic electronics, i.e., thermoelectric converters, photovoltaic devices, supercapacitors and sensors, etc. It has excellent solution processing ability and miscibility with functional films, usually drop-casting, and spin-coating. and spray coating to demonstrate high and adjustable conductivity. In addition, it has excellent chemical and electrochemical stability, good optical transparency and good biocompatibility.[115] Here we focus on the ability to monitor ammonia (NH_3) concentrations in the low ppb range. Rather than a mere case study, the choice of

ammonia as a pollutant gas is based on solid scientific evidence that comprehensive monitoring of ammonia concentrations and fluxes is key to reducing risks to human health and vegetation. The widespread use of ammonia and its derivatives as agricultural nitrogen fertilizers has greatly increased ammonia emissions into the atmosphere, which has caused many environmental problems. These include the eutrophication of semi-natural ecosystems, soil acidification, generation of fine particles in the atmosphere, and changes in the balance of the global greenhouse. A growing number of studies highlight the importance of ammonia as a precursor to secondary fine particles (PM_{10} and $PM_{2.5}$), which pose a serious threat to human health.[116] Ammonia could thus be used as a local indicator of secondary particle formation, which would allow indirect control of particle emission sources. However, the detection of atmospheric ammonia concentrations in urban areas has been largely neglected until now because its average level is usually low, i.e., between 20 and 30 ppb, as Chiesa et al. [117] For realistic outdoor ammonia (NH_3) concentration monitoring in urban environments, chemically resistant gas sensors (CGS) should provide sensitivities well below the ppm scale, hopefully at the ppb level. In addition, hyperammonemia (increased ammonia levels) can cause serious consequences for human health. During treatment, it is necessary to measure the level of ammonia several times very accurately. To date, a limited number of cost-effective methods are available for the rapid, inexpensive, and accurate estimation of ammonia at room temperature. There is literature [118] on the detection of ammonia in exhaled breath, which is considered to be one of the non-invasive diagnostics, but poor selectivity and high humidity are the main disadvantages. Therefore, the detection of ammonia in human serum, breath and sweat is limited. Here, we aim to create a more efficient sensor for use in biological samples, including cancer cells, as well as for environmental monitoring. In this study, we present several strategies to improve the sensitivity of NH_3 at room temperature (RT) as a potential emerging medical diagnostic.

1.5. REFERENCES

1. T. Someya, Z. Bao & G. G. Malliaras, *Nature*, 2016, 540,379-385.
2. M. Sheliakina, A. B. Mostert and P. Meredith, *Mater. Horiz.*, 2018, 5, 256.
3. M. Ghittorelli, L. Lingstedt, P. Romele, N. Irina Crăciun, Z. M. Kovács-Vajna, P. W.M. Blom & F. Torricelli, *Nature Communications*, 2018, 9, 1441.
4. J. T. Friedlein, R. R. McLeod, J. Rivnay, *Organic Electronics,* 2018, 63, 398–414.

5. V. Venkatraman, J. T. Friedlein, A. Giovannitti, I. P. Maria, I. McCulloch, R. R. McLeod, and J. Rivnay, *Adv. Sci.*, 2018, 5, 1800453.
6. H. Liu, W. Shen and X. Chen, *RSC Adv*., 2019, 9, 24519.
7. S. Pandey, G. K. Goswami & K. K. Nanda, *Scientific Reports*, 2013, 3, 2082.
8. W. Gao, H. Li, Y. Zhang, S. Pu, *Tetrahedron*, 2019, 75, 17, 26, 2538-2546.
9. H. Xu, W. Chen, W. Zhang, L. Jua and H. Lu, *New J. Chem*., 2020,44, 15195-15201.
10. P. S. Kumar, P. R. Lakshmi, *New J. Chem*., 43,2019,675-680.
11. A. J. Blok, M. R. Johnston, & C. E. Lenehan, *Scientific Reports*, 7, 2512.
12. R.M. Duke, E.B. Veale, F.M. Pfeffer, P.E. Kruger, T. Gunnlaugsson, *Chem. Soc. Rev*., 2010, 39, 3936-3953.
13. C. Chatterjee, S. Sethi, V. Mukherjee, P.K. Sahu, N. Behera, *Spectrochim. Acta - Part A: Mol. Biomol. Spect. A*., 2020, 226, 117566.
14. S. K. Dhawan, D. Kumar, M. K. Ram, S. Chandra, D. C. Trivedi, *Sens. Actuators B*, 1997, 40, 3, 99-103.
15. W. Guo, T. Liu, W. Zeng, D. Liu, Y. Chen, Z. Wang, *Mater. Lett.*, 2011, 65, 3384–3387.
16. L. Xue, W. Wang, Y. Guo, G. Liu, P. Wan, *Sens. Actuators B Chem*., 2017, 244, 47–53.
17. P. Wei, F. Xue, Y. Shi, R. Strand, H. Chen and T. Yi, *Chem. Commun*., 2018, 54, 13115.
18. A. Panja, K. Ghosh, *Supramol. Chem*., 2019,31, 239-250.
19. R. M. Duke, B. V. Emma, M. P. Frederick, E. K.Paul and T. Gunnlaugsson, *Chem. Soc. Rev*., 2010, 39, 3936–3953.
20. F. Pfeffer, A. M. Buschgens,N. W. Barnett, T. Gunnlaugsson, *Tetrahedron Letters*, 2005, 46,6579-6584.
21. Y.-M. Dong, Y. Peng, M. Dong and Y.-W. Wang, *J. Org. Chem*., 2011, 76, 6962–696.
22. R. K. Jakku, N. Mirzadeh, S. H. Privér, G. Reddy, A. K. Vardhaman, G. Lingamallu, R. Trivedi and S. K. Bhargava, *Chemosensors,* 2021, 9,10, 285.
23. C. Chatterjee, S. Sethi, V. Mukherjee, P.K. Sahu, N. Behera, *Spectrochim. Acta - Part A: Mol. Biomol. Spect. A.*, 2020, 226, 117566.
24. Z. Deng, C. Wang, H. Zhang, T. Ai, K. Kou, *Front Chem.*, 2021, 19, 9, 666450.
25. A. Chellappa, C. Fischer, W. Thomson, *Appl. Catal. Gen.,* 2002,227,231–240.

26. T. Hejze, J.O. Besenhard, K. Kordesch, M. Cifrain, R.R. Aronsson, *J.Power Sources*, 2008,176, 490–493.
27. G.K. Mani, J.B.B. Rayappan, *Appl. Surf. Sci*., 2014,311, 405–412.
28. B.Timmer, W. Olthuis, A. Van Den Berg, *Sensor.B. Actuator. B Chem*., 2005, 107, 666–677.
29. (a) G.K. Mani, J.B.B. Rayappan, *Mater. Sci. Eng. B*, 2015,191 ,41–50.
    (b) G.K. Mani, J.B.B. Rayappan, *Sensor. Actuator. B Chem*., 2013, 183, 459–466.
    (c) V. Talwar, O. Singh, R.C. Singh, *Sensor. Actuator. B Chem*., 2014,191,276–282.
30. A.K. Prasad, P.I. Gouma, D.J. Kubinski, J.H. Visser, R.E. Soltis, P.J. Schmitz, *Thin Solid Films*, 2003, 436, 46–51.
31. P. Gouma, K. Kalyanasundaram, X. Yun, M. Stanaćević, L. Wang, *IEEE Sens. J.* , 2010, 10, 49–53.
32. L. Tabrizi, H. Chiniforoshan, *Sensor. Actuator. B Chem*., 2017, 245, 815–820.
33. P. Werle, R. Mucke, F. Slemr, *Appl.Phys. B Photophysics Laser Chem*.,1993, 57, 131–139.
34. G. Korotcenkov, *Mater. Sci. Eng. B Solid-State Mater. Adv. Technol*., 2007, 139, 1–23.
35. S. Carquigny, J.B. Sanchez, F. Berger, B. Lakard, F. Lallemand, *Talanta*, 2009,78, 199–206.
36. T. Zhang, M.B. Nix, B.Y. Yoo, M.A. Deshusses, N.V. Myung, *Electroanalysis*, 2006,18, 1153–1158.
37. B. Timmer, W. Olthuis, A. Van Den Berg, *Sensor. Actuator. B Chem*., 2005,107, 666–677.
38. R. Peeters, G. Berden, A. Apituley, G. Meijer, *Appl. Phys. B*, 2000, 71, 231–236.
39. D.J. Miller, K. Sun, L. Tao, M.A. Khan, M.A. Zondlo, *Atmos. Meas. Tech*., 2014,7, 81–93.
40. H.J. Kim, J.H. Lee, *Sensor. Actuator. B Chem*., 2014,192, 607–627.
41. L. Tao, K. Sun, D.J. Miller, D. Pan, L.M. Golston, M.A. Zondlo, *Appl. Phys. B Laser Opt*., 2015,119, 153–164.
42. Atmos. C.A. Skjøth, C. Geels, *Chem. Phys*., 2013,13, 117–128.
43. M. A. Sutton, J. W. Erisman, F. Dentener, D. Moller, *Environ. Pollut*., 2008,156, 583–604.
44. R. Kincaid, K. Johnson, G.H. Mount, D. Yonge, J. Havig, H.Westberg, B. Lamb,B. Rumburg, *Atmos. Environ*., 2002, 36, 1799–1810.

45. R. Lewicki, A.A. Kosterev, D.M. Thomazy, T.H. Risby, S. Solga, T.B. Schwartz, F.K. Tittel, *Society of Photo-Optical Instrumentation Engineers (SPIE)*, 2011, 79450K1-79450K7.

46. B.H. King, A. Gramada, J.R. Link, M.J. Sailor, *Adv.Mater*., 2007,19, 4044–4048.

47. J. F. M. Oudenhoven, W. Knoben, R. Van Schaijk, *Procedia Eng*., 2015,120, 983–986.

48. P. K. Sekhar, J. S. Kysar, *J. Electrochem. Soc,* 2017,164, B113–B117.

49. K. Sawicka, P. Gouma, S. Simon, *Sensor. Actuator. B Chem*., 2005,108, 585–588.

50. A. Kassim, Z.B. Basar, H.N.M.E. Mahmud, *Proc. Indian Acad. Sci. Chem. Sci.*, 2002, 114, 155–162.

51. E. Krivan, C. Visy, R. Dobay, G. Harsanyi, O. Berkesi, *Electroanalysis*, 2000,12, 1195–1200.

52. A.G. MacDiarmid, *Angew.Chem. Int. Edit*., 2001, 40,2581-2590.

53. V.C. Nguyen, K. Potje-Kamloth, *Thin Solid Films*, 1999, 338, 142-148.

54. C.N.Van , K.Potje-Kamloth, *Thin Solid Films*, 2001,392, 113-121.

55. K.H An, S.Y.Jeong, H.R.Hwang, Y.H.Lee*, Adv. Mater*., 2004,16, 1005-1009.

56. (a) H.Yoon, M.Chang, , J.Jang, *J. Phys. Chem. B*, 2006,110, 14074-14077.

(b) N.V.Bhat, A.P.Gadre, V.A Bambole, *J. Appl. Polym. Sci*., 2003,88, 22-29.

(c) K. Kate S.R Damkale P. K. Khanna, G H Jain, Journal *of Nanoscience and Nanotechnology*, 2011, 11, 7863-9.

(d) A. Grinou, H. Bak, Y. Soo Yun, H.-J. Jin, *J of Disper. Sci. and Tech.*, 2011, 33,5.

(e) V. Osuna, A. Vega-Rios, E. A. Zaragoza-Contreras, I. A. Estrada-Moreno, R. B. Dominguez, *Biosensors,* 2022, 12(3), 137.

57. C.H.Hsieh,, L.H.Xu, J.M.Wang, T.M. Wu, *Mater. Sci. Eng. B*, 2021, 272, 115317.

58. S. Virji, J. Huang, R.B. Kaner, B.H. Weiller, *Nano Lett.*, 2004, 4, 491–496.

59. D. Xie, Y.D. Jiang, W.Pan, D.Li, Z.M.Wu, Y.R. Li, *Sens. Actuators B*, 2002, 81, 158-164.

60. L.Y. Yang, W.B. Liau, *Synth. Metals*, 2010,160, 609-614.

61. J. C. Bittencourt, B. H. D. S. Gois, V. J. R. D. Oliveira, D. L. D. S. Agostini and C. D. A. Olivati, *J Appl Polym Sci*, 2019,136, 47288.

62. G.F. Li, M. Josowicz, J. Janata, S. Semancik, *Appl. Phys. Lett*., 2004, 85, 1187-1189.

63. A. L. Kukla, Y. M. Shirshov, S. A. Piletsky, *Sensor. Actuator. B Chem.*, 1996, 37, 135–140.
64. J. Sarfraz, P. Ihalainen, A. Maattanen, J. Peltonen, M. Linden, *Thin Solid Films*, 2013, 534, 621–628.
65. J. Elizalde-Torres, H. Hu, A. Garcia-Valenzuela, *Sens. Actuators B*, 2004, 98, 218-226.
66. X. Liu, S. Cheng, H. Liu, S. Hu, D. Zhang, H. Ning, Sensors, 2012, 12, 9635–9665.
67. V.Sethumadhavan, S. Rudd, E. Switalska, K. Zuber, P. Teasdale and D. Evans, *BMC Mat*., 2019,1,1-14.
68. Y.Wang, A. Liu, Y. Han and T. Li, *Polym Int*, 2020,69, 7–17.
69. F. Faridbod, M. R. Ganjali, R. Dinarvand and P. Norouzi, *Sensors*, 2008,8, 2331-2412,
70. H. Bai and G. Shi, *Sensors*,2007, 7, 267-307,
71. M.K. Ram, O. Yavuz, M. Aldissi, *Synth. Met*. 2005,151, 77-84.
72. K. Zakrzewska, *Thin Solid Films*, 2001, 391, 229-238.
73. K. Suri, S. Annapoorni, A. K. Sarkar, R. P. Tandon, *Sens. Actuators B*, 2002,81, 277-282.
74. Z. Jin, Y. X. Su, Y. X. Duan, *Sens. Actuators B*, 2001,72, 75-79.
75. M. E. Nicho, M. Trejo, A. Garcia-Valenzuela, J.M. Saniger, J. Palacios, H. Hu, *Sens. Actuators B*, 2001,76, 18-24.
76. S. T. McGovern, G. M. Spinks, G. G. Wallace, *Sens. Actuators B*, 2005,107, 657-665.
77. J. Stejskal, I. Sapurina, M. Trchova, *Prog. Poly. Sci.*, 2010, 35, 1420-1481.
78. X. Yu, Y. Li, K. Kalantar-zaheh, *Sens. Actuators B*, 2009,136, 1-7.
79. X. Wang, M. Shao, G. Shao, Z. Wu, S. Wang, *J. Colloid Interface Sci*., 2009, 332, 74-77.
80. Y. Wang, X. Jing, *J. Phys. Chem. B*, 2008, 112, 1157-1162.
81. H. Hu, M. Trejo, M. E. Nicho, J. M. Saniger, A. Garcia-Valenzuela, *Sens. Actuators B*, 2002, 82, 14-23.
82. S. A. Rafaela, M. S. Flávio, M. M. Celina, R. Jr Antonio, M. Danilo, J.L. R. Sidney, N. O. Jr Osvaldo, H.C. M. Luiz, S. C. Daniel, *Sensors and Actuators B*, 2017,238,795–801
83. L. K. Buckley, G. E. Collins, *Synth. Met.,* 1996, 78, 93–101.
84. G. Ciric-Marjanovic, *Synthetic Metals*, 2013, 177,1-47.

85. M. Eising, C. E. Cava, R. V. Salvatierra, A. J. G. Zarbin, L. S. Roman, *Sens. Actuators B Chem*., 2017,245, 25–33.
86. L. Xue, W. Wang, Y. Guo, G. Liu, P. Wan, *Sens. Actuators B Chem*., 2017, 244, 47–53.
87. E. Bekyarova, M. Davis, T. Burch, M. E. Itkis, B. Zhao, S. Sunshine, R. C. Haddon, *J. Phys. Chem*., 2004, B108, 19717-19720.
88. Z. Pang, Z. Yang, Y. Chen, J. Zhang, Q. Wang, F. Huang, Q. Wei, *Colloids Surf. A Physicochem. Eng. Asp*., 2016,494, 248–255.
89. H. Sheng-Zhe, H. Qing-Yi and W. Tzong-Ming, *Polymers*, 13, 2021,3676-3694.
90. C. Liu, H. Tai, P. Zhang, Z. Yuan, X. Du, G. Xie, Y. Jiang, *Sens. Actuators B Chem*., 2018,261, 587–597.
91. S. Li, P. Lin, L. Zhao, C. Wang, D. Liu, F. Liu, P. Sun, X. Liang, F. Liu, X. Yan, *Sens. Actuators B Chem*., 2018, 259, 505–513.
92. P. N. Bartlett, S. K. Ling-Chung, *Sens. Actuators,* 1989,20, 3, 287-292.
93. (a) H. S. Kang, J. K. Lee, J. W. Lee, J. Joo, J. M. Ko, M. S. Kim, J. Y. Lee, *Synth. Met,*. 2005,155, 176-179.
(b) S. H. Yu, M. S. Choi, P. J. Yoo, J. H. Park, J. H. Park, J. H. Cho, G. S. Chung, J. Y. Lee, *Synthetic Metals*, 2013,185–186, 52-55.
(c) A. Pasha, S. Khasim, F. A. Khan, N. Dhananjaya, *Iranian Polymer Journal*, 2019, 28,183–192.
(d) L. Aba, Y. Yusuf, M. Mitrayana, K. Triyana, *Journal of Modern Physics*, 2012, 3, 529-533.
(e) S. Radhakrishnan, C. Sumathi, V. Dharuman and J. Wilson, *Anal. Methods*, 2013,5, 684-689.
(f) S. Rudd, M. Dalton, P. Buss, A. Treijs, M. Portmann, N. Ktoris, D. Evans, *Scientific Reports*, 2017, 7, 1-6.
(g) J. Wang, D. Wang, N. Hui, *Bioelectrochemistry*, 2020, 136,107595.
(h) R. S. Andre, J. Chen, D. Kwak, D. S. Correa, L. H. C. Mattoso, Y. Lei, *Synthetic Metals*, 2017, 233, 22-27.
(i) T. Alamro, M. Ram, *Electrochimica Acta*, 2017, 235.
(j) S. Kim, S. Y. Kim, J. Kim and J. H. Kim, *J. Mater. Chem. C*, 2014, 2, 5636–5643.
(k) X. H. Nguyen, H. N. Luong, H. A. Pham, N. M. Nguyen and V. Q. Dang, *RSC Adv*., 2021, 11, 36340–36347.

(l) N. Gao, J. Yu, Q. Tian, J. Shi, M. Zhang, S. Chen, L. Zang, *Chemosensors,* 2021, 9(4), 79.

94. (a) A. Bibi, Y. R. M. Rubio, K. S. Santiago, H. W. Jia, M. M. M. Ahmed, Y. F. Lin, J. M. Yeh, *Polymers*, 2021,13, 1457.

(b) H. Tan, S.-Y Park, *ACS Sens*., 2021, 6, 3, 1039–1048.

(c) Y. Hu, H. Yu, Z. Yan, and Q. Ke, *RSC Adv*., 2018, 8,16, 8747–8754.

95. L. H. Xu, T. M. Wu, *J. Mater. Sci. Mater*., 2020,31, 7276–7283.

96. D. K. Chaudhary, Y. S. Maharjan, S. Shrestha, S. Maharjan, S. P. Shrestha and L. P. Joshi, *Journal of Physical Science*, 2022, 33, 97–108.

97. R. S. Andre, D. Kwak, Q. Dong, W. Zhong, D. S. Correa, L. H. C. Mattoso, and Y. Lei, Sensors, 18, 2018, 1058.

98. C. Piloto, F. Mirri, E. A. Bengio, M. Notarianni, B. Gupta, M. Shafiei, M. Pasquali, N. Motta, *Sens. Actuators B Chem*., 2016, 227, 128–134.

99. P.-G. Su, L.-Y Yang, *Sens. Actuators B Chem*., 2016, 223, 202–208.

100. J. Wang, P. Yang, X. Wei, *Appl. Mater. Interfaces*, 2015, 7, 3816–3824.

101. Y. Wang & W. Feng, *Springer Nature Singapore*., 2022, 275–347.

102. Q. Feng, X. Li, J. Wang, A. M. Gaskov, *Sens. Actuators B Chem*., 2016, 222, 864–870.

103. S. Park, S. An, H. Ko, C. Jin, C. Lee, *Appl. Mater. Interfaces*, 2012, 4, 3650–3656.

104. Y. Qiu, M. Yang, H. Fan, Y. Xu, Y. Shao, X. Yang, S. Yang, *J. Mater. Sci*., 2014, 49, 347–352.

105. L. A. Mercante, V. P. Scagion, F. L. Migliorini, L. H. C. Mattoso, D.S. Correa, *TrAC Trends Anal. Chem*., 2017,91, 91–103.

106. S. Zhu, J. Zhang, C. Qiao, S. Tang, Y. Li, W. Yuan, B. Li, L. Tian, F. Liu, R. Hu, *Chem. Commun*., 2011, 47, 6858–6860.

107. J. Shen, Y. Zhu, X. Yang, C. Li, *Chem. Commun*., 2012, 48, 3686–3699.

108. J. Zhao, G. Chen, L. Zhu, G. Li, *Electrochem. Commun*., 2011,13, 31–33.

109. S. Xu, K. Kan, Y. Yang, C. Jiang, J. Gao, L. Q. Jing, P. K. Shen, L. Li, K. Y. Shi, *J. Alloys Compd*., 2015,618, 240–247.

110. A.T. Güntner, M. Righettoni, S.E. Pratsinis, *Sensors Actuators B Chem*., 2016, 223, 266– 273.

111. C. Van Tuan, M.A. Tuan, N. Van Hieu, T. Trung, *Curr. Appl. Phys.,* 2012, 12, 1011–1016.

112. T. Trung, *Int. J. Nanotechnol*., 2011, 8, 174-187.

113. L. Herous, M. Nemamcha, M. Remadnia, L. Dascalescu, *J. Electrostat*., 2009,67, 198–202.

114. Akos Markovics, & Barna Kovacs, Talanta, 2013, 109. 101-6.

115. N. Gao, J. Yu, Q. Tian, J. Shi, M. Zhang, S. Chen and L. Zang, *Chemosensors*, 2021, 9(4), 79.

116. K. E. Wyer, D. B. Kelleghan, V. Blanes-Vidal, G. Schauberger, T. P. Curran, *Journal of Environmental Management*, Volume, 2022, 323, 116285.

117. M. Chiesa, F. Rigoni, M. Paderno, P. Borghetti, G. Gagliotti, M. Bertoni, A. Ballarin Denti, L. Schiavina, A. Goldoni and Luigi Sangaletti, *J. Environ. Monit*., 2012, 14, 1565.

118. A. T. Güntner, M. Righettoni, S. E. Pratsinis, *Sensors and Actuators B: Chemical*, Volume 223, February 2016, Pages 266-273.

Chapter – 2

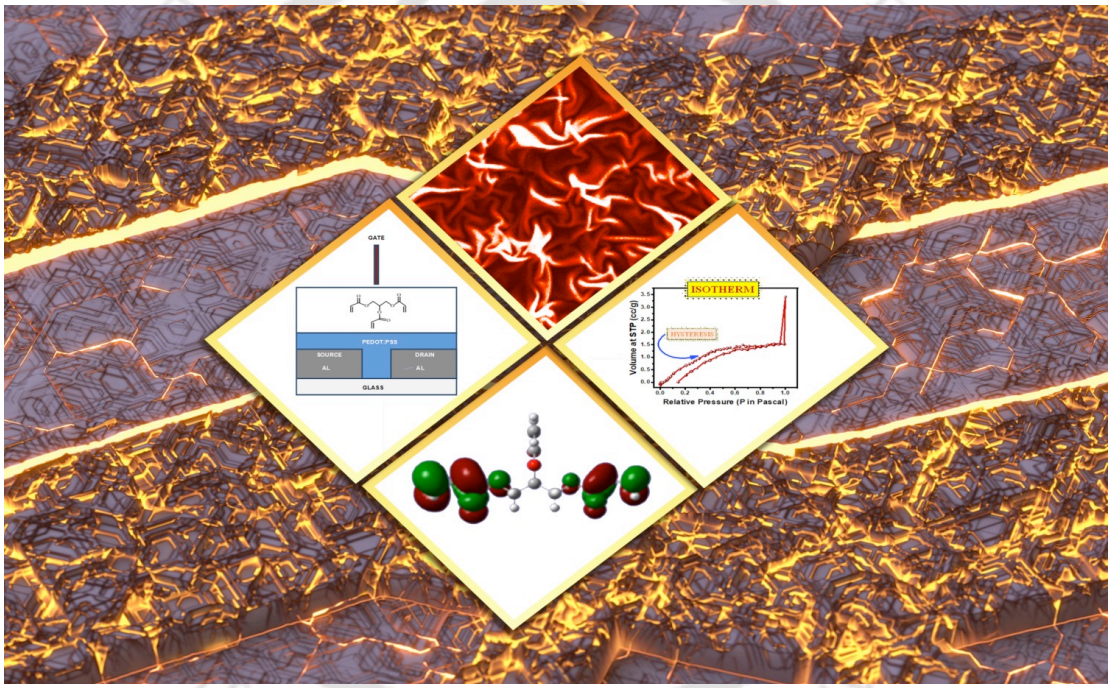

ABSTRACT

The development of an improved design methodology via an organic electrochemical transistor (OECT)-based organic transistor device is presented here. A polyhydroxyl layer is strategically added to the OECT sensor assembly, which mainly consists of poly(3,4-ethylenedioxythiophene) doped with polystyrene sulfonate (PEDOT: PSS). By introducing this layer, a higher selectivity of ammonia was observed compared to other analytes tested in the aqueous environment. A very small order of magnitude of ammonia concentration was detected with this device at very low operating voltages at room temperature. This excellent performance of the OECT device is due to the formation of an intelligent mesoporous layer with electronic properties; which helped to achieve an ammonia limit of detection (LOD) of 71.6 ppb. This approach involves an OECT device platform where the sensitivity of the sensor system is improved to achieve better device performance while maintaining cost-effectiveness.

2.1. INTRODUCTION

Although countless sensors are available for ammonia detection and are used in various industries and environmental monitoring, the sensitivity of the device is very important for medical applications. It is particularly difficult to detect ammonia produced in very low concentrations during diseases or human metabolism. Among several techniques, hybrid nanostructures formed by mixing metal/metal oxide nanoparticles with polymer or its derivatives have been used for environmental hazard assessment.[1-3] These air and environmental monitoring systems can detect analytes in the <1 ppb range. Some optical gas sensors are suitable for ammonia detection, but they are large and expensive, with reagent consumption and maintenance requirements causing additional problems, making them less affordable. [4,5] Relatedly, studies on sensitivity, selectivity, response time, and reliability must be done. considered in addition to miniaturization to reduce cost and power consumption. Nanostructured materials are widely used as gas sensors due to their high volume ratio, good morphology and excellent electrical conductivity. These sensors are either metal oxide-based or conducting polymer sensors.[6-8] Conducting polymers have proven useful due to their advantages such as easily tunable chemical structure, easy processing and morphology compared to other materials. In this context, conjugated polymers and their nanocomposites have been proposed as active sensing materials to achieve advantages in optoelectronic properties, and improved sensitivity to various acidic or basic gases for use in advanced devices and at room temperature. The high demand for analytical equipment requires the development of intelligent technologies that enable faster and more efficient detection of the desired analytes. Various combinations of device architectures and improved methods of existing technology platforms are currently being developed to improve the sensitivity and selectivity of analyte detection.[9-16]

The main goal of developing such devices is to achieve better device efficiency at an affordable and lower cost. publishing Examples of analytical devices include portable and readily available glucose sensors that are widely used in medical practice and home testing. However, the development of such analytical devices involves a trade-off between manufacturing costs and device sensitivity. Thus, hardware improvements can be further explored without compromising the sensitivity of the analytical device.

Sl No.	Reference	Active Material	Detection Method	Temperature	LOD
1.	Hussain *et al*, Anal. Chem., 2016, 88, 12453−12460	ionic liquid (RTIL) 1-ethyl-3-methylimidazolium bis(trifluoromethylsulfonyl)imide([C2mim]-[NTf2])/ microarray thin film electrode (MATFE)	Voltammetric	Room Temperature	0.1 to 2 ppm
2.	Mackin *et al*, ACS Appl. Mater. Interfaces, 2018, 10, 16169−16176	Graphene	Chemiresistive	Room Temperature	160ppm
3.	Kannan *et al*, J. Mater. Chem. A, 2014, 2,394	α-Fe_2O_3	Impedimetric	Room Temperature	100–1000 ppm
4.	Meng *et al*, J. Mater. Chem. A, 2015, 3, 1174	Cu_2O nanorods/rGO	Surface-controlled Adsorption	Room Temperature	200 ppm
5.	Ghosh *et al*, RSC Adv., 2015, 5, 50165	RGO–SnO_2 hybrid	Conducting hetero junctions	Room Temperature	25-2800 ppm
6.	Kim *et al*, J. Mater. Chem. A, 2017, 5, 19116	Chemically fluorinated graphene oxide (CFGO)	Chemoresistive	Room Temperature	100-500 ppb
7.	Wang *et al*, Sensors and Actuators: B. Chemical, 2022, 350, 130854	SnO2/bionic porous (BP) carbon composites	Microwave Transduction Technology	Room Temperature	10–200 ppm
8.	Singh *et al*,ACS Appl. Nano Mater., 2020, 3, 9375−9384	$MoSe_2$ Crystalline Nanosheets	Resistive	Room Temperature	1 ppm
9.	Kanaparthi *et al*, Organic Electronics ,2019, 68, 108–112	polyaniline (PANI)	Chemiresistive	Room Temperature	200 ppb to 3.15 ppm
10.	Seekaew *et al*, ACS Omega, 2019, 4, 16916−16924	Sn−TiO2@rGO/CNT	Resistive	Room Temperature	250 ppm
11.	Murugappan *et al*, Electrochemistry Communications, 2011, 13, 1435–1438	Room temperature ionic liquids (RTILs)	Electrochemical	Room Temperature	50 ppm and 185 ppm
12.	Liu *et al*, Sensors & Actuators: B. Chemical, 2020, 320 ,128318	biomass hydrogel poly-L-glutamic acid and L-glutamic acid (PGA/GA)	Impedance	Room Temperature	0.5 ppm
13.	Yin *et al*, Journal of Alloys and Compounds, 2019, 789, 941-947	mesoporous NiO	Resistive	Room Temperature	0.001 ppm (1 ppb)
14.	Chen *et al*, Applied Surface Science, 2022, 598,153821	Core-shell Au@SiO2 nanocrystals doped PANI	Resistive	Room Temperature	10 ppb
15.	Tang *et al*, J Mater	graphene oxide (GO)	Love mode	Room	500 ppb

	Sci, 2019, 54:11925–11935		Surface acoustic wave (SAW)	Temperature	
16.	Song *et al*, ACS Appl. Mater. Interfaces, 2021, 13, 14377−14384	ultrathin silicon nanowires (SiNWs)	Field-Effect transistor	Room Temperature	100 ppb
17.	Garg *et al*, ACS Omega, 2020, 5, 27492−27501	zeolite imidazole framework / reduced graphene oxide (ZIF-67/rGO) composite	Chemoresistive	Room Temperature	74 ppb
18.	Present Work	PEDOT:PSS/Polyhydroxyl Derivative (PHD)	Organic Electrochemical Transistor (OECT)	Room Temperature	71.6 ppb

Table 2.1. A comparative study of room temperature ammonia detection considering varied techniques.

Organic electrochemical transistors (OECTs) are promising in this regard due to their low operating voltage, ability to operate in aqueous environments, and ease of fabrication. In addition, OECTs can detect desired analytes, especially through activation of the active material or through a chemical reaction in which the analytes participate as a starting material or as a by-product. In addition, OECTs based on poly(3,4-ethylenedioxythiophene) doped with polystyrene sulfonate (PEDOT: PSS) can be integrated into microfluidic systems used in logic circuits. Such integration facilitates the detection of biomolecules such as glucose, deoxyribonucleic acid (DNA), neurotransmitters, and certain other biomarkers. These devices follow an ion-to-electron conversion mechanism that allows easy coupling of biology with electronics.[17 – 24] Thus, these devices have the advantage of detecting large changes in electron flow even with a relatively small ion drift. As such, here we introduced a polyhydroxyl layer (PHD) to design a PEDOT: PSS-based OECT to investigate its ability to improve transistor efficiency. In addition to being ammonia-selective, the PHD layer also ensures device stability, protects the transistor in aqueous environments, and ensures operation under room temperature ambient conditions. We confirmed the presence of strong hydrogen bonds, N-H stretching and cavity condensation. All these remarkable properties, together with the mesoporous nature of the PHD film, contribute to the remarkable response of the PHD-OECT-treated solution to ammonia at very low operating voltages of <1V. Table 2.1 presents a comparative study of ammonia detection at room temperature using different techniques developed by researchers.

2.2. EXPERIMENTAL SECTION

2.2.1. MATERIALS AND METHODS

PEDOT: PSS, Acrylic acid and 30% Ammonia solution were purchased from Sigma-Aldrich. Glycerol was purchased from Merck and p-toluene sulfonic acid from Loba Chemie. CV measurements were carried out using a CH instruments Model 700D series. Ag/AgCl was used as the reference electrode and 0.1M NaCl as an aqueous electrolytic solution. The thickness of the deposited films was optimized using a Profilometer (Dektat-150). Field emission scanning electron microscope (FESEM) images were recorded on a Sigma Carl ZEISS SEM instrument. FT-IR was recorded on a Perkin Elmer spectrometer with samples prepared using KBr into pellets.

2.2.2. SYNTHESIS

A polyhydroxyl derivative was synthesized by mixing 0.03 mol of Glycerol, 0.09 mol of acrylic acid and 0.05 g of p-toluene sulfonic acid together for 30 min. A viscous solution was formed after mixing which was used for coating the device. The material has been found to be chemically, thermally, and mechanically rather stable for room temperature experiments that can be attributed to the cross-linked homogenous texture.[25]

2.2.3. SENSOR FABRICATION

Microscopic Glass slides of dimensions 1cm X 2 cm were utilized as substrates which were cleaned in Piranha solution for 1 hour and washed several times with deionised water followed by sanitation prior to use. The cleaned substrates were then dried; ionized and subsequently 100 nm thickness aluminium contacts were thermally deposited on them inside the Glove Box. A channel of dimensions 30 mm length (L) and 2 mm width (W) was obtained which was used as the Source (S) and Drain (D). 30 nm thick PEDOT: PSS films were coated on these aluminium deposited substrates. The coated substrates were again heated at 130 °C for 1 hour. The synthesized poly-hydroxyl layer was coated over the PEDOT: PSS region and heated at 50 °C for 30 minutes. An ammonia concentration of 1μM was used for all the experiments.

2.3. CHARACTERIZATION

2.3.1. ELECTRICAL MEASUREMENTS

All the electrical characterizations of the devices were carried out under ambient conditions at room temperature using a Keithley2614B. A positive Gate bias (V_g) was applied with Ag/AgCl electrode and the two aluminium electrodes served as a source (S) and drain (D). The ammonia sensing experiments were performed at Drain voltage V_d= -0.2 V with a Gate voltage V_g sweep ranging from 0 to 1V in 5ml electrolyte solution at pH = 7. The analyte and ammonia solutions were confined in 10 mL beaker and mixed with electrolyte prior to testing.

2.3.2. FIELD EMISSION SCANNING ELECTRON MICROSCOPE (FESEM) AND X-RAY DIFFRACTION (XRD)

FESEM images of PHD film on glass slides were recorded on a Sigma Carl ZEISS scanning electron microscope at an accelerating voltage of 15kV at different magnifications. XRD was recorded on a Bruker D8 Advance model.

2.3.3. BRUNAUER-EMMETT-TELLER (BET) AND BARRETT-JOYNER-HALENDA (BJH)

BET/BJH experiments of PHD were performed on Autosorb-IQ MP instrument to understand the porosity of the selective Layer.

2.3.4. FOURIER TRANSFORM INFRARED ANALYSIS (FT-IR)

FT-IR was recorded on a Perkin Elmer spectrometer with solid samples prepared using KBr into pellets. Selected IR peaks with tentative assignments (nmax/cm^{-1}) were recorded.

2.4. RESULTS AND DISCUSSION

2.4.1. ELECTRICAL MEASUREMENTS

The OECT and poly-hydroxyl derivative used for coating are shown in Fig. 2.1(a). The electronic transfer characteristic is indicated at V_d = -0.2V and drain characteristics at different gate voltages are shown in Fig. 2.1(b).

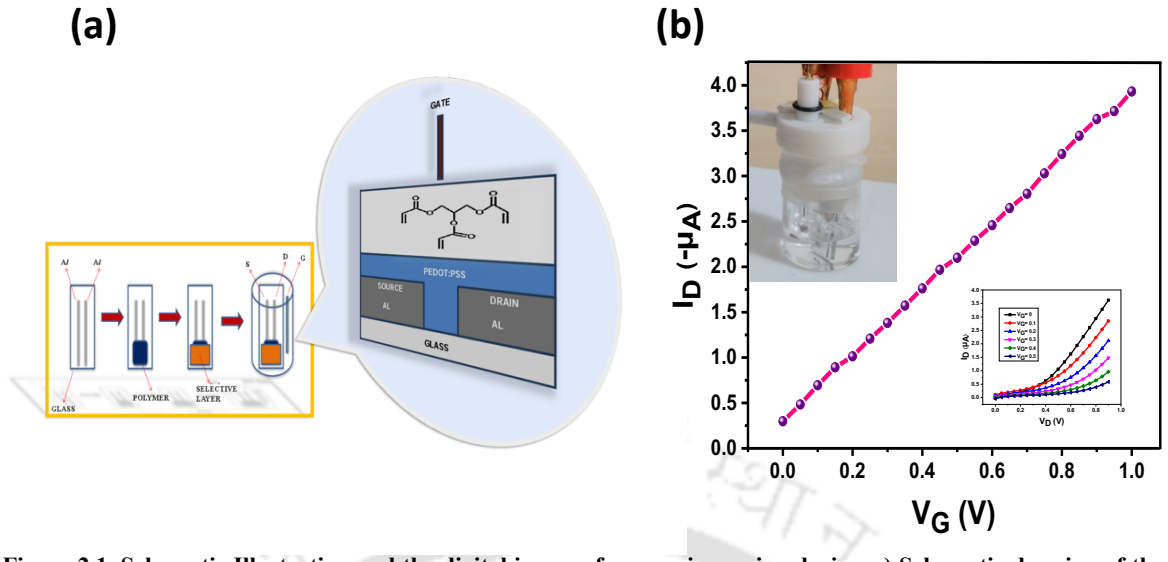

Figure 2.1. Schematic Illustration and the digital image of ammonia sensing device. a) Schematic drawing of the device showing various layers and Incorporation of a Mesoporous Layer immersed in an electrolyte solution. b) Transfer Characteristics (I_D-V_G). (Inset top left device setup; inset down right output curves).

The measurements were done under positive gate bias which subsequently changes the channel conductance through the injection of ions from the aqueous medium. This process, in turn, affects the conductivity of the PEDOT: PSS layer which is referred to as doping/de-doping of PEDOT: PSS as depicted in equation 1.

$$PEDOT^+: PSS^- + M^+ + e^- \rightleftharpoons PEDOT^0 + M^+: PSS^- \ldots\ldots\ldots (1)$$

where, M^+ represents a cation and e^- an electron.

The transistor characteristics of the PHD-OECT are due to ions acting as charged carriers contributing to its high sensitivity. Therefore, these characteristics result in a built-in amplification entity (Fig. 2.1b). This system is found to be highly sensitive towards ammonia, i.e., it forms an ammonia-sensitive layer. Hence, the presence of a small concentration of ammonia is selectively detected. It is found that the electron transfer curve shifts significantly upon exposure to different concentrations of ammonia. Various analytes, such as urea, thiourea, ethanolamine, diethylamine, $FeCl_3$, hydrazine, NaCl and KCl have been tested with this sensor assembly.

2.4.2. FESEM and XRD

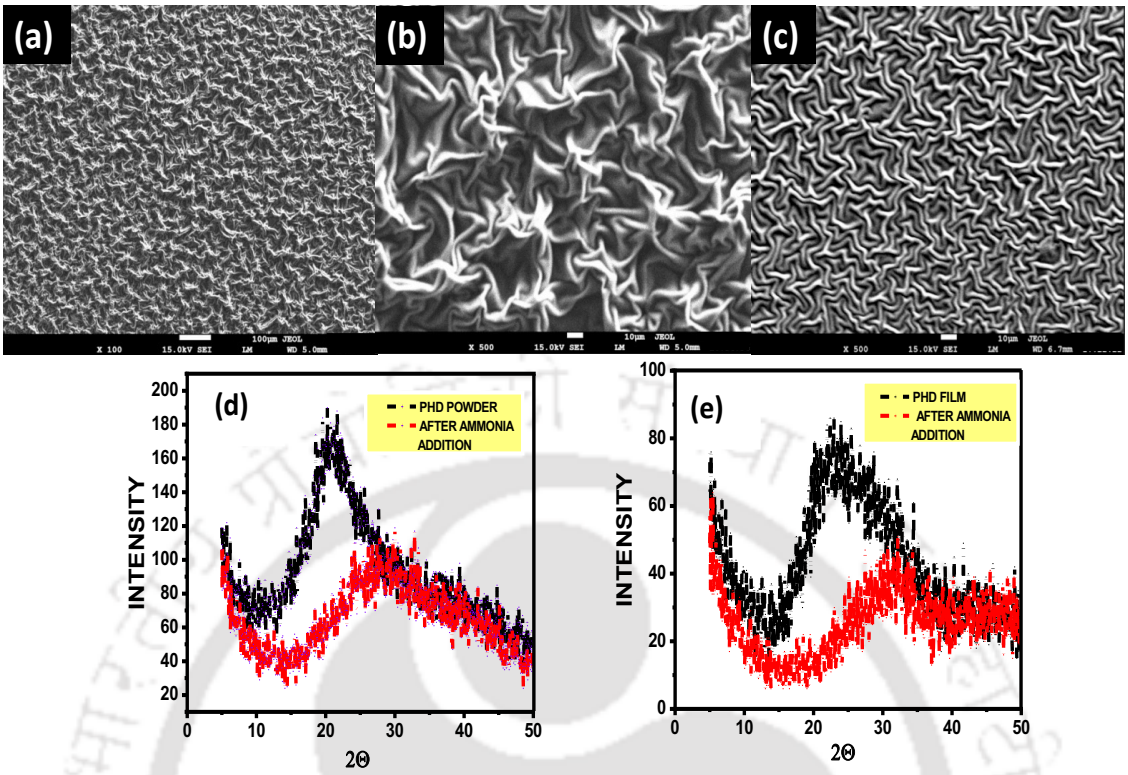

Figure 2.2 Analytical Imaging and Qualitative Evaluation of Polyhydroxyl Derivative. a) FESEM image of PHD at 100X. b) FESEM image of PHD at 500X before exposure to ammonia. c) FESEM image of PHD at 500X after exposure to ammonia. d) XRD images of PHD in powder form before and after exposure to ammonia. e) XRD images of PHD in film form before and after exposure to ammonia.

The surface morphology of the PHD film layer before and after exposure to ammonia can be seen in Fig. 2.2 b & c. In Fig. 2.2 a & b, the PHD layer before exposure to ammonia at 100X and 500X magnification respectively shows well-defined grooves. Exposing it to ammonia changes the structural pattern. The XRD data show a shift of peaks after exposure to ammonia. Both in powder and film form, PHD is mostly amorphous in nature (Fig. 2.2 d & e). This could be one of the factors contributing to the PHD-OECT device's high performance at low operating voltages. However, the peak at 20.8° for PHD powder (Fig. 2.2 d) shows a shift to 28.48° after exposure to ammonia. Similarly, the peak at 23.04° for PHD film (Fig. 2.2 e) shows a shift to 32.08° after exposure to ammonia.

2.4.3. BRUNAUER-EMMETT-TELLER (BET) AND BARRETT-JOYNER-HALENDA (BJH)

The adsorption and desorption of N_2 in an isotherm determine the presence of pores in the material and the likeable cavity condensation. The appearance of hysteresis highlights the presence of mesoporous pores in the material (Fig. 2.3a). Since pores of a specific size are

filled at higher pressures and expelled at lower pressures, cavity condensation takes place during adsorption; and cavity evaporation takes place during desorption. BET experiment performed on the samples revealed the porosity of the selective layer. In Figs. 2.3b & 2.3c, the pore distributions of the selective layer are observed which is in direct contact with the electrolyte. Fig. 2.3b shows the pore size distribution calculated through the DFT method while Fig. 2.3c is averaged data. In both the figures 2.3 b&c, the presence of different pore sizes is observed; however, a maximum of 3 nm pore sizes was noticed. Thus, the ions in the electrolyte could easily pass through the porous selective layer to dope or de-dope the PEDOT: PSS layer. Although it is possible for the ions of the analyte to infiltrate, the selectivity factor, along with attraction and repulsion forces comes into play and allows more ammonium ions to be detected. [26-29]

2.4.4. FOURIER TRANSFORM INFRARED (FT-IR) ANALYSIS

FT-IR performed at room temperature on the selective layer, (Figs. 2.3d & 2.3e) on pristine and after ammonia exposure confirm the changes occurring after the addition of ammonia and resulted in broad peaks at ~3406 cm^{-1} for PHD w.r.t. 3138 cm^{-1} for PHD without ammonia corresponding to the -OH groups. The peak at 3172 cm^{-1} and 2947 cm^{-1} present in PHD with ammonia is not seen in PHD without ammonia and the peaks at 1732 cm^{-1} for PHD without ammonia and 1724 cm^{-1} for PHD with ammonia confirms the formation of ester. The idea of detecting a hydrogen bond (HB) solely on one single site can be done by quantum chemical calculation. However, the prediction of H-bonding can be made by observing the easily accessible basic sites of PHD for interacting with NH_3. First, we assume that the interaction with these sites results in H-bonded complexes. It could also be demonstrated from the classification of acceptor atoms types in order to form hydrogen-bonded complexes and also for forming more effective sites. In this context three regions may be recommended to associate with NH_3 through hydrogen bonds with specific acceptor atoms, say –C-O-C- and –C=O. Accordingly, the utility of these sites as criterion sensing of NH_3 through H-bond can be understood. These groups can be connected to the H-atom of NH_3 by a HB and the strength of the bond as well as the sensitivity depends on the electron density of these groups to attract hydrogen. HBs are ubiquitous in this structure and have been the important focus in sensing processes. Many studies have shown that sensing mechanisms can be well-explained by HB interactions.[30-34] The probe PHD shown in Fig.2.3 d & 2.3 e taken by the IR vibration

analysis before and after interaction with NH_3 shows that relevant vibrational peaks are distinctly shifted.

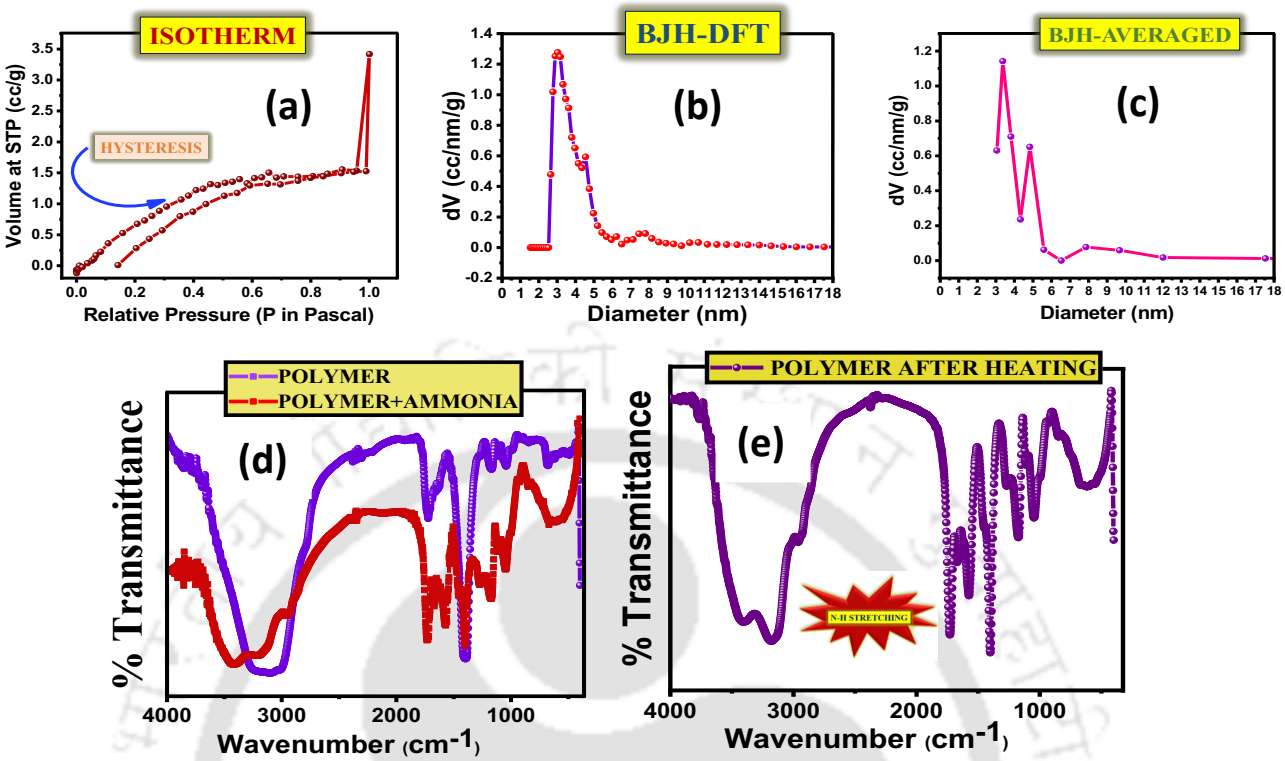

Figure 2.3. Surface Area Evaluation for determination of pores, functional groups and characterizing chemical bonds formation. a) Isotherm of a Mesoporous PHD Layer when exposed to nitrogen. b) Pore size distribution of PHD calculated using BJH-DFT method. c) Pore size distribution of PHD calculated using BJH-Averaged method. d) FTIR analysis of PHD before and after exposure to ammonia. e) FTIR analysis of PHD after heating and exposure to ammonia resulting in N-H stretching.

The FTIR spectra of functional groups, -C=O, -C-O-C- and H-N related to HBs show the red-shift in vibration frequencies of up to 268 cm^{-1} (3406→3138 cm^{-1}) (Figs.2.3d & 2.3e). This red shift indicates the existence of a Hydrogen bond (HB), whereas the blue shift indicates its weakening. Analysis of sensing mechanisms can be demonstrated from the six nucleophilic sites of PHD. Out of these sites, the most electronegative sites attract the H of NH_3 although these sites cannot be distinguishable from experimental results. Thus, the vibrational spectra confirm the mechanism of HB in the ground state. Presence of hydrogen bonding between -C=O group of PHD and ammonia results in the increase of -C=O as well as H-N bond length. Fundamentally, the vibrational frequency for these bonds will decrease leading to a change in IR stretching frequencies of -C=O (PHD) and H-N (ammonia). The IR spectra of PHD after the addition of ammonia have also been examined. On heating for 20 minutes, the IR spectra were again taken, showing a slight impression of ammonia in the spectra. In Fig. 2.3e, the difference after the application of heat could be ascertained. The original IR of PHD could be observed with N-H stretching

at 3175 cm^{-1} which was not found before exposure to ammonia. This can be attributed to the formation of strong hydrogen bonds between PHD and ammonia. It proves stable hydrogen bond formation between -C=O (PHD) and ammonia at the exposed -C=O groups of the material. Moreover, the formation of hydrogen bonds may weakly polarize the ammonia molecule which can facilitate the accumulation of more NH_3 molecules inside the pores of the material and thereby undergo cavity condensation. Thus, both hydrogen bonding and cavity condensation operate in this system. The possibility of reversibility in this configuration indicates that the device can be reusable with a baseline correction. Aggregation of NH_3 at the nucleophilic sites i.e. –C=O and –C-O-C- can significantly affect the extent of reactivity or selectivity at these regions. Here, the presence of NH_3 in IR spectra on heating reveals the importance of H-bond networks where it forms strong HB with the analyte.

2.4.5. GAUSSIAN STUDIES

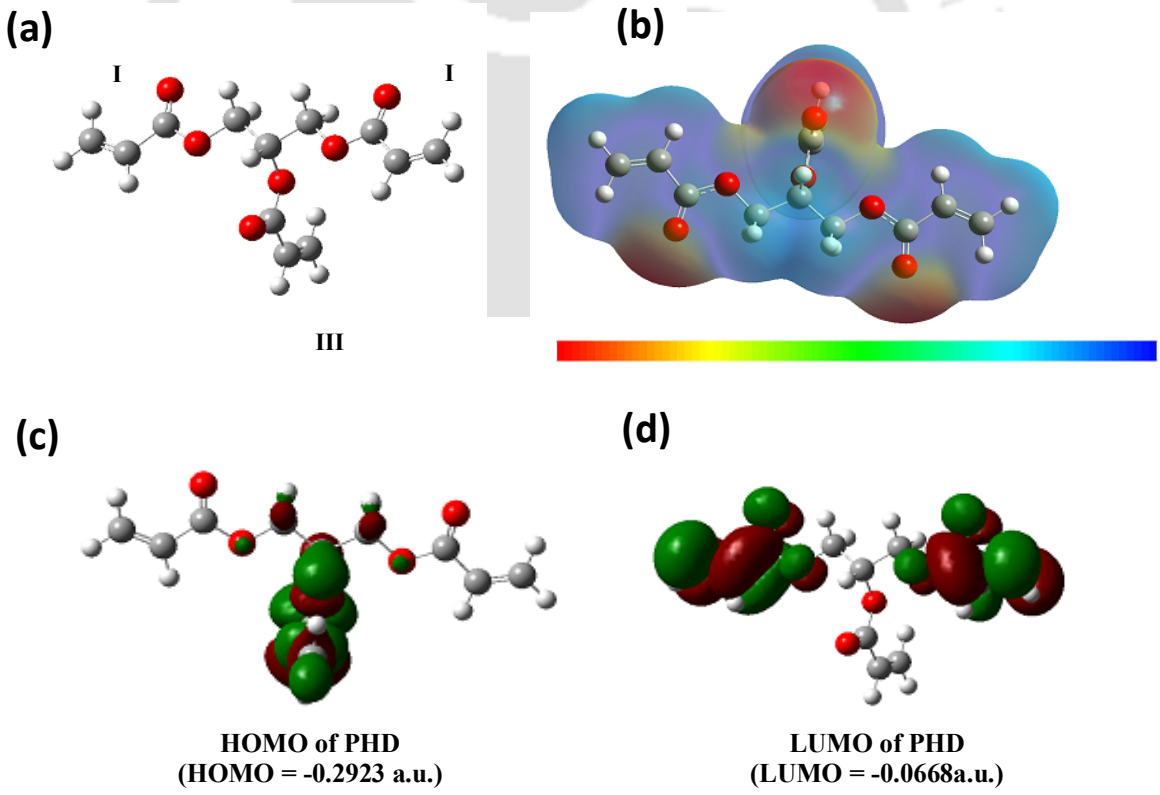

Figure 2.4. Computational Study and molecular electronic structure calculations of PHD. a) Gaussian model of the 3D structure of PHD with three acrylate subunits. b) Electronic Cloud Density distribution of PHD. c) HOMO of PHD. d) LUMO of PHD.

The Structure of the PHD derivative may be analysed in the three subunits I, II and III (Fig. 2.4a). The configuration of subunit I and II maintain along the same axial plane,

whereas unit III lie along the perpendicular of this plane. The acrylate groups are bonded to primary carbon centres in subunit I and II, whereas in subunit III the acrylate group is attached to the tertiary carbon centre through a carboxylate bond. Hence, the nature of electrostatic potential around this monomer PHD may indicate a distinguishable variation in electron density. The completely optimized poly-hydroxyl derivative with B3LYP/6-31G (d,p) method was used for calculating electrostatic potential (Fig. 2.4b). Thus, we have computed the EPS profile in the 3D structure of monomer PHD.

More negative values are found around –C=O of these three regions and less negative or positive are found around the rest of the regions. The maximum negative value in regions I and II is approximately -4.31 X 10^{-2} a.u. whereas the value for region III is -4.58 X 10^{-2} a.u. Hence, region III may be more perceptive for NH_3 or NH_4OH (in an aqueous solution) than regions I and II. This may be the reason why the PHD material is very sensitive towards NH_3 or NH_4OH (in an aqueous solution). The electron labile property of poly-hydroxyl derivative can be related to the energy gap of Frontier orbitals, i.e., HOMO-LUMO (Fig. 2.4c). The optimized structure of the PHD derivative using B3LYP/6-31G (d,p) was used for calculating HOMO and LUMO energies and Fig. 2.4c & 2.4d show the electron density distribution. The HOMO-LUMO gap is found to be -6.1 eV, but the value is much large for electronic conductive material. According to the electronic property of the PHD derivative, -C=C- and –C=O groups generally undergo n-π^* and π-π^* transitions, but such transition occurs only in the excited states. Hence, electronic conduction may not occur in the process of NH_3 or NH_4OH (in aqueous solution) sensing. It is essential to analyze electrostatic potential in the 3D structure of poly-hydroxyl derivative.

2.4.6. SENSING MECHANISM

The sensing of the transistor is based on the integration of ions in an aqueous solution repelled by the positively charged gate and attracted by a negative channel. The species sensed acquires a positive charge in an aqueous medium which then associates with the poly-hydroxyl layer and gets absorbed by it to further de-dope the PEDOT: PSS polymer film to create changes in the I-V characteristics of the device. The absorption /association with acrylate polymer film involves different intermolecular interactions like H-bonding, Dipolar interaction, London forces, dispersion forces and individual ionic conductivities of ions furnished by various species taken into consideration. In this study, we have analyzed a large set of species commonly found in Industrial Wastes and Biological

Processes, such as Ammonia, Urea, thiourea, diethylamine (DA), ethanolamine (EA), Hydrazine, and ionic salts like NaCl, KCl, $FeCl_3$ in order to extract the highest sensitivity. The sensitivity profiles of these species depend on attraction forces, repulsion forces, and different intermolecular interactions between acrylate polymer and ions furnished by the species taken into consideration. As per the results obtained in the process, ammonia shows the maximum sensitivity due to H-bonding between the acrylate and NH_3 which after absorption through the polymer film de-dope the PEDOT: PSS polymer up to the maximum extent (Fig. 2.5a).

In ionic cases like NaCl and KCl, the sensitivity is less due to poor interaction between the polymer and Na^+/K^+ ions. The sensitivity profile clearly shows approximately similar values for NaCl and KCl which can be explained on the basis of almost similar ionic properties and dissociation of both the salts in water. As NaCl is slightly more soluble in water hence it shows a bit more value than KCl. In the case of ionic salts like $FeCl_3$, due to more solubility than NaCl and KCl, $FeCl_3$ is showing slightly higher sensitivity but the overall sensitivity when compared to NH_3 is fairly low due to rapid complexation of Fe^{3+} ions with water molecules to form $[Fe(H_2O)_6]^{3+}$ hexaaquairon(III) complex ion. Hence, the interaction of Fe^{3+} has been reduced with the sensing polymer layer which led to a sensitivity profile as seen in Fig 2.5a.

In the case of other organic samples taken into consideration for this study, Urea and Thiourea molecules due to high electronegativity of oxygen (O) in urea molecule polarization take place leading to less electron density on both the $-NH_2$ groups. This results in less association of urea molecule with the acrylate group and is indicated by reduced sensitivity of Urea as compared to thiourea. However, overall, they have a very high tendency to form Hydrogen bonding with the polymer hence their sensing profile is high as compared to other organic samples. In the case of Hydrazine, the molecule exists as NH_2-NH_3^+ in water which will associate with polymer but repulsions due to nearby second $-NH_2$ group led to less sensitivity than ammonia, urea and thiourea but can be comparable to that of ionic salts like KCl and NaCl. The sensitivity of ethanolamine is least as compared to rest due to the presence of intra-molecular Hydrogen bonding between the -OH group and $-NH_2$ group which will result in less association of ethanolamine with the acrylate group of the PHD layer.

In the case of Diethylamine, the association is somewhat more due to the absence of such an electron-rich group. It is less repelled and more associated with the polymer as compared to Ethanolamine as seen in the sensitivity profile. Repeatability and

reproducibility are two distinguished features of a sensor. The device characteristics were measured for the same device multiple times in the same electrolyte solution (Fig. 2.5b). The device does not deter away from its original value and is repeatable even after successive 10 scans. Four different devices fabricated under the same conditions scanned in the same electrolyte solution indicate that our device is reproducible (Fig. 2.5c). The values for different concentrations of ammonia were plotted to get the calibration curve for the calculation of the limit of detection (LOD) (Fig. 2.5d). Increasing concentrations of 1µM ammonia are injected in the electrolyte solution where the device is immersed as seen in Fig. 2.1a and the LOD was calculated to be 71.6 ppb. Ammonia exposure of about 25 ppm for 8 hours is hazardous to health.[35] As such; this approach to fabricating OECTs could be further explored for improved detection of various analytes in a cost-effective manner.

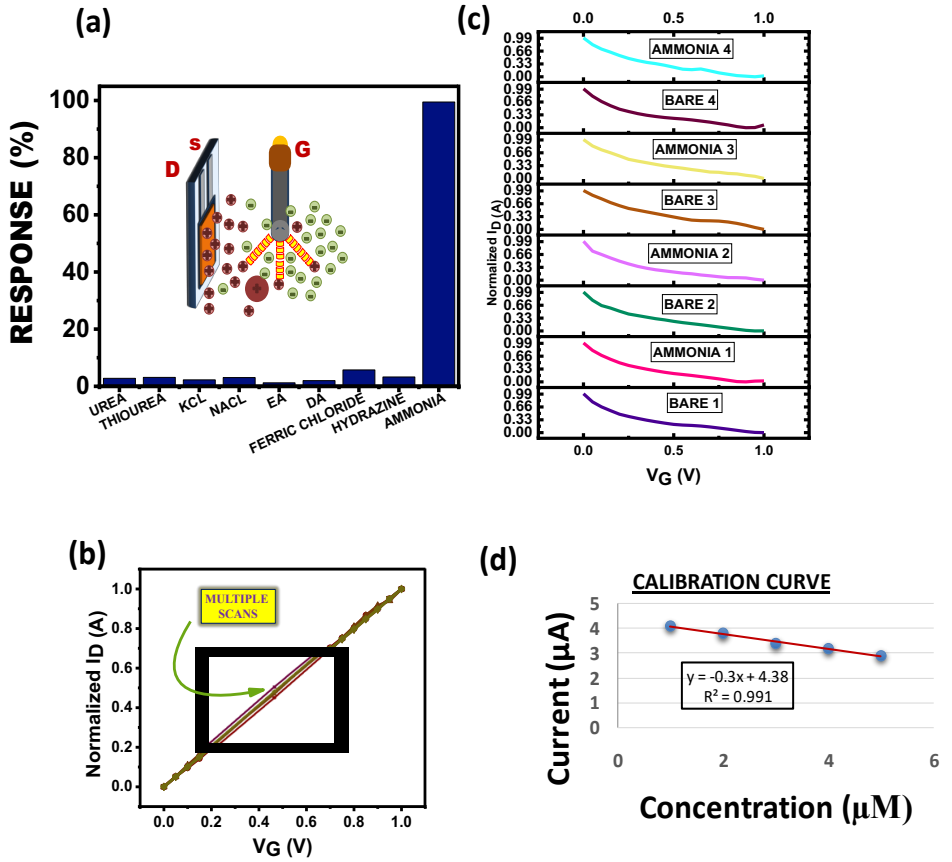

Figure 2.5. Response of PHD-OECT to common Industrial and Biological Waste Products. a) Sensitivity of PHD compared to other analytes. b) Repeatability of the device kept in electrolytic solution. c) Analyzing different devices in the same electrolytic solution. d) Calibration Curve of PHD incorporated device after exposure to ammonia.

2.5. CONCLUSION

In conclusion, a mesoporous film platform using a vertical OECT has been developed utilizing poly(3,4-ethylenedioxythiophene) doped with polystyrene-sulfonate (PEDOT: PSS), and ammonia sensing at 71.6 ppb has been achieved. We have demonstrated that the sensor assembly has excellent transistor characteristics and can be operated with voltages <1V. The poly-hydroxyl film is optimal in an aqueous environment at room temperature due to its cross-linked homogenous texture. The developed PHD-OECT is highly sensitive and selective for ammonia with the presence of strong hydrogen bond formation and N-H stretching. It has been observed that mesoporous pores on the PHD film enhance the sensing attributes of PHD-OECT towards ammonia with an excellent electrical response. Due to the economic viability of our developed PHD-OECT sensor, this approach can be further explored to detect other biological and chemical analytes efficiently.

2.6. REFERENCES

1. (a) B. Timmer, W. Olthuis, A. van den Berg, *Sens. Act. B*, 2005, 107, 666–677. (b) J.F.M. Oudenhovena, W. Knobena, R. van Schaijka, *Procedia Eng*., 2015,120, 983–986. (c) R.A. Michaels, *Environ. Health Perspect*., 1999, 107 (8), 617–627. (d) D. Leduc, P. Gris, P. Lheureux, P. A. Gevenois, P. De Vuyst, J. C. Yernault, *Thorax*, 1992, 47, 755–757.

2. (a) Jun-Ch. Jin, J. Wu, Guo-P. Yang, Yun-L.Wua and Yao-Y. Wang, *Chem. Commun*., 2016, 52, 8475—8478.(b) R. Ghosh, A. K. Nayak, S. Santra, D. Pradhan and P. Kumar Guha, *RSC Adv*., 2015, 5, 50165. (c) N. Sharma, N. Sharma, P. Srinivasan, S. Kumar, J. B. B. Rayappan and K. Kailasam, *J. Mater. Chem. A*, 2018, 6, 18389.

3. (a) T. Someya, Z. Bao, G. G. Malliaras, *Nature*, 2016, 540, 379-385. (b) M. Berggren, A. Richter-Dahlfors, Adv. Mater., 2007, 19, 3201-3213.

4. (a) T. Grady, T. Butler, B. D. MacCraith, D. Diamond and M. A. McKervey, *Analyst*, 1997, 122, 803–806. (b) W. Cao, Y. Duan, *Sensors and Actuators B*, 2005, 110, 252–259.

5. Z. Jin, Y. Su, Y. Duan, *Sensors and Actuators B*, 2001, 72, 75-79.

6. (a) N. R. Stradiotto, H. Yamanaka and M. V. B. Zanoni, *J. Braz. Chem. Soc.*, 2003, 14, 2, 159-173. (b) U. Yogeswaran and Shen-M. Chen, Sensors, 2008, 8, 290-313.

7. (a) F. Rigoni, S. Tognolini, P. Borghetti, G. Drera, S. Pagliara, A. and L. Sangaletti, *Analyst*, 2013, 138, 7392–7399. (b) A. Kalita, S. Hussain, A. H. Malik, N. V. V. Subbarao and P. K. Iyer, *J. Mater. Chem. C*, 2015, 3, 10767—10774.

8. P. K. Sekhar, and J. S. Kysar, *J. Electrochem. Soc*., 2017, 164 (4), 113-117.

9. (a) S. Stříteský, A. Marková, J. Víteček, E. Šafaříková, M. Hrabal, L. Kubáč, L. Kubala, M. Weiter, M. Vala, *J. Biomed. Mater. Res. A*, 2018,106A, 4,1121-1128. (b) V. Rani, K.S.V. Santhanam, *J. Solid State Electrochem*, 1998, 2, 99-101. (c) S. Singh, J. Deb, U. Sarkar, and S. Sharma, *ACS Appl. Nano Mater*., 2020, 3, 9375−9384.

10. (a) M. Chen, D. Nilsson, Th. Kugler, and M. B.T. Remonen, *Appl. Phys. Lett*., 2002, 81, 11, 2107355-210365. (b) Chang-S. Lee, S. K. Kim and M. Kim, *Sensors*, 2009, 9, 7111-7131. (c) S. Kanaparthi, S. G. Singh, *Organic Electronics*, 2019, 68, 108–112.

11. (a) Y. H. Kim, J. S. Park, Y.-R. Choi, S. Y. Park, S. Y. Lee, W. Sohn, Y.-S. Shim, J.-H. Lee, C. R. Park, Y. S. Choi, B. H. Hong, J. H. Lee, W. H. Lee, D. Lee and H. W. Jang, *J. Mater. Chem. A*, 2017, 5, 19116. (b) H. Meng, W. Yang, K. Ding, L. Feng and Y. Guan, *J. Mater. Chem. A*, 2015, 3, 1174. (c) Y. Seekaew, W. Pon-On, and C. Wongchoosuk, *ACS Omega*, 2019, 4, 16916−16924.

12. (a) S. Pandey, G. K. Goswami and K. K. Nanda, *Sci. Rep*., 2013,3, 2082. (b) S. Arya, M. Riyas, A. Sharma, B. Singh, Prerna, P.Bandhoria, S. Khan, V. Bharti, *Appl. Phys. A*, 2018, 124,538. (c) L. Liu, T. Fei, X. Guan, X. Lin, H. Zhao, T. Zhang, *Sensors & Actuators: B. Chemical*, 2020, 320 ,128318.

13. (a) S. C. Hernandez, D. Chaudhuri, W. Chen, N. V. Myung, A. Mulchandani, *Electroanalysis*, 2007, 19, 2125−2130. (b) K. Murugappan, J. Lee, D. S. Silvester, *Electrochemistry Communications*, 2011, 13, 1435–1438. (c) M. Yin, Z. Zhu, *Journal of Alloys and Compounds*, 2019, 789, 941-947.

14. (a) C. Mackin, V. Schroeder, A. Zurutuza, C. Su, J. Kong, T. M. Swager, and T. Palacios, *ACS Appl. Mater. Interfaces*, 2018, 10, 16169−16176. (b) N. Wang, N. Zhang, T. Wang, F. Liu, X. Wang, X. Yan, C. Wang, X. Liu, P. Sun, G. Lu, *Sensors and Actuators: B. Chemical*, 2022, 350, 130854. (c) G. Chen, Y. Yuan, M. Lang, Z. Lv, W. Ma, N. Gu, H. Liu, J. Fang, H. Zhang, Y. Cheng, *Applied Surface Science*, 2022, 598,153821.

15. (a) G. Hussain and D. S. Silvester, *Anal. Chem*., 2016, 88, 12453−12460. (b) Q. B. Tang, Y. J. Guo, Y. L. Tang, G. D. Long, J. L. Wang, D. J. Li, X. T. Zu, J. Y. Ma, L. Wang, H. Torun, and Y. Q. Fu, *J Mater Sci*, 2019, 54:11925–11935. (c) X. Song, R. Hu, S. Xu, Z. Liu, J. Wang, Y. Shi, J. Xu, K. Chen, and L. Yu, *ACS Appl. Mater. Interfaces*, 2021, 13, 14377−14384.

16. (a) P. K. Kannan and R. Saraswathi, *J. Mater. Chem. A*, 2014, 2,394. (b) N. Garg, M. Kumar, N. Kumari, A. Deep, and A. L. Sharma, *ACS Omega*, 2020, 5, 27492−27501.

17. H. S. White, G. P. Kittlesen, and M.S. Wrighton, *J. Am. Chem. Soc*., 1984, 106, 5375-5377.

18. D. A. Bernards, G. G. Malliaras, G. E. S. Toombes and Sol M. Gruner, *Appl. Phys. Lett.*, 2006, 89, 053505-053508.

19. S. Pecqueur, S. Lenfant, D. Guérin, F. Alibart and D.Vuillaume, *Sensors*, 2017, 17, 570. (Book)

20. (a) M. Ghittorelli, L. Lingstedt, P. Romele, N. I. Crăciun, Z. M. Kovács-Vajna, P. W.M. Blom and F. Torricelli, *Nature Commun*., 2018, 9, 1441-1451. (b) M. J. Donahue, A. Williamson, X. Strakosas, J. T. Friedlein, R. R. McLeod, H. Gleskova, and G. G. Malliaras, *Adv. Mater*., 2018, 30, 1705031-5.

21. N. Stutzmann, R. H. Friend and H. Sirringhaus, *Science*, 2003, 299, 1881-1884.

22. M. Uno, Y. Tominari, J. Takeya, *Appl. Phys. Lett*., 2008, 93, 173301-173303.

23. J. Rivnay, P. Leleux, M. Ferro, M. Sessolo, A. Williamson, D. A. Koutsouras, D. Khodagholy, M. Ramuz, X. Strakosas, R. M. Owens, C. Benar, Jean-M. Badier, C. Bernard, G. G. Malliaras, *Sci. Adv*., 2015, 1, 1400251-1400255.

24. M. Demelas, E. Scavetta, L. Basiricò, R. Rogani, and A. Bonfiglio, *Appl. Phys. Lett*., 2013, 102, 193301-193304.

25. P. Dutta, B. Kalita, B. Gogoi, and N. Sen Sarma, *J. Phys. Chem. C*, 2015, 119, 17260−17270.

26. R. Bardestani, G. S. Patience, S. Kaliaguine, *J. Chem. Eng*., 2019, 97, 2781–2791.

27. P. Kuhn, A. Forget, D. Su, A. Thomas, and M. Antonietti, *J. Am. Chem. Soc*., 2008, 130, 13333–13337.

28. J. C. Groen, L. A.A. Peffer, J. Pérez-Ramírez, *Micro. Mes. Mater*., 2003, 60, 1–17.

29. R.J.C. Brown, *J. Mol. Str*., 1995, 345, 77-81.

30. B. Kojić-Prodić and K. Molčanov, *Acta Chim. Slov*., 2008, 55, 692–708.

31. A.D. Buckingham, J.E. Del Bene, S.A.C. McDowell, *Chemical Physics Letters*, 2008, 463, 1–10.

32. P. A. Colman and L. C. Allen, *Chem. Rev.*, 1972, 72, 283-303.

33. M. C. Etters, *Acc. Chem. Res*., 1990, 23, 120-126.

34. I. V. Alabugin, M. Manoharan, S. Peabody and F. Weinhold, *J. Am. Chem. Soc*., 2003, 125, 5973-5987.

35. T. N. I. f. O. S. a. H. (NIOSH), Ammonia, https://www.cdc.gov/niosh/pel88/7664-41.html.

Chapter – 3

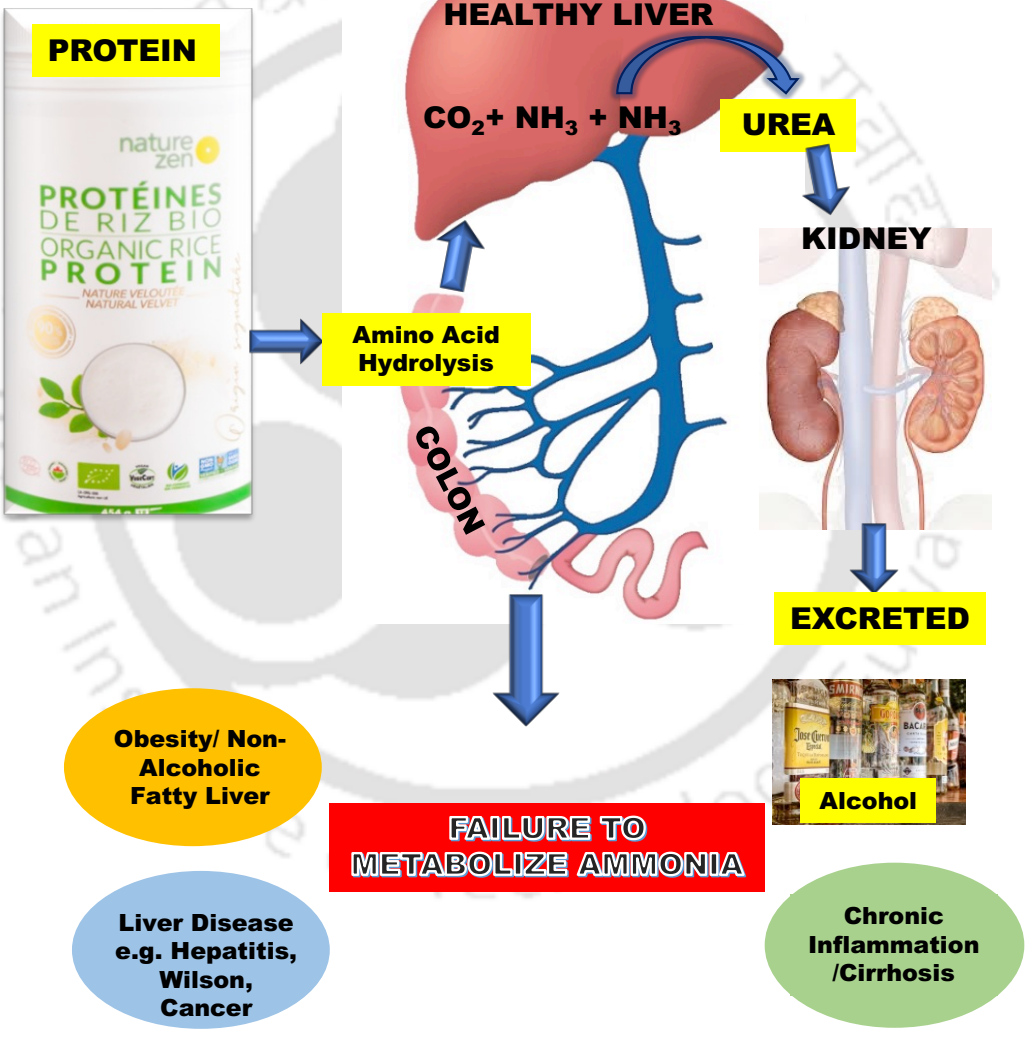
PROTEIN
nature zen
PROTÉINES DE RIZ BIO
ORGANIC RICE PROTEIN
HEALTHY LIVER
CO_2+ NH_3 + NH_3
UREA
KIDNEY
Amino Acid Hydrolysis
COLON
EXCRETED
Alcohol
Obesity/ Non-Alcoholic Fatty Liver
FAILURE TO METABOLIZE AMMONIA
Liver Disease e.g. Hepatitis, Wilson, Cancer
Chronic Inflammation /Cirrhosis

ABSTRACT

The disadvantages of ammonia may be illustrated in two ways i.e., exposure to an environment of high ammonia concentration and other is the presence of ammonia inside the body. In one direction exposure to ammonia indeed affects the biochemistry of many vital organs like kidneys, liver, and stomach in Humans by incorporating it into metabolism processes. On the other way, clinically the outcome of the reduced Liver and Kidney functions is due to the increase of Blood Urea Nitrogen (BUN) in humans which led to higher levels of ammonia concentration in the Skin, nose and Mouth. For both these strategies one needs to monitor the ammonia concentration accurately. The techniques of detecting precise ammonia concentration are promising for application as a biomarker which indeed is essential for the potential identification of these severe diseases in Humans. There is a constant need to develop a non-invasive, real-time, precise and fast screening device to detect ammonia concentrations for better monitoring of such diseases. In this context, low concentrations of ammonia, location and abundance of interference are considered great challenges for monitoring specific diseases. Still, almost no suitable devices are available to tackle the problems faced in ammonia detection and continuous real-time monitoring of ammonia for underlying diseases. Organic Electrochemical Transistor (OECT) based device demonstrates the precise and selective detection of ammonia suitable for varied applications in health screening protocols. The sensing data and results obtained from the OECT device were found to be highly selective for ammonia detection as compared to other analytes and interferents thereby making it highly useful for clinical applications.

3.1. INTRODUCTION

The excessive presence of ammonia both in the environment and in the human body is harmful. [1-3] Clinically the presence of ammonia in the human blood serum is a signal of developing diseases inside the human organs. [4,5] So, it always gives negative impacts on health if abundant in the environment as well as inside the body. [6,7] Hence, effective monitoring of NH_3 at a very low concentration is of great importance. [8-11] Among the various NH_3 detection technologies reported so far, chemiresistive, electrochemical, and mass-sensitive counterparts due to the distinct merits of handy measurement, easy fabrication, and high cost-effectiveness may be mentioned. [12-14] Direct exposure to NH_3 poses a high health risk due to disturbances in the functioning of several organs. Hence long exposure to high concentrations of ammonia in the human body is usually related to the development of deadly diseases like Chronic Kidney Disease (CKD), Peptic Ulcers and even prone to epidemic diseases as well as COVID-19 (SARS - CoV - 2) due to reduced immune response. On the other hand, Peptic ulcers commonly caused by Helicobacter pylori (H. Pylori) infections can produce ammonia from urea developed in the stomach itself. Ammonia is one of the main by-products of human metabolism. Ammonia is usually formed in muscles and peripheral tissues, which is further transported to the liver for conversion into urea by the urea cycle. The urea cycle takes place in the mitochondrion and cytoplasm of hepatocytes (Liver Cells) where conversion of ammonia into urea occurs, which is again excreted by kidneys. The main signal for acute and chronic liver injury is the elevated level of ammonia, a life-threatening metabolic condition known as Hyperammonemia which is considered the main outcome of acute and chronic liver injury. Hyperammonemia is the outcome of Child-Pugh grade liver cirrhosis [15]. It is a life-threatening condition unless detected at the early stages of the disease and in such situations frequent monitoring of quantities of ammonia liberated during the metabolic process is necessary. There are several ammonia levels lowering therapies that have been constantly used clinically for improvements in acute liver failure and chronic liver disease in patients. Under such circumstances monitoring ammonia from time to time during therapy is essential. Hyperammonemia is also associated with the development of a neuropsychiatric condition known as hepatic encephalopathy which complicates the already critical clinical course in such patients. [15-28] In recent studies it has been deduced that lowering ammonia concentration by therapies can reverse sarcopenia of cirrhosis by restoring skeletal muscle proteostasis.[29-32] Apart from hepatic

diseases, Hyperammonemia also causes severe neuro-developmental complications and neurodegenerative diseases. Higher ammonia concentrations are evidently related to many diseases like urea cycle disorders, hepatic encephalopathy, skeleton muscle proteostasis, carcinomas, cirrhosis, renal dysfunction, hepatitis etc.[33-35] The disturbance of ammonia cycle enhances the concentration of NH_3 and NH_4^+ in the blood which can be detected from the measurement of ammonia concentration in exhaled breath.

The urea cycle is an energy-dependent process responsible for the conversion of toxic ammonia into urea, which can then be excreted. Five major steps are involved in this metabolic process, each step requiring a different enzyme. These include N-acetyl-glutamate synthase, carbamoyl phosphate synthetase (CPS), ornithine transcarbamylase, argininosuccinate synthetase (AS), argininosuccinic acid lyase (AL), and arginase. A defect in any of these enzymes results in impaired function of the urea cycle, leading to the accumulation of ammonia. [36-37]

Hepatocellular damage and enzymatic defect lead to reduced metabolism of ammonia during the urea cycle. Also, infection of certain microorganisms elevates ammonia production in the human body. Ammonia being a neurotoxin causes acute or chronic neurological symptoms which can be led to life-threatening complications such as cerebral edema and herniation of the brain. [38-39] Renal dysfunction attributes to the non-removal of urea causing excessive build-up of ammonia. This excessive ammonia is further transfers the ammonia and ammonium ions into the blood and finally detected in exhaled breath. Hence, ammonia in exhaled breath can be a biomarker for identifying and monitoring renal disorders. Unfortunately, the COVID-19 pandemic increases patients with limited liver and kidney function worldwide. Recent research on the COVID-19 virus has confirmed the variations in values of various biochemicals in serious patients. One of the most common variations is high levels of Blood Urea Nitrogen (BUN) which indicates kidney dysfunction based on proteinuria and hematuria. [40-43] Further study inferred that high BUN directly indicates a high concentration of ammonia in the breath. Also, it has been reported that patients with high Blood Urea Nitrogen (BUN) are the indirect way of understanding kidney dysfunction, which can be proteinuria and hematuria.

So, it is evident that ammonia can be used as a biomarker for several infectious and terminal diseases. Currently, modelling and quantification of ammonia in whole blood are widely used to monitor such diseases. Albeit, current techniques are less effective due to the limited range of identification, fewer resolutions, large and complex sensor sizes, low

preciseness with high error probability etc. [44] Apart from these limitations, ammonia detection techniques require specific sample preparation analyzed by mass spectroscopy which requires modern and sophisticated instruments available in big laboratories only. At present a precise, fast, non-invasive, inexpensive method to detect ammonia concentration is still unavailable for clinical procedures. Alternative methods include the quantification of ammonia directly from liver biopsy for accurate diagnosis using commercially available kits which are unfriendly to organs. These kits are made up of expensive calorimetric assays and are highly sensitive towards ammonia. Also, another disadvantage is that even below -80˚C, prolonged tissue storage affects the ammonia concentration of the sample which results in lower-than-expected ammonia readings. Hence, there is a constant need for developing a novel, precise, non-invasive, inexpensive method to measure ammonia in tissue samples.

Our simple and inexpensive Organic Electrochemical Transistor (OECT) based device is able to detect ammonia in blood serum efficiently. The OECT sensor is based on PEDOT: PSS polymer with a polyhydroxyl derivative membrane deposited over it resists interference from other components of blood [11]. The device exhibits high selectivity and sensitivity for ammonia with reliable and precise quantification of ammonia in blood serum. The device shows the detection of ammonia at the lowest concentrations which is clinically useful for the detection of rare hyperammonemia-related hepatic, kidney and neural disorders at the early stage. Our Organic Electrochemical Transistor (OECT) based device may be highly useful for the early detection of ammonia-related diseases and provide convenient clinical management.[11]

3.2. EXPERIMENTAL SECTION

3.2.1. MATERIALS AND METHODS

PEDOT: PSS, Acrylic acid, 30% Ammonia solution, Dulbecco's modified Eagle's medium (DMEM) was purchased from Sigma-Aldrich. Fetal Bovine Serum (FBS), Trypsin, and Pen Strep (Antibiotic) were from Gibco. Glycerol was purchased from Merck and p-toluene sulfonic acid from Loba Chemie. All the chemicals were used in this experiment as obtained from the supplier. Electrochemical measurements were carried out using CH instruments Model 700D series and Keithley 2614B. Ag/AgCl was used as the reference electrode and Phosphate buffer solution (10 mM PBS, pH 7.4) as an aqueous electrolytic solution.

3.2.2. SENSOR DESIGN AND CONSTRUCTION

As discussed in Chapter 2, 1cm X 2 cm sensor dimensions were fabricated and placed in a beaker with PBS as an electrolyte.

3.2.3. SEM/EDX Characterization of PHD

SEM/EDX mapping for PHD was performed in FESEM GEMINI 300 (CIF, IIT Guwahati). The samples were fixed using carbon tape and characterized in FESEM GEMINI 300.

3.2.4. DYNAMIC LIGHT SCATTERING (DLS)

Malvern, Zetasizer Nano ZS90 was used for the measurement of zeta potential and particle size in suspensions.

3.3. RESULTS AND DISCUSSION

3.3.1. Electrical Characterization

All the electrical characterizations of the devices were carried out under ambient conditions at room temperature using a Keithley2614B. A positive Gate bias (V_g) was

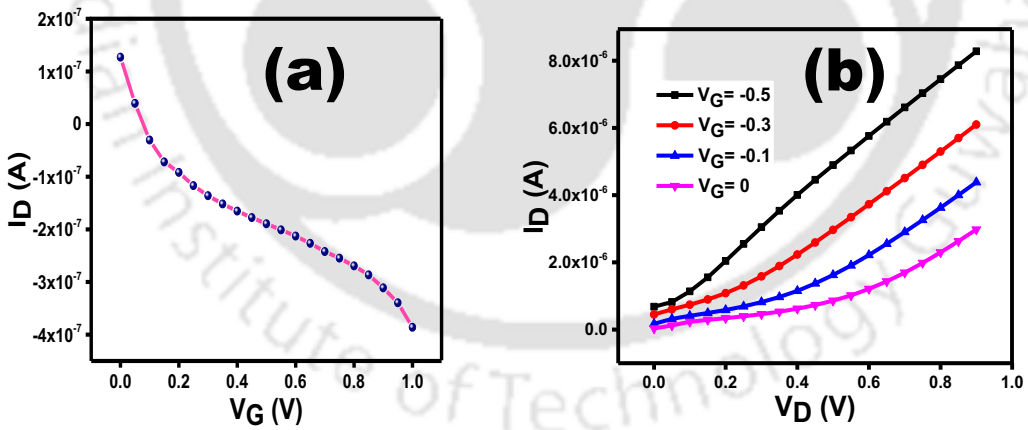

Figure 3.1. Response of the Device. a) Transfer Characteristics (I_D-V_G). b) Drain Characteristics (I_D-V_D).

applied with Ag/AgCl electrode and the two aluminium electrodes served as a source (S) and drain (D). The ammonia sensing experiments were performed at Drain voltage V_d = -0.2 V with a Gate voltage V_g sweep ranging from 0 to 0.9V in 5ml electrolyte solution at a pH of 7 (Fig. 3.1). The analyte and ammonia solutions were confined for some time in a 10 mL beaker and mixed with electrolyte prior to testing.

3.3.2. STUDY ON SENSING MECHANISM

Human liver serum specimens were acquired from patients with liver disease undergoing treatment at GNRC Hospital (Sixmile, Amingaon). Healthy human serum samples from donors were used as controls. Studies clearly demonstrate that the OECT devices can function as highly sensitive sensors for the detection of ammonia in PBS. To better understand the effect of ammonia on the electrical properties of the sensor device, the current intensity of the device was plotted against solution gate voltage in PBS. The device recorded a consistent variation of shifts (decreasing shift) with increasing ammonia concentrations and an analysis of p-type material was performed. This decreased shift can be attributed to the doping effect of PEDOT: PSS upon the binding of ammonia to the polyhydroxyl derivative (PHD) which increases the overall resistance of the device thereby decreasing the shift in current.

3.3.3. SELECTIVITY AND FUNCTIONALITY OF SENSOR IN PHYSIOLOGICAL SOLUTIONS.

For achieving practicability of the PHD along with sensitivity, the selectivity of OECT towards ammonia in an electrolytic system was also tested. During these experiments, OECT with several amino acids of biological importance, i.e., amines, and anionic and cationic analytes were examined to monitor the selectivity of OECT for ammonia under identical conditions (Fig. 3.2). It was observed that other amino groups, such as urea, glycine, and tert-butyl-amine, could not give significant current values of OECT. The less sensitivity of amino acids is due to their feeble interaction with the PHD sensing layer as they exist as Zwitter-ionic form (Intramolecular Acid-Base interactions between the carboxylic group and amine group). However, in case of urea and tert-butyl-amine interaction with the sensing layer is poor due to less ability for H-Bond formation. Thus, the OECT responded to ammonia with outstanding sensitivity and selectivity even in the presence of commonly interfering analytes in 10mM PBS; which is a very unique feature of this configuration. Ammonia is highly volatile in nature; sophisticated special instruments that could work at low pressure for the effective vaporization of ammonia have been used. Our OECT-PHD overcomes the room temperature sensing as well as low sensitivity and challenges faced by the existing probes. All the above hurdles have been subsided completely owing to the very strong hydrogen bonds formed with the newly designed OECT sensor (Refer Chapter 2). These observations with extraordinary efficacy

endorse huge application potential for onsite, simple and cost-effective detection of ammonia.

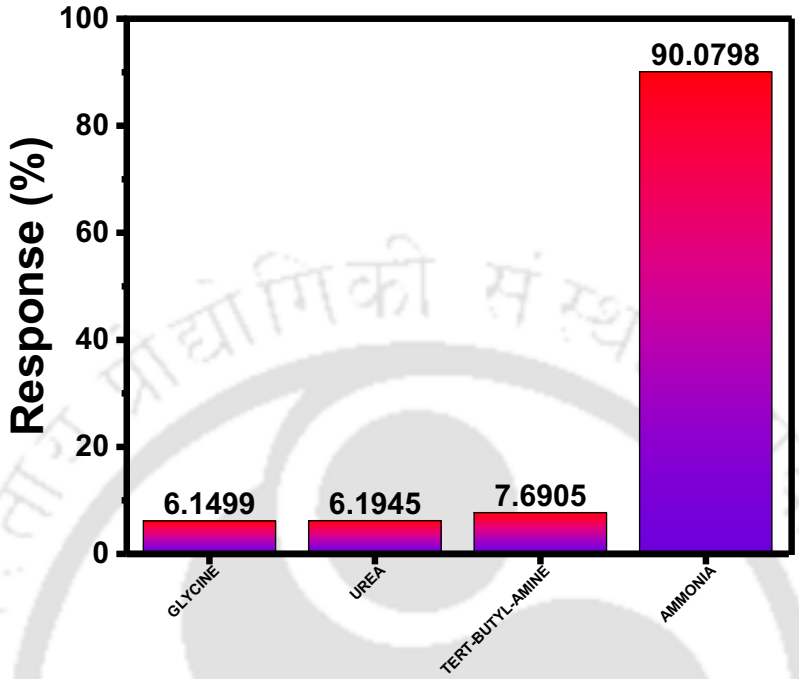

Figure 3.2. Selectivity Study of OECT-PHD in Physiological Conditions.

3.3.4. SEM/EDX STUDY

EDX (Energy Dispersive X-ray) microanalysis is a method of elemental analysis linked to electron microscopy, based on the generation of characteristic X-rays that indicate the presence of elements in samples. Many scientists and doctors use EDX microanalysis in various fields of biomedicine. However, most of the scientific community is not fully aware of its potential applications. EDX is also used in the study of environmental pollution and the characterization of mineral bioaccumulating tissues. SEM/EDX studies have been widely used to analyze the surface morphology of samples. Surface morphology can play a key role in determining the activity, selectivity and stability of a material. The position of the peak in the spectrum and its energy identifies the element (Fig. 3.3); the area under the peak is proportional to the number of atoms of the element in the irradiated region. Figure 3.4a shows a typical EDX pattern for PHD before and after NH_4^+ absorption. EDX pattern (Fig. 3.4a) for unloaded (native) PHD showed no characteristic signal for NH_4^+, while for NH_4^+-loaded PHD (Fig. 3.4b). A clear signal for the presence of NH_4^+ was observed; which is confirmed by Figure 3.4b.

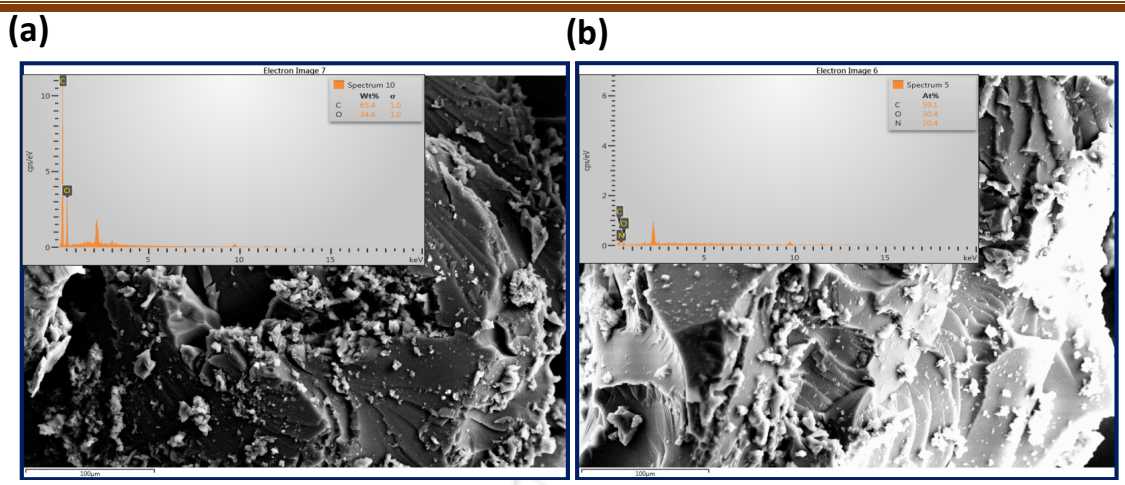

Figure 3.3 Surface Morphology and Elemental Analysis of PHD. a) Before the addition of Ammonia (Inset top left C map; inset top middle O map; inset top right N map). b) After the addition of Ammonia (Inset top left C map; inset top middle O map; inset top right N map).

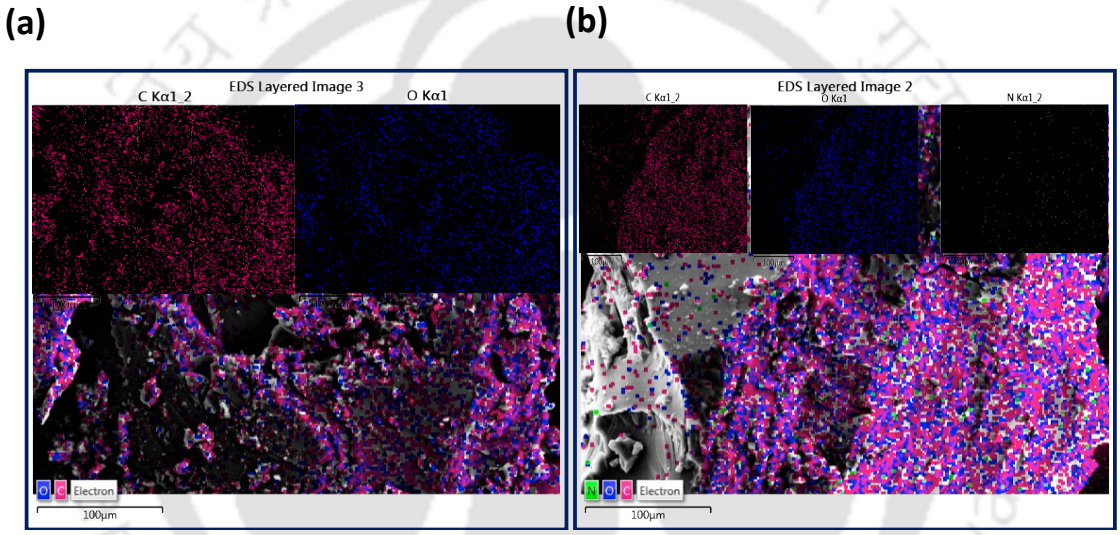

Figure 3.4. EDX Mapping of PHD Layer. a) Before the addition of ammonia (Inset top left C map; inset top right O map). b) After the addition of ammonia (Inset top left C map; inset top middle O map; inset top right N map).

3.3.5. DLS STUDY

Furthermore, DLS studies (Table 3.1) performed in aqueous media showed a decrease in particle size after the addition of ammonia due to the formation of hydrogen bonds. Along with the size, a zeta potential shift has been observed after the addition of ammonia.

	SIZE (nm)	MEAN (mV)	Z-AVERAGE (nm)
PHD	105.7	-1.55	3890
PHD+AMMONIA	135.4	-21.3	332

Table 3.1. Particle Size and Zeta Potential Values of PHD.

3.3.6. PERFORMANCE OF A NEWLY-DEVELOPED HUMAN SERUM-BASED HYBRID OECT SENSOR

Using an OECT sensor, we previously demonstrated the performance of a competitive assay for the measurement of ammonia molecules. In our previous work, the OECT was placed inside the electrolytic chamber, with an average pore size distribution of the PHD membrane of 3nm. This pore size is shown to influence the response time of the sensor by accelerating the permeation rate of the ammonia molecules, thereby, promoting the overall performance of the system. The pore size distribution of the membrane helps to contribute to the improvement of the response time of the sensor. We have also tested the reversibility and reproducibility of the OECT sensor and compared the outcome results to those obtained by the standard colourimetric sensor. This analysis revealed that both sensors could detect the varied ammonia concentrations, and in fact, our system produced more reproducible results. However, due to the presence of the PHD membrane, the OECT sensor remains protected from electrolytes for a relatively long period required for the determination of ammonia levels. The presence of a small amount of protein strongly affects the indophenol reaction, leading to a complete cessation of the reaction. Therefore, it is important to separate NH_3 from whole blood and discard proteins. In this process, a mesoporous PHD layer is used as a cation exchange membrane. Thus, another possible source of interference with the indophenol reaction is proteins. Small amounts of protein can inhibit the reaction completely. A PHD cation exchange membrane was used to rapidly separate ammonia from whole blood, excluding all proteins. When cast into films, usually from a hot-pressed solution, the PHD block is assembled in long-range pores surrounded by a cross-linked polymer matrix. The pores are strongly negatively charged due to the COO– and OH– groups and are typically 3 nm in size. These pores allow the rapid diffusion of hydroxyl-containing molecules and cations, preventing the diffusion of anions and macromolecules. The analyte recovery mechanism is ammonium ion exchange using a PHD membrane (refer to Chapter 2). Ammonia concentrations were added to the spike when ammonia was detected in whole blood. The response to serum ammonia was observed at different concentrations (Fig. 3.5). To validate the FDA guidelines and effectively quantify human serum NH_3 concentrations, future studies can be investigated to improve the efficient detection of blood ammonia concentrations that represent levels of healthy and diseased cells.

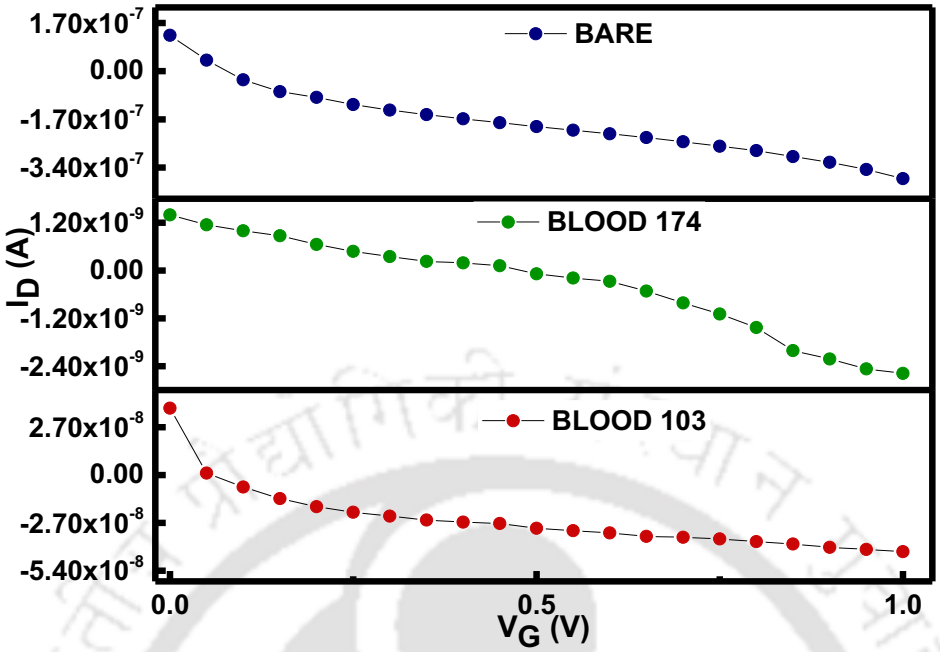

Figure 3.5. Current outputs for different ammonia concentrations in patient samples.

3.4. CONCLUSIONS

In summary, we have first demonstrated the utility of a bi-layer OECT sensor for label-free ammonia detection. This sensor was able to detect the clinical ammonia in human serum. Moreover, our device proved to be a stable method and has several key advantages: (1) it does not consume any enzymes; (2) it is a label-free system; (3) signals generated by the device are directly responsible for the analyte; and (4) cost-effective. Thus, we believe that this OECT sensor platform will represent a technique for the advancement in biomedical sensor technology, and can be further developed into a robust and compact wearable online ammonia monitoring system.

3.5. REFERENCES

1. S. Dey, N. Haripavan, S.R. Basha, G.V. Babu, *Current Research in Chemical Biology*, 2021, 1, 100005.

2. L. Ampollini, E. F. Katz, S. Bourne, Y. Tian, A. Novoselac, A. H. Goldstein, G. Lucic, M. S. Waring, and P. F. DeCarlo, *Environ. Sci. Technol.,* 2019, 53, 15, 8591–8598.

3. P.P. Ricci, O.J. Gregory, *Sci Rep 11*, 2021, 7185.

4. M. M. Adeva, G. Souto, N. Blanco, C. Donapetry, *Metabolism*, 2012, 61, 11, 1495-1511.

5. T. Shroff, K. Aina, C. Maass, M. Cipriano, J. Lambrecht, F. Tacke, A. Mosig, P. Loskill, *Open Biol.,* 12: 210333.

6. T. Hibbard & A. J. Killard, *Critical Reviews in Analytical Chemistry*, 2011, 41, 1.

7. I. Horváth, J. Hunt, P. J. Barnes On behalf of the ATS/ERS Task Force on Exhaled Breath Condensate, *European Respiratory Journal*, 2005 26: 523-548.

8. M. Serafini, F. Mariani, I. Gualandi, F. Decataldo, L. Possanzini, M. Tessarolo, B. Fraboni, D. Tonelli and E. Scavetta, *Sensors*, 2021, 21(23), 7905.

9. D. Germanese, S. Colantonio, M. D'Acunto, V. Romagnoli, A. Salvati and M. Brunetto, *Sensors*, 2019, 19(17), 3656.

10. D. R. Seshadri, R. T. Li, J. E. Voos, J. R. Rowbottom, C. M. Alfes, C. A. Zorman & C. K. Drummond, *npj Digital Medicine,* 2019, 2, 72.

11. I. Medhi and P. K. Iyer, *Sens. Diagn*., 2022,1, 1176-1184.

12. Y. Wang, S. Cheng, C. Sun and T. Wang, *Chemosensors* 2023, 11(3), 202.

13. H. Shen, A. Abtahi, B. Lussem, B. W. Boudouris, and J. Mei, *ACS Appl. Electron. Mater*., 2021, 3, 6, 2434–2448.

14. F. Gao, C. Liu, L. Zhang, T. Liu, Z. Wang, Z. Song, H. Cai, Z. Fang, J. Chen, J. Wang, M. Han, J. Wang, K. Lin, R. Wang, M. Li, Q. Mei, X. Ma, S. Liang, G. Gou & N. Xue, *Microsystems & Nanoengineering*, 2023, 9, 1.

15. S. Deutsch-Link, A. M. Moon, Y. Jiang, A. S. Barritt IV, E. B. Tapper, *Clinical Therapeutics*, 2022, 44, 3.

16. N. D. Vaziri, M. Khazaeli, A. C. F. Nunes, K. T. Harley, H. Said, O. Alipour, W. L. Lau, M. V. Pahl, *Hemodial Int.*, 2017, 21(3): 343–347.

17. C. Ming-Jen, L. Yi-Jung, W. Chao-Ching, L. Yu-Chen, Z. Hsiao-Wen, M. Hsin-Fei, H. Meng-Hsuan, L. Chao-Sung and T. Ya-Chung, *Biomedicines,* 2020, 8(11), 468.

18. N. Savy, D. Brossier, C. Brunel-Guitton, L. Ducharme-Crevier, G. Du Pont-Thibodeau, P. Jouvet, *Hepatic Medicine: Evidence and Research*, 2018: 10:105-115.

19. V. Walker, *Ann Clin Biochem*, 2012; 49: 214–228.

20. J. Y. Findlay, O. K. Fix, C. Paugam-Burtz, L. Liu, P. Sood, S. J. Tomlanovich, J. Emond, *Liver Transplantation*, 2011, 17:496-510.

21. T. Wang, Z. Sun, D. Huang, Z. Yang, Q. Ji, N. Hu, G. Yin, D. He, H. Wei, Y. Zhang, *Sensors and Actuators B: Chemical,* 2017, 252, 284-294.

22. D. Huang, X. Li, S. Wang, G. He, W. Jiang, J. Hu, Y. Wang, N. Hu, Y. Zhang, Z. Yang, *Sensors and Actuators B: Chemical,* 2017, 252, 956-964.

23. F. Haitao, Y. Xiaohong, A. Xizhong, F. Weiren, J. Xuchuan, Y. Aibing, *Sensors and Actuators B: Chemical,* 2017, 252, 103-115.

24. T. Wang, D. Huang, Z. Yang, S. Xu, G. He, X. Li, N. Hu, G. Yin, D. He, L. Zhang, *Nano-Micro Letters,* 2016, 8, 95–119.

25. W. Meng, L. Dai, W. Meng, H. Zhou, Y. Li, Z. He, L. Wang, *Sensors and Actuators B: Chemical* 2017, 240, 962-970.

26. J. G. Kusters, A. H. M. van Vliet, and E. J. Kuipers, *Clin Microbiol Rev.,* 2006 Jul; 19(3): 449–490.

27. S. Selorm F. Kenston, X. Song, Z. Li, J. Zhao, *Journal of Gastroenterology and Hepatology,* 2019 34, 31–39.

28. J. A. Frontera, *Current Treatment Options in Neurology*, 2014,16, 297.

29. N. D. Hawkes, G. A. O. Thomas, A. Jurewicz, O. M. Williams, C. E. M. Hillier, I. N. F. McQueen, G. Shortland, *Postgrad Med J*, 2001, 77:717–722.

30. M. Rovegno, M. Vera, A. Ruiz, C. Benítez, *Annals of Hepatology,* 2019, 18, 543–552.

31. C. Mangini and S. Montagnese, *J. Clin. Med.*, 2021, 10(18), 4050.

32. G. Tarantino, V. Citro, P. Esposito, S. Giaquinto, A. de Leone, G. Milan, F. S. Tripodi, M. Cirillo & R. Lobello, *BMC Gastroenterol,* 2009, 9, 21.

33. L. Jing, L. Enkhchimeg, C. Hea-Jong, K. Hyeon-Jin and H. Seong-Tshool, *Nutrients*, 2018, 10(2): 140.

34. M.C. Machado, F. Pinheiro da Silva, *j intensive care,* 20142, 22.

35. C. F. Rose, P. Amodio, J. S. Bajaj, R. K. Dhiman, S. Montagnese, S. D. Taylor-Robinson, H. Vilstrup & R. Jalan, *Journal of Hepatology*, 2020.

36. U. Lichter-Konecki, *Translational Science of Rare Diseases,* 2016, 1, 23–43.

37. N. Haskins, S. Bhuvanendran, C. Anselmi, A. Gams, T. Kanholm, K. M. Kocher, J. LoTempio, K. I. Krohmaly, D. Sohai, N. Stearrett, E. Bonner, M. Tuchman, H. Morizono, J. K. Jaiswal and L. Caldovic, *Front. Physiol.*, 11:542950.

38. E A Jones, K Weissenborn, *Journal of Neurology, Neurosurgery, and Psychiatry,* 1997, 63, 279–293.

39. C. Rubinos, S. Ruland, *Curr Neurol Neurosci Rep,* 2016, 16, 57.

40. P. Letelier, N. Encina, P. Morales, A. Riffo, H. Silva, I. Riquelme, N. Guzmán, *J Med Biochem,* 2021, 40, 115–128.

41. H. Zhou, Z. Zhang, M. Dobrinina, Y. Dong, Z. Kang, V. Chereshnev, D. Hu, Z. Zhang, J. Zhang, A. Sarapultsev, *Diagnostics,* 2022, 12, 602.

42. L. Ye-Mao, X. Jing, C. Ming-Ming, Z. Xiao, C. Xu, L. Haomiao, Z. Feng, Q. Juan-Juan, L. Fang, C. Ze, L. Lijin, Y. Chengzhang, M. Weiming, C. Guohua, L. Haofeng, X. Xigang, W. Daihong, L. Xiaofeng, Y. Jun, H. Xiaodong, Z. Bing-Hong, Y. Yufeng, C. Jingjing, Z. Xiao-Jing, W. Yibin, Z. Xin, S. Zhi-Gang, L. Hongliang, *Med*, 2021, 2, 1, 38-48.

43. T. Xia, W. Zhang, Y. Xu, B. Wang, Z. Yuan, N. Wu, Y. Xiang, C. Li, Y. Shan, W. Xie, Y. Wang, Y. Zhang, L Bai & Y. Li, *BMC Infectious Diseases,* 2021, 21, 1012.

44. I. Chaudhri, R. Moffitt, E. Taub, R. R. Annadi, M. Hoai, O. Bolotova, J. Yoo, S. Dhaliwal, H. Sahib, F. Daccueil, J. Hajagos, M. Saltz, J. Saltz, S. K. Mallipattu, F. M. Koraishy, *Kidney Blood Press Res*, 2020;45, 1018–1032.

Chapter – 4

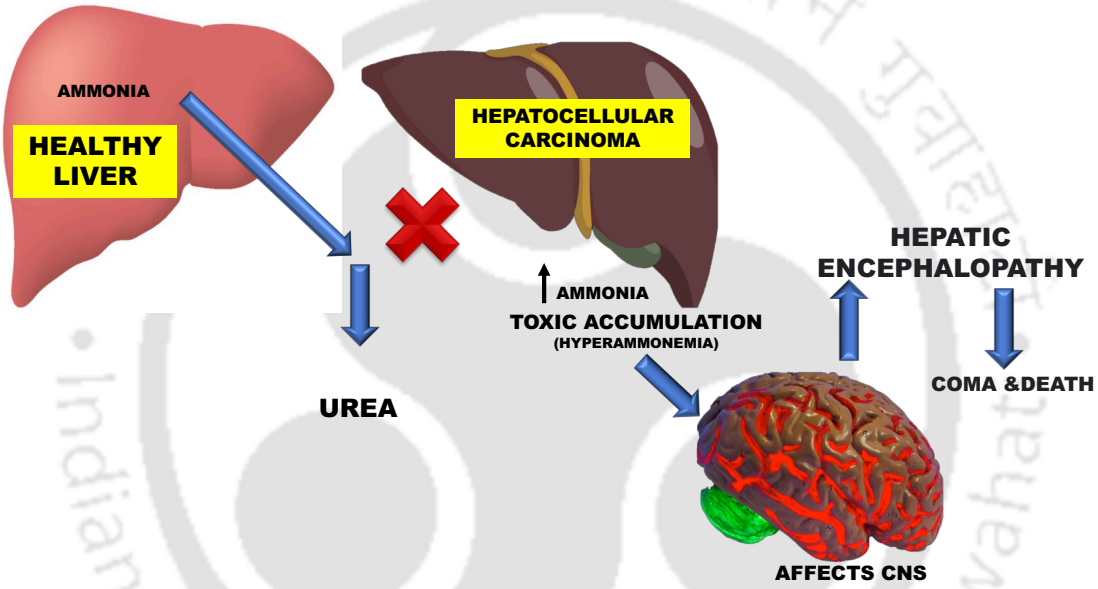

ABSTRACT

Hepatocellular carcinoma (HCC) is highly malignant affecting particularly in China. The poor prognosis of HCC is one of the reasons for late diagnosis during treatment. There are many new biomarkers available for HCC diagnosis. However, limited numbers are clinically used in clinical practice. It is still a clinical challenge to develop an early and differential diagnosis of HCC from cirrhosis and/or hepatitis. Metabolomics and biochemical methods were used to reveal specific serum biomarkers of HCC. Not only urea was the specifically elevated serum biomarker of HCC patients but also the plasma ammonia of HCC patients was significantly found higher than normal adults. As such normal liver cells can better cooperate to metabolize ammonia into urea in comparison to cancer cells. If we consider the urea cycle, detoxification of high concentrations of ammonia lead to cancer cell proliferation. Therefore, urea was a by-product of ammonia metabolism and could be a potential serum biomarker for HCC. Rapidly growing cells, particularly cancer cells, consume nutrients voraciously and generate excess metabolic waste. One such by-product, ammonia, is normally transported in blood vessels to the liver, where it is converted into less toxic substances and excreted from the body as urea. Tumours, however, have few blood vessels, and as a result, ammonia accumulates in the tumour's local environment at concentrations that would be toxic for many cells. The combined application of metabolomics and biochemical methods can discover new biomarkers for the early diagnosis of HCC and be quickly applied to clinical diagnosis. So, the PEDOT: PSS-based PHD has been used as an efficient biosensor for the detection of HCC.

4.1. INTRODUCTION

According to the World Health Organization (WHO) reports more than 1 million patients will die of liver cancer by 2030. New cases and deaths related to liver cancer in developing countries like China account for about 50% of the world's. [1-6] Hepatocellular carcinoma (HCC) is highly malignant and usually diagnosed at an advanced stage, accounting for over 80% of primary liver cancers. [7-8] The diagnosis of HCC still depends on imaging (ultrasound B, CT or MRI) and alpha-fetoprotein (AFP) in clinical practice. [9-13] Early diagnosis and a better understanding of the molecular mechanisms leading to HCC occurrence and progression may be considered urgent clinical research. Detection of HCC at the early stage is not easy work despite tremendous efforts that have been made to discover new biomarkers.[14-16] However, their sensitivity and/or specificity are not satisfactory. Metabolic reprogramming is a recognized hallmark of cancer. [17] Metabolites can regulate gene and protein expressions, and metabolic proteins and/or metabolites are potential diagnostic and prognostic biomarkers. [18-21] It has been known that certain metabolites, such as lactate and amino acid, and their changes in serum may reflect metabolic changes in tumour tissue. [22-23] Many studies were devoted to discovering serum biomarkers of HCC diagnosis from the aspect of metabolites. Ping Luo et al. [24] defined a group of biomarkers of serum metabolites, including phenylalanyl-tryptophan and glycine chelate. This panel has a higher diagnostic performance. Tomoyoshi Soga et al. [25] revealed that γ-glutamyl dipeptides are new biomarkers for liver disease and can distinguish different liver disease progressions. These studies may reflect various metabolic aspects of HCC. Still, lack of sufficient validation restricts further clinical applications of these biomarkers, because most laboratories cannot access mass spectrometers for easily detecting metabolites. Moreover, it is not possible to elucidate the underlying molecular mechanism. Usually, cancer cells are highly dependent on glutamine for survival and cell proliferation**.** Glutamine catabolism is accompanied by the secretion of alanine and ammonia, leading to most of the amino groups of glutamine being lost from the cell instead of being incorporated into other molecules [26]. Together with another amino acid metabolism, they lead to the accumulation of ammonia in the tumour microenvironment. Hence ammonia metabolism plays different roles in cancers. Most researchers believe ammonia is a toxic cellular by-product of glutamine metabolism [27,28] and needs to be metabolized into a non-toxic form, such as urea, to be excluded from the body. But Jessica B et al. prove that breast cancer cells can recycle glutamine amide for

biosynthesis. [29] Therefore, the role of ammonia in cancer cells remains to be determined. The liver represents a perfect metabolic model that governs body energy metabolism through different metabolites' physiological regulation, including sugars, lipids, amino acids, and the urea cycle.

So, one can consider ammonia (NH_3) as a toxic cellular by-product of glutamine metabolism and accumulates in all tissues of the body during the metabolism of a variety of compounds. At physiological pH, ammonia exists as the ammonium ion (NH_4^+). The body produces ammonia mainly through transamination and deamination of biogenic amines, amino groups from nitrogenous bases such as purine and pyrimidine, and intestinal bacteria by the action of urease on urea in the intestine. Ammonia disposal takes place primarily by the hepatic formation of urea. Hence, the blood level of ammonia must remain very low because even slightly elevated concentrations (hyperammonemia) are toxic to the central nervous system (CNS). [30]

On the other hand, a metabolic mechanism exists by which nitrogen is moved from peripheral tissues to the liver for its ultimate disposal as urea, while at the same time maintaining low levels of circulating ammonia. Enzymes that function in the urea cycle synthesize NH_3 in vitro. Myeloma is associated with an excess of NH_3 in the cellular microenvironment. This condition may be due to the reliance of tumour cells on glycolysis for the production of energy, which reduces the requirement for mitochondrial phosphorylation. The analysis of protein biomarkers is of great importance in the diagnosis of diseases.[31]

Although many convenient and low-cost electrochemical approaches have been extensively investigated, they are not sensitive enough in the detection of protein biomarkers with low concentrations in physiological environments. Here, this study reports a novel organic-electrochemical-transistor-based biosensor that can successfully detect cancer protein biomarkers with ultrahigh sensitivity. The ultrahigh sensitivity of the protein sensors is attributed to the inherent amplification function of the organic electrochemical transistors. In this work, we focus on developing highly sensitive and low-cost biosensors and the clinical application for the detection of ammonia biomarkers in future.

4.2. EXPERIMENTAL SECTION

4.2.1 MATERIALS AND METHODS

PEDOT: PSS, Acrylic acid, 30% Ammonia solution, Dulbecco's modified Eagle's medium (DMEM) was purchased from Sigma-Aldrich. Fetal Bovine Serum (FBS), Trypsin, and Pen Strep (Antibiotic) were from Gibco. Glycerol was purchased from Merck and p-toluene sulfonic acid from Loba Chemie. All the chemicals were used in this experiment as obtained from the supplier. Electrochemical measurements were carried out using CH instruments Model 700D series and Keithley 2614B. Ag/AgCl was used as the reference electrode and Phosphate buffer solution (10 mM PBS, pH 7.4) as an aqueous electrolytic solution.

4.2.2. THERMOGRAVIMETRIC ANALYSIS (TGA) AND DIFFERENTIAL SCANNING CALORIMETRY (DSC)

TGA of the polymers was performed on a Perkin Elmer TGA 4000 instrument at a heating rate of 10 °C/min with a nitrogen flow rate of 20 mL/min.

4.2.3. SENSOR DESIGN AND CONSTRUCTION

As discussed in Chapter 2, 1cm X 2 cm sensor dimensions were fabricated and placed in a beaker with PBS as an electrolyte.

4.2.4. CELL STUDIES

For undertaking cancer cells studies, the cell lines liver hepatocellular carcinoma cells (HepG2), Human cervical carcinoma (HeLa), Human breast adenocarcinoma cells (A549) and human embryonic kidney cells (HEK-293) were procured from NCCS, Pune. The cells were grown in Dulbecco's modified Eagle's medium (DMEM) supplemented with 10% FBS (Fetal Bovine Serum) and antibiotics (Pen Strep) maintained at 5% CO_2 and 37 °C in a humidified incubator.

4.2.5. CELL CULTURE FOR CONFOCAL MICROSCOPY IMAGING

For the experiments, the cells HEPG2, HeLa, A549 and HEK-293 were trypsinized and 10^5 cells/mL were seeded in 35 mm tissue culture plates and were allowed to attach for 24 h at 5% CO2 at 37 °C in a humidified incubator. 0.1M NH_4Cl was added to the cells. The attached cells were given PBS wash once and were added to the tissue culture plates. The

cells were then allowed to incubate with 0.1M NH_4Cl for 3 hrs. The cells not treated with 0.1M NH_4Cl served as the control group.

4.2.6. ELECTRICAL CHARACTERIZATION

All the electrical characterizations of the devices were carried out under ambient conditions at room temperature using a Keithley2614B. A positive Gate bias (Vg) was applied with Ag/AgCl electrode and the two aluminium electrodes served as a source (S) and drain (D). The cell sensing experiments were performed at Drain voltage V_d = -0.2 V with a Gate voltage V_g sweep ranging from 0 to 0.9V in 5ml electrolyte solution at a pH of 7.4.

4.3. RESULTS AND DISCUSSION

4.3.1 ELECTROCHEMICAL DETECTION OF HepG2 CELLS

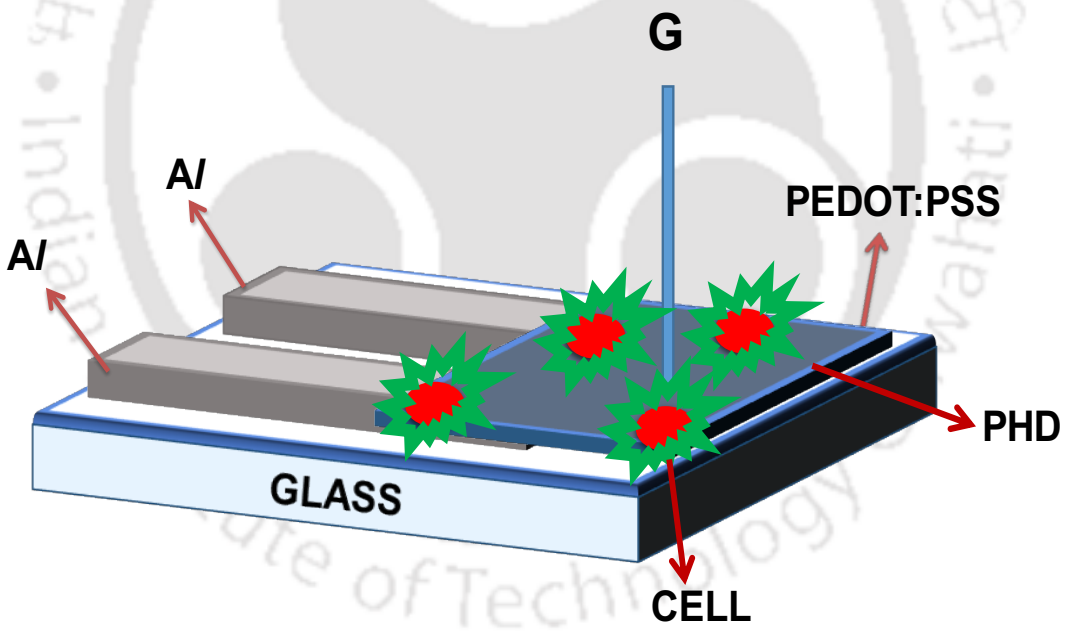

Figure 4.1. Schematic Illustration of cell sensing device showing various layers and Incorporation of a Mesoporous Layer.

Ammonia metabolism of hepatocytes was monitored for efficient local transduction of biological signals and diagnosing pathological conditions. Traditional devices used to record electrophysiological signals are passive electrodes that require pre-amplification with downstream electronics. Here, we show that the uptake of ionic charge from an electrolyte into a poly(3,4-ethylenedioxythiophene) doped with polystyrene sulfonate

(PEDOT: PSS) OECT channel leads to a dependence of the effective capacitance on the entire volume of the film (Fig. 4.1). Subsequently, device characteristics and time response vary with channel thickness, a defining characteristic that differentiates OECTs from field effect transistors and provides a new degree of freedom for device engineering to impart richer signal content without the need for additional amplification circuitry (Fig. 4.2). We also show that the materials of merit OECTs is the product of hole mobility and volumetric capacitance of the channel, leading to design rules for novel high-performance materials. The NH_3 readily diffuses across the cell membrane, following the chemical potential gradient. Thus, the real-time imaging of NH_3 release from cells to the cellular microenvironment could play a vital role in exploring the behaviour and heterogeneity among tumour cells. However, analyzing metabolites released from cells to the surroundings is difficult due to rapid fluctuations and dilution which obscures the cellular activities.

Rapidly growing cells, especially cancer cells, voraciously consume nutrients and produce excess metabolic waste. However, tumours have few blood vessels and as a result, ammonia accumulates in the local environment of the tumour in concentrations that would be toxic for many cells. Normal cells have an extracellular pH between 7.2 and 7.4, while cancer cells have a pH between 6.2 and 6.9. With a dissociation constant (pKa) of 9.3, NH_4^+ constitutes ≈ 99% of the total ammonia (NH_3 + NH_4^+) concentration at a physiological pH (7.1–7.5). In its ionized form, NH_4^+ is relatively impermeable to cell membranes. At pH > 6.8, exhibiting rapid protonation of NH_3 in the cellular microenvironment causes a constant flow of NH_3 from the cells to the surroundings, which raises the pH of the cellular microenvironment. Hence, the NH_4^+ in the cellular microenvironment interacts with the opposite charge COO^- of PHD. This reduces the net charge density and forms hydrogen bonding, leading to the detection of cancerous cells.

Therefore, our research uses quantitative targeted metabolomics to screen for HCC and in-depth verification using biochemical analysis methods. Ammonia is a potential biomarker of HCC, and combining it with an OECT configuration could improve the detection efficiency of HCC. Normal liver cells and cancer cells metabolize ammonia into urea, leading to a decrease or elevated serum urea in HCC patients. These cells have a high rate of glutaminolysis and release ammonia (NH_3) as a by-product, which may function as a

diffusible signal among cancer cells and can reveal cellular heterogeneity. An organic electrochemical transistor (OECT) coupled with a porous polyhydroxyl derivative

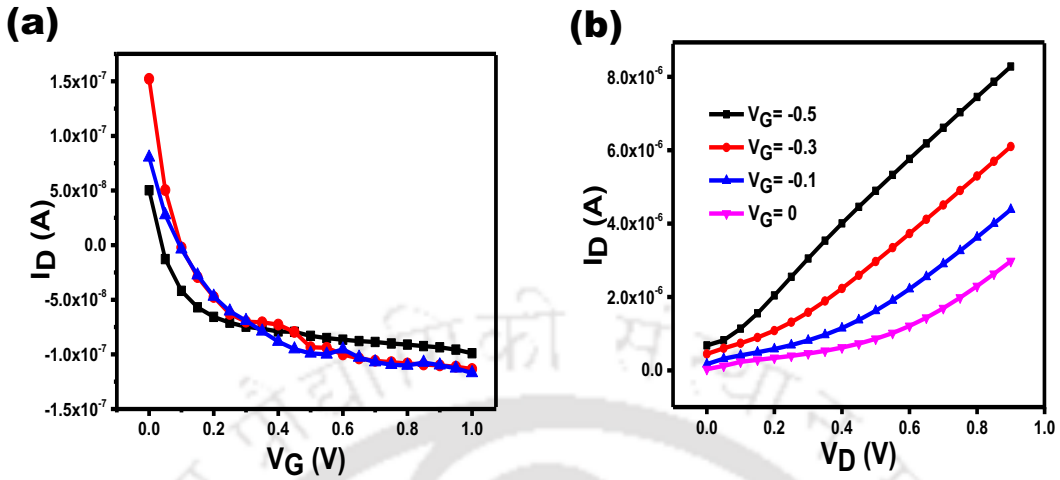

Figure 4.2. OECT-PHD Hybrid Sensor Characteristics. a) Transfer Characteristics (I_D-V_G). b) Drain Characteristics (I_D-V_G).

(PHD) serves as a tool to investigate the release of NH_3. The designed device is able to detect NH_3 release from the cell when put in an unstable stressful environment. The various cell lines significantly differ in their response. The sensor comprises a modified OECT configuration, which resists sources of destructive interferences, in conjunction with a cation-exchange membrane. The presented sensing scheme is selective against other amine-containing molecules such as amino acids and is room temperature stable (Chapter 2 & 3). Additionally, the resulting system has high sensitivity and allows for the accurate reliable detection of ammonia, which is clinically relevant for rare hyperammonemia disorders and liver disease.

One major advantage of using the OECT-PHD for determining HepG2 concentrations is that it does not require any biological components such as enzymes, which are high in cost and may arise certain stability issues. A concentration of 0.1M was utilized for ammonia to ensure the selectivity of HepG2. In order to rapidly detect HepG2 from other cell lines, PHD: ammonia selective layer. When cast into films, usually from solution in a hot press, the PHD aggregates into a porous matrix. The pores are highly negatively charged due to the presence of oxygen centres and are generally 3 nm in size. These pores allow for the rapid diffusion of hydroxyl-containing molecules and cations while inhibiting the diffusion of anions and macromolecules.

The ion exchange of ammonia through the use of a PHD membrane is the mechanism utilised for detecting HepG2. Furthermore, we proved the underlying mechanism by direct contact cell model. Normal liver cells metabolize the ammonia to urea whereas HCC cells are unable to which may be the reason for the elevated serum ammonia in HCC patients.

4.3.2. THERMOGRAVIMETRIC ANALYSIS (TGA) AND DIFFERENTIAL SCANNING CALORIMETRY (DSC)

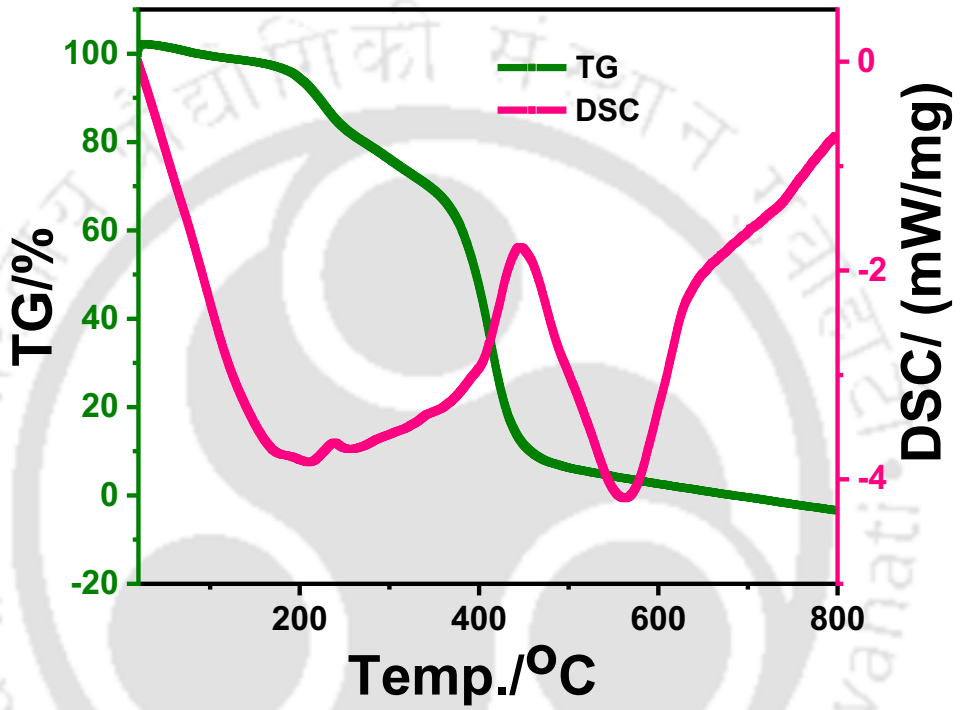

Figure 4.3. Thermal Degradation of PHD showing the stability of the material.

In figure 4.3, Thermogravimetric Analysis (TGA) and Differential Scanning Calorimetry (DSC) of the selective layer were recorded for the temperature range of 20-800 °C. This test was done to know the stability of the material. From the TGA data, we can see the selective layer undergoes a weight loss due to breaking of weak bonds of the polymer at around 180 °C. A second humf around 340°C signifies further weight loss due to breaking of strong bonds of the polymer. Sudden drop in TGA curve at around 450°C represents the complete degradation of the polymer. The DSC Curve shows the Glass transition of the polymer at 210 °C and the crystallisation exothermic peak at 447°C. On further heating, the polymer melts which can be associated with endothermic inverted peak around 570 °C. After melting, the polymer exhibits strong crosslinking and oxidation (decomposition) leads to continuos energy release (exothermic profile) which is evident by monotonously increasing DSC curve at end.

4.3.3. REAL-TIME ELECTRICAL DETECTION OF HEPG2 CELL LINE USING AMMONIA AS BIOMARKER

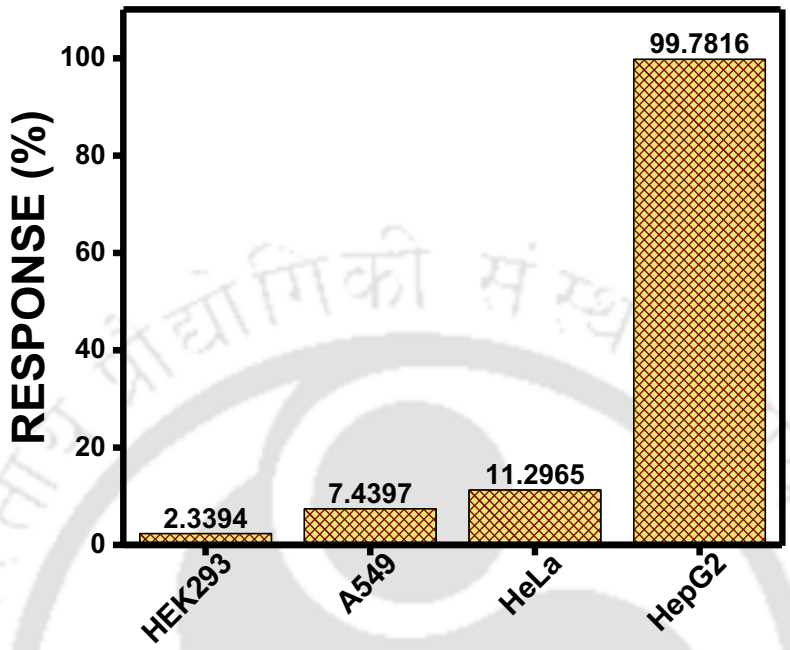

Figure 4.4. Selectivity Study of different cell lines.

We also evaluated real-time monitoring of ammonia released by living cells. Going a step further, we also performed in vitro studies to test the performance of the OECT-PHD ammonia sensor for real-time detection. Here, the real-time electrical measurements were conducted at a constant bias voltage. Devices were kept in a 10 mM phosphate-buffered saline (PBS) (pH 7.4). Our device exhibited current readouts on the addition of untreated/treated cells. We used 0.1M NH_4Cl as a precursor to releasing ammonia in PBS (pH 7.4) and DMEM. Upon the introduction of HepG2 cells in PBS the conductance of our device exhibits a noticeable change. On the contrary, such changes in conductance were not shown/negligible for other cell lines like HeLa, A549 and HEK-293 etc. As a control experiment, cells were cultured in culture media and taken out before the electrical measurement. In another set of experiments, cells were incubated in ammonia for 3 hrs and electrical measurements were carried out. When cells were added to the aqueous solution, a change of conductance was observed (Fig. 4.4). The conductance of another control device with ammonia stimulation further shift of current was observed. These studies further demonstrate the capability of our device to detect cancer cell lines with fast response in complex biological systems.

This study clearly demonstrates that the OECT-PHD device can indeed respond specifically to HepG2 in PBS and DMEM solutions. As the conductance change of the sensor originates from the doping effect, it is expected that the sensor should exhibit higher sensitivity. Thus, the OECT–PHD devices can function as highly sensitive sensors for the detection of HepG2 in both PBS and cell media. To better understand the effect of ammonia on the electrical properties of the sensor device, the conductance of the device was plotted against the solution gate voltage. The OECT-PHD devices show a consistent shift with increasing ammonia concentration as seen in Chapter 2. This shift can be attributed to the doping effect of the OECT-PHD complex on the PEDOT: PSS channel upon the binding of HepG2. Therefore, the binding of ammonia to PHD is equivalent to partial electron doping to an OECT-PHD device. This electron-doping effect explains the shifting of the current upon the introduction of HepG2 and is consistent with the reduction of conductance in the hole transport branch of the OECT-PHD devices.

4.3.4. CELL IMAGING

The cell imaging studies were performed with a fluorescence microscope (480nm) and confocal microscope (488nm). For performing the studies on the cells HEPG2, HeLa, A549 and HEK-293 were grown and seeded at a density of 1,00,000 cells/mL in tissue culture plates. The cells treated with 0.1M NH_4Cl were given PBS wash and 10µL of Acridine orange (for staining live cells) of a concentration of 1mg/mL was added evenly on the cells and were incubated for 15 min at 37 °C. The excess dye was removed using PBS wash. This was followed by the addition of 10µL Propidium Iodide (for staining the dead cells; 1mg/mL) and incubation of 15 min at 37 °C. The excessive dye was washed using PBS and the cells were fixed using 0.1% formaldehyde and 70% chilled ethanol. The cells were observed under a fluorescence cell imager (Bio-Rad, ZOE) and Confocal Laser Scanning Microscope (Zeiss, LSM 880).

This study confirms the selectivity of HEPG2 cell line with ammonia as biomarker (Fig. 4.4) detected by our OECT-PHD Hybrid Platform. As seen in Figure 4.5 & 4.6, fluorescence was negligible in case of HEK-293 and A549 respectively. Confocal Study of Hela and HepG2 (Fig. 4.7 & 4.8) was performed to get better realization of the difference in selectivity of the two cell lines). HepG2 cell line (Fig. 4.8) gives better fluorescence confirming our device selectivity.

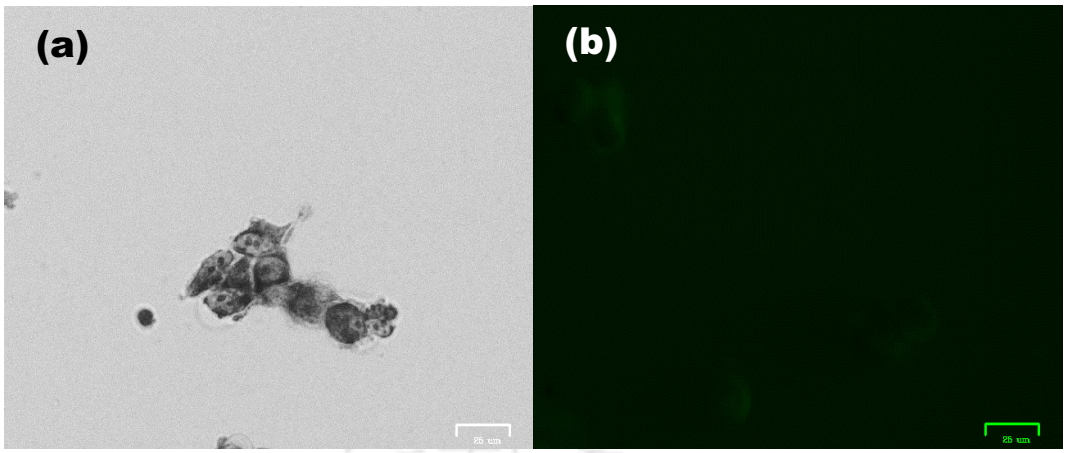

Figure 4.5. Fluorescence Imaging of HEK-293 in a) Before the addition of ammonia (Bright field); b) After the addition of ammonia (Green Field).

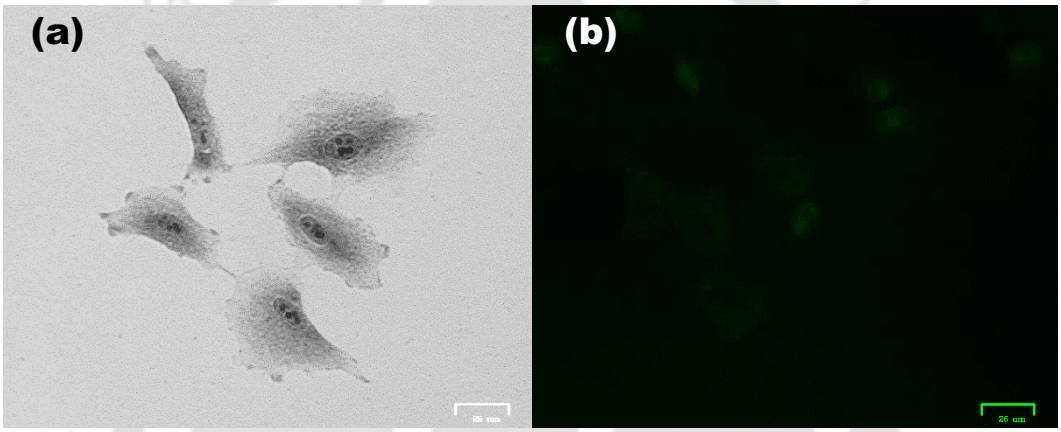

Figure 4.6. Fluorescence Imaging of A549 in a) Before addition of ammonia (Bright field); b) After addition of ammonia (Green Field).

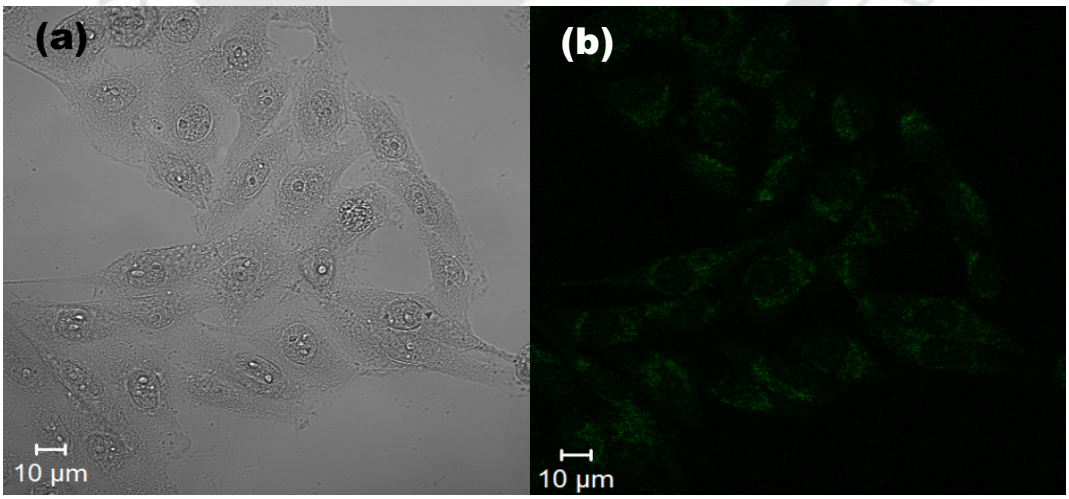

Figure 4.7. Confocal Imaging of HeLa in a) Before addition of ammonia (Bright field); b) After addition of ammonia (Green Field).

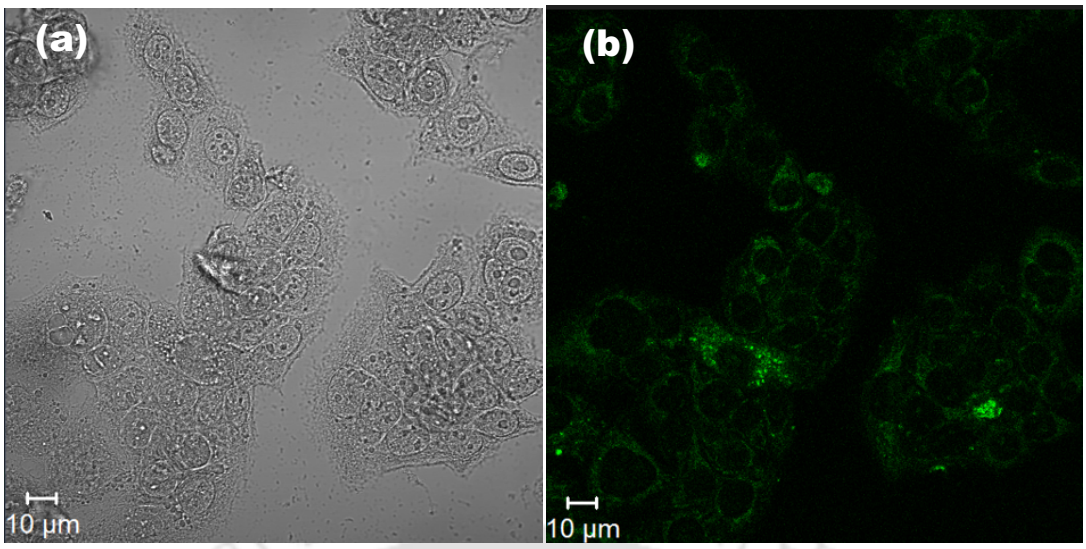

Figure 4.8. Confocal Imaging of HEPG2 in a) Before addition of ammonia (Bright field); b) After addition of ammonia (Green Field).

4.4. CONCLUSION

Direct measurement of ammonia with OECT–PHD sensor can be readily used to measure ammonia released by liver cells. This study demonstrates the utility of ultra-microscale ammonia detection and quantification. Here, we have demonstrated the detection of ammonia with respect to HCC cells compared to other standard end-point assays, such as immune fluorescence. Hence, the combination of metabolomics and routine testing can reveal the potential serum biomarkers of HCC, and quickly promote the application. Ammonia is a potential biomarker of HCC, and combining it with an OECT–PHD sensor can improve the diagnostic efficiency of HCC. The prospect of this work will benefit from harnessing the development of the hybrid OECT-polymer devices, as an example of cheap, easy-to-fabricate as well as real-time monitoring of metabolites.

4.5. REFERENCES

1. (a) I. D. Weiner, J. W. Verlander, *Compr Physiol.,* 2013, 3(1), 201-20. (b) L. A. Torre, F. Bray, R. L. Siegel, J. Ferlay, J. Lortet-Tieulent, A. Jemal, *CA: A Cancer Journal for Clinicians*, 2015, 65, 87-108.

2. (a) O. W. van Assendelft, W. G. Zijlstra, *Anal Biochem.*, 1975, 69(1), 43-8. (b) J. Fu, H. Wang, *Cancer Letters,* 2018, 412, 1, 283-288.

3. (a) P. L. Rayford, T. A. Miller, J. C. Thompson, *N Engl J Med.*, 1976, 294(20), 1093-1101. (b) M. J. Thun, J. O. DeLancey, M. M. Center, A. Jemal and E. M. Ward, *Carcinogenesis,* 2010, 31, 100–110.

4. (a) G. T. Nagami, L. L. Hamm, *Adv Chronic Kidney Dis.*, 2017, 24(5), 274-279. (b) R. Zheng, C. Qu, S. Zhang, H. Zeng, K. Sun, X. Gu, C. Xia, Z. Yang, H. Li, W. Wei, W. Chen, J. He, J. Chin, *Cancer Res.,* 2018, 30(6), 571-579.

5. (a) M. Ruscák, H. Hager, J. Orlický, *Acta Neuropathol.,* 1976, 34(2), 149-55. (b) H. Rumgay, M. Arnold, J. Ferlay, O. Lesi, C. J. Cabasag, J. Vignat, M. Laversanne, K. A. McGlynn, I. Soerjomataram, *Journal of Hepatology*, 2022, 77, 1598–1606.

6. (a) M. Zatz, *J Neural Transm Suppl.*, 1978, 13, 97-114. (b) J. D. Yang, P. Hainaut, G. J. Gores, A. Amadou, A. Plymoth, L. R. Roberts, *Nat Rev Gastroenterol Hepatol.*, 2019, 16(10), 589–604.

7. (a) H. Crossland, K. Smith, P. J. Atherton, D. J. Wilkinson, *J Cell Physiol.*, 2018, 233(12), 9663-9673. (b) J. M. Llovet, R. K. Kelley, A. Villanueva, A. G. Singal, E. Pikarsky, S. Roayaie, R. Lencioni, K. Koike, J. Zucman-Rossi & R. S. Finn, *Nat Rev Dis Primers*, 2021, 7, 6.

8. (a) A. Hagiwara, T. Sakamoto, *J Trauma.*, 2009, 67(1), 115-20. (b) A. Forner, M. Reig, J. Bruix, *The Lancet*, 2018, 391, 10127, 1301-1314.

9. E. S. Bialecki, A. M. Di Bisceglie, *HPB (Oxford)*, 2005, 7(1), 26-34.

10. S. D. Ryder, *Gut*, 2003, 52, 1-8.

11. R. Montal, C. Andreu-Oller, L. Bassaganyas, R. Esteban-Fabró, S. Moran, C. Montironi, A. Moeini, R. Pinyol, J. Peix, L. Cabellos, A. Villanueva, D. Sia, V. Mazzaferro, M. Esteller & J. M. Llovet, *British Journal of Cancer*, 2019, 121, 340–343.

12. T. A. Auer, U. Fehrenbach, C. Grieser, T. Penzkofer, D. Geisel, M. Schmelzle, T. Müller, H. Bläker, D. Seehofer & T. Denecke, *Eur Radiol*, 2020, 30, 3497–3506.

13. C. J. Zech, A. Ba-Ssalamah, T. Berg, H. Chandarana, G.-Y. Chau, L. Grazioli, M.-J. Kim, J. M. Lee, E. M. Merkle, T. Murakami, J. Ricke, C. B. Sirlin, B. Song, B. Taouli, K. Yoshimitsu & D.-M. Koh, *Eur Radiol*, 2020, 30, 370–382.

14. W. Wang, C. Wei, *Genes Dis.*, 2020, 7(3), 308-319.

15. S. Schlosser, D. Tümen, B. Volz, K. Neumeyer, N. Egler, C. Kunst, H. C. Tews, S. Schmid, A. Kandulski, M. Müller, K. Gülow, *Front Oncol.*, 2022, 12, 1016952.

16. J. Chen, C. Niu, N. Yang, C. Liu, S.-S. Zou, S. Zhu, *Pharmacological Research*, 2023, 189, 106674.

17. D. Hanahan, R. A. Weinberg, *Cell*, 2011, 144(5), 646-74.

18. R. J. DeBerardinis, N. S. Chandel, *Sci Adv.*, 2016, 2(5), e1600200.

19. Pavlova NN, Thompson CB., Cell Metab. 2016 Jan 12;23(1):27-47.

20. N. N. Pavlova, J. Zhu, C. B. Thompson, *Cell Metab*., 2023, 34, 3, 355-377.

21. A. J. Wolpaw, C. V. Dang, *Biochim Biophys Acta Rev Cancer.*, 2018, 1870(1), 43-50.

22. S. D. Matteis, A. Ragusa, G. Marisi, S. D. Domenico, A. C. Gardini, M. Bonafè, A. M. Giudetti, *Oxidative Medicine and Cellular Longevity*, 2018, 7512159, 13.

23. N. Fujiwara, S. L. Friedman, N. Goossens, Y. Hoshida, *J Hepatol*., 2018, 68(3), 526-549.

24. P. Luo, P. Yin, R. Hua, Y. Tan, Z. Li, G. Qiu, Z. Yin, X. Xie, X. Wang, W. Chen, L. Zhou, X. Wang, Y. Li, H. Chen, L. Gao, X. Lu, T. Wu, H. Wang, J. Niu, G. Xu, *Hepatology*, 2018, 67(2), 662-675.

25. T. Soga, M. Sugimoto, M. Honma, M. Mori, K. Igarashi, K. Kashikura, S. Ikeda, A. Hirayama, T. Yamamoto, H. Yoshida, M. Otsuka, S. Tsuji, Y. Yatomi, T. Sakuragawa, H. Watanabe, K. Nihei, T. Saito, S. Kawata, H. Suzuki, M. Tomita, M. Suematsu, *J Hepatol*., 2011, 55(4), 896-905.

26. R. J. DeBerardinis, A. Mancuso, E. Daikhin, I. Nissim, M. Yudkoff, S. Wehrli, Thompson CB., *Proc Natl Acad Sci U S A.*, 2007, 104(49), 19345-50.

27. S. A. Khan, S. Tavolari, G. Brandi, *Liver Int.,* 2019, 39(Suppl. 1), 19– 31.

28. X. Li, H. Zhu, W. Sun, X. Yang, Q. Nie, X. Fang, *Cancer Cell Int*., 2021, 9, 21(1), 479.

29. J. Spinelli, H. Yoon, A. Ringel, S. Jeanfavre, C. Clish, and M. Haigis, *Science*, 2017, 358, 941-946.

30. I. D. Limón, I. Angulo-Cruz, L. Sánchez-Abdon and A. Patricio-Martínez, *Front. Neurosci.*, 2021, 15, 578922.

31. J. M. Curry, M. Tuluc, D. Whitaker-Menezes, J. A. Ames, A. Anantharaman, A. Butera, B. Leiby, D. M. Cognetti, F. Sotgia, M. P. Lisanti, U. E. Martinez-Outschoorn, *Cell Cycle*, 2013, 12(9), 1371-84.

Chapter – 5

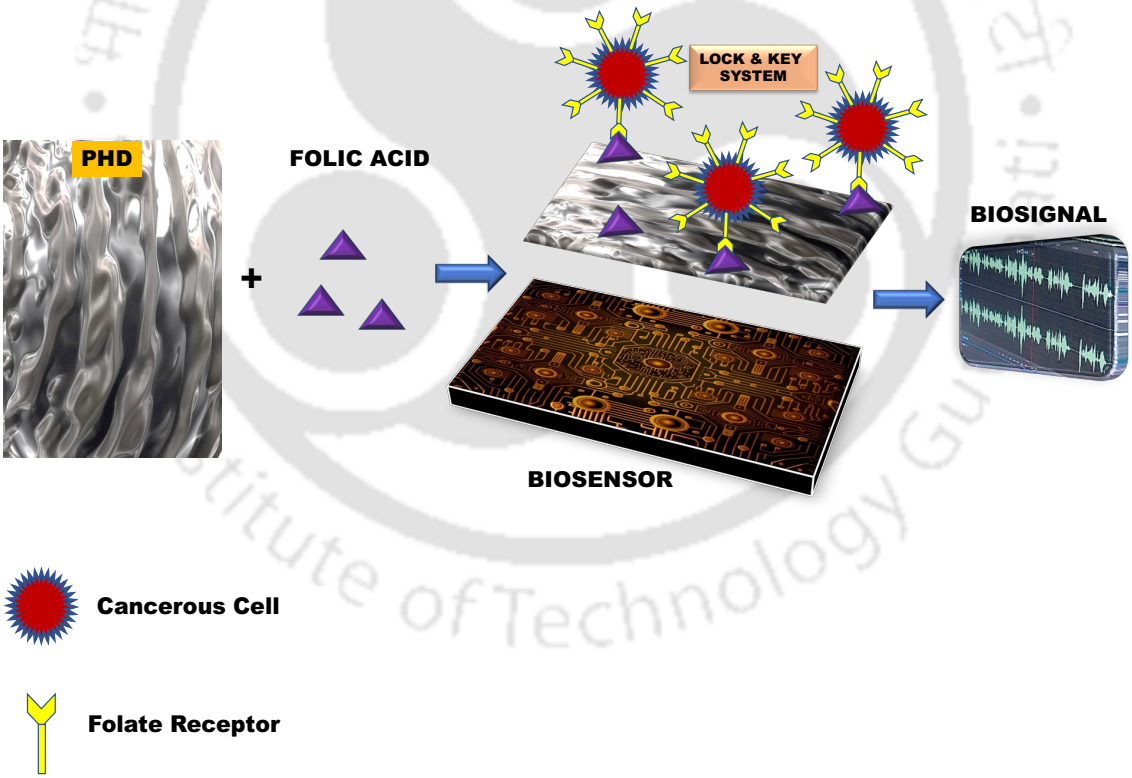

ABSTRACT

Cancer cells grow very quickly, consuming nutrients from the body and also producing additional metabolic waste. Ammonia is one such metabolic waste by-product that is normally transported through blood vessels to the liver, where it is converted into less toxic substances and excreted from the body in the form of urea. It was also found that ammonia accumulates in the local environment of the tumour, where there are few blood vessels. The concentration of ammonia in such an environment causes toxicity to the surrounding cells. Due to the lack of early screening strategies, cancer is the most lethal cause of malignancy and death. Thus, the work showed an effective method to detect cancer cells using folic acid (FA) conjugated with our modified organic electrochemical transistor (OECT). Electrochemical biosensors offer rapid detection, low cost, portability, and ease of use. There are many applications in the field of nanotechnology to improve the sensitivity of biosensors, especially in the context of polyhydroxy derivative OECT prepared by thermal decomposition and then covalently conjugated with FA. The OECT-FA configuration can stably adhere to the surface of HeLa cells by binding to the overexpressed folate receptor (FR), enabling cell detection. The study suggested the possibility of early detection of HeLa cells, which can improve the overall survival of cancer patients in clinical applications. Here, we present an FA-modified substrate integrated with an organic electrochemical transistor. Our goal is twofold: first, to establish a platform for host cells in a more physiologically relevant environment, and second, to demonstrate the efficient integration of different cancer cell detection techniques. Overall, this platform enables large-scale screening for in vitro drug development and toxicology testing and addresses the existing gap in sensor integration in microfluidic devices. This platform provides development and evaluation for oncologists to effectively expand cancer treatment research.

5.1. INTRODUCTION

In recent years, cancer is rapidly becoming the number one killer in many countries. In preclinical testing research, there is a great need to develop faster and easier methods to investigate cancer cells, especially the development of a strategy to identify cancer cells would greatly affect the clinic, suppressing additional therapies. Traditional methods currently used mostly in preclinical testing and cancer cell biology include cytological testing, fluorescent imaging, and radioactive detection [1-4]. These techniques often require extensive experimental processes and rigorous laboratory conditions in addition to instrumentation and expense. However, there is still no universally accepted test. Therefore, it is necessary to develop a viable method sensitive and specific enough to detect cancer cells. Although many biochemical and physical assays are used to study cell physiology and pathology in various environments, label-free methods are preferred for cell characterization or monitoring. As we know, one of the non-invasive methods for cell characterization has been the use of electrochemical impedance spectroscopy (EIS), which provides the frequency-dependent electrical properties of cells related to cell physiology or morphology[5-9]. In this approach, the electrical properties of a single cell were quantitatively evaluated from the measured impedance of cell suspensions [10,11] or of cells embedded in a nucleopore filter[12]. Cancer cells are captured and immobilized before detection on the electrode surface.

A major challenge in cancer treatment today is to achieve a satisfactory balance between the destruction of cancerous tissues and the destruction of healthy tissues, including damage to the immune system and highly proliferative cells (gastrointestinal epithelium and hair follicles). Thus, the detection of cancer cells at a fairly early stage, i.e. in a manageable stage for possible treatment, is essential. As such, recently developed nanotechnology techniques bring hope to the world of oncology research [13]. Nanotechnology is currently being tested and used, but improvements to current technologies and the development of new ones are needed for cancer detection, prevention and treatment. When we look at the tumour microenvironment, passive targeting is a well-known process. In cancer cells, the cytosol tends to be acidic, and at its low pH, some drug conjugates can degrade entering the cancer cells, resulting in the release of the active drug into the target tissues [14]. Even when the drug is administered locally to the tumour tissue, systemic blood flow to the surrounding tissues is usually blocked [15]. Therefore,

locally elevated drug concentrations are allowed in cancer cells without causing toxicity to the surrounding tissues [14]. The advantage of passive targeting is that it can distinguish cancer cells from healthy cells and tissues. In general, cancer cells leak into the vasculature and maintain an acidic tumour microenvironment [15]. This is because rapidly growing cancer cells consist of defective vascular structures that are more permeable to macromolecules than normal tissues. This increased permeability makes cancer tissues easily accessible to chemotherapeutic agents, and the lack of lymphatic drainage in the tumour bed leads to the accumulation of drugs in cancer cells [15]. This effect is called the enhanced permeability and retention (EPR) effect, which can interfere with the cell's ability to take up essential nutrients and oxygen [16]. Some studies have used the high-affinity vitamin folic acid receptor (folate receptor) as a target [17]. The folic acid receptor appears to be a promising target for cancer therapy and detection.

In recent years, folate receptors (FRs) have been used as a strategic target in cancer detection and diagnosis. [21-23] FRs are folate-binding proteins with a high affinity for folic acid (FA) (Kd ¼ 0.1-10 nM) and a molecular weight of 38 kDa. They are overexpressed on the surface of cancer cells or cells infected with parasites that cause tropical diseases such as leishmaniasis [24,25]. Various methods have been developed to detect FR, including cytological testing, fluorescence imaging, and radio labeled assays.[26-28] Although the effectiveness of these methods has not yet been questioned, most of them are expensive and time-consuming processes to implement. Also, some of these approaches involve more serious radioactive risks due to the use of radio labeled tests in the testing process[26, 27]. It is extremely important and important to develop new methods and techniques for FR expression. Electrochemical methods have received considerable attention in the development of biosensors for the detection of disease markers due to their simplicity, speed, and convenience. [29,30]

FA is an attractive ligand useful for targeting cell membranes. The high affinity between FA and FR suggests the use of FA as a biosensing element in the construction of electrochemical sensors. This interaction leads to the blocking of electron transfer across the insulating cell membrane and an accompanying decrease in current.[31-33] Cyclic voltammetry and impedance spectroscopy were used to characterize the interaction between an FR cell and an FA-operated transducer. Various materials such as gold nanoparticles, polydopamine-coated carbon nanotubes, polyaniline nanofibers/gold

nanoparticles, and boron-doped diamond electrodes functionalized with folic acid for electrochemical detection of cellular folate receptors have been used as sensors. [34-36]

The folate receptor, a glycosylphosphatidylinositol-anchored cell surface receptor, is overexpressed in most cancer tissues, while its expression is limited in healthy tissues and organs [18]. Folic acid receptors are highly expressed in epithelial, ovarian, cervical, breast, lung, renal, colorectal, and brain tumours [19]. Folate, also known as pteroyl glutamate, is a nonimmunogenic water-soluble B vitamin essential for DNA synthesis, methylation, and repair (folate is used to synthesize thymine). Folic acid is compact (441 Da), stable over a wide temperature and pH range, inexpensive and non-immunogenic, and retains its ability to bind to the folate receptor after conjugation species or diagnostic markers [20]. The folic acid/folate receptor interaction can be targeted to imaging cancer cells by attaching imaging probe molecules to folate. Probe/folate conjugate detection methods are non-invasive, making them very attractive for use in localizing and staging folate receptor-positive cancers. FR is also an identified tumour antigen/biomarker.[13][23][37] Therefore, diagnostic and therapeutic methods for cancer are being developed that utilize FR activity. FR is a growing therapeutic target in the diagnosis and treatment of cancer and chronic inflammatory diseases.[25] FR expression is selectively increased in certain malignant cells and activated macrophages. [38,39]

FA has a high affinity for cell surface receptors. In addition, it is non-immunogenic, very stable, inexpensive and of small molecular size. Among the various forms of cancer, solid tumours are a particularly aggressive and fast-growing form, most of which overexpress the folic acid receptor, such as ovaries, kidneys, lungs, brain, endometrium, pancreas, stomach, prostate, testicles, bladder, head and neck cancer, breast cancer, and non-small cell lung cancer.[13][23] The voltammetric behaviour of HeLa cells was measured using a graphite electrode as the working electrode and cell suspensions in phosphate-buffered saline (PBS). The analysis showed a peak anodic current but no peak cathodic current. The oxide peak was significantly reduced or disappeared in the second scan compared to the first scan [40,41]. Since electron transfer rates at carbon electrodes are often slower than at metal electrodes, the gold electrode potentially offers very favourable electron transfer kinetics and a large anodic potential range. We currently used immobilized living HeLa cells for electrochemical detection and viability of living cancer cells. [42-44] The emerging field of organic bioelectronics provides access to unique tools for label-free real-time

sensing, potentially bridging the gap between rigid, difficult-to-integrate sensors. An OECT is an organic electrochemical transistor (OECT), a class of organic devices. which contains a thin layer of conductive polymer as active material. OECTs are tripolar devices (source, drain and gate) where a conductive layer is deposited between the source and drain to form a transistor channel. The transistor channel is usually in direct contact with the electrolyte, which also has a gate electrode inside. Poly(3,4-ethylenedioxythiophene): poly (styrene sulfonic acid) (PEDOT: PSS) is a conductive polymer commonly used as an active OECT layer due to its easy processability, chemical tunability, and biocompatibility.

This work involved the fabrication of an OECT folic acid-modified biosensor for the detection of human cervical cancer cells (HeLa). The OECT-FA conjugate could improve the proliferation and attachment of FR and HeLa cancer cells. This may indicate a decrease in faradic current. Developed may be useful for selective monitoring of living cells targeting folic acid receptors in physiologically relevant fluid environments. The OECT-FA configuration is used to diagnose diseases in which FRs are overexpressed in cancer cells.

5.2. EXPERIMENTAL SECTION

5.2.1. MATERIALS AND METHODS

PEDOT: PSS, Acrylic acid, 30% Ammonia solution, Dulbecco's modified Eagle's medium (DMEM) was purchased from Sigma-Aldrich. Fetal Bovine Serum (FBS), Trypsin, and Pen Strep (Antibiotic) were from Gibco. Glycerol was purchased from Merck and p-toluene sulfonic acid from Loba Chemie. All the chemicals were used in this experiment as obtained from the supplier. Electrochemical measurements were carried out using CH instruments Model 700D series and Keithley 2614B. Ag/AgCl was used as the reference electrode and Phosphate buffer solution (10 mM PBS, pH 7.4) as an aqueous electrolytic solution.

5.2.2. CELL STUDIES

For undertaking cancer cells studies, the cell lines liver hepatocellular carcinoma cells (HepG2), Human cervical carcinoma (HeLa), Human breast adenocarcinoma cells (MDA_MB_231) and human embryonic kidney cells (HEK-293) were procured from

NCCS, Pune. The cells were grown in Dulbecco's modified Eagle's medium (DMEM) supplemented with 10% FBS (Fetal Bovine Serum) and antibiotics (Pen Strep) maintained at 5% CO_2 and 37 °C in a humidified incubator.

5.2.3 SENSOR DESIGN AND CONSTRUCTION

As discussed in Chapter 2, 1cm X 2 cm sensor dimensions were fabricated and placed in a beaker with PBS as an electrolyte.

5.2.4 CELL CULTURE AND CONFOCAL MICROSCOPY IMAGING

For the experiments, the cells HEPG2, HeLa, MDA_MB_231 and HEK-293 were trypsinized and 10^5 cells/mL were seeded in 35 mm tissue culture plates and were allowed to attach for 24 hour at 5% CO2 at 37 °C in a humidified incubator. - 30mg/mL was added to the cells. The attached cells were given PBS wash once and were added to the tissue culture plates. The cells were then allowed to incubate with Folic acid for 3 hrs. The cells not treated with Folic acid served as the control group.

5.2.5 CELL IMAGING

The cell imaging studies were performed with a fluorescence microscope. For performing the studies on the cells HeLa and MDA_MB_231 were grown and seeded at a density of 1,00,000 cells/mL in tissue culture plates. The cells treated with Folic acid were given PBS wash and 10µL of Acridine orange (for staining live cells) of a concentration of 1mg/mL was added evenly on the cells and were incubated for 15 min at 37 °C. The excess dye was removed using PBS wash. This was followed by the addition of 10µL Propidium Iodide (for staining the dead cells; 1mg/mL) and incubation of 15 min at 37 °C. The excessive dye was washed using PBS and the cells were fixed using 0.1% formaldehyde and 70% chilled ethanol. The cells were observed under a fluorescence cell imager (Bio-Rad, ZOE) (480nm).

5.2.6. ELECTRICAL CHARACTERIZATION

All the electrical characterizations of the devices were carried out under ambient conditions at room temperature using a Keithley2614B. A positive Gate bias (Vg) was applied with Ag/AgCl electrode and the two aluminium electrodes served as a source (S) and drain (D). The cell sensing experiments were performed at Drain voltage V_d = -0.2 V with a Gate voltage V_g sweep ranging from 0 to 0.9V in 5ml electrolyte solution at a pH of 7.4.

5.3. RESULTS AND DISCUSSION

5.3.1. ELECTROCHEMICAL DETECTION OF HeLa CELLS

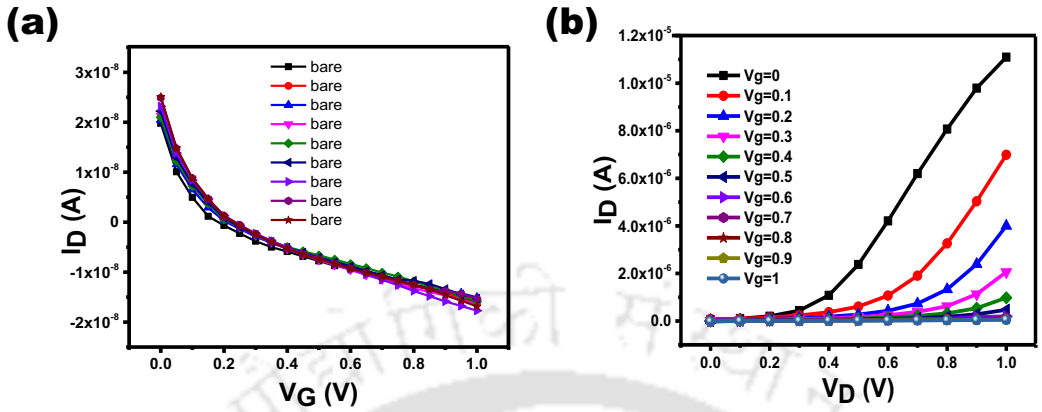

Figure 5.1. OECT-PHD/FA Hybrid Sensor Characteristics. a) Transfer Characteristics (I_D-V_G). b) Drain Characteristics (I_D-V_D).

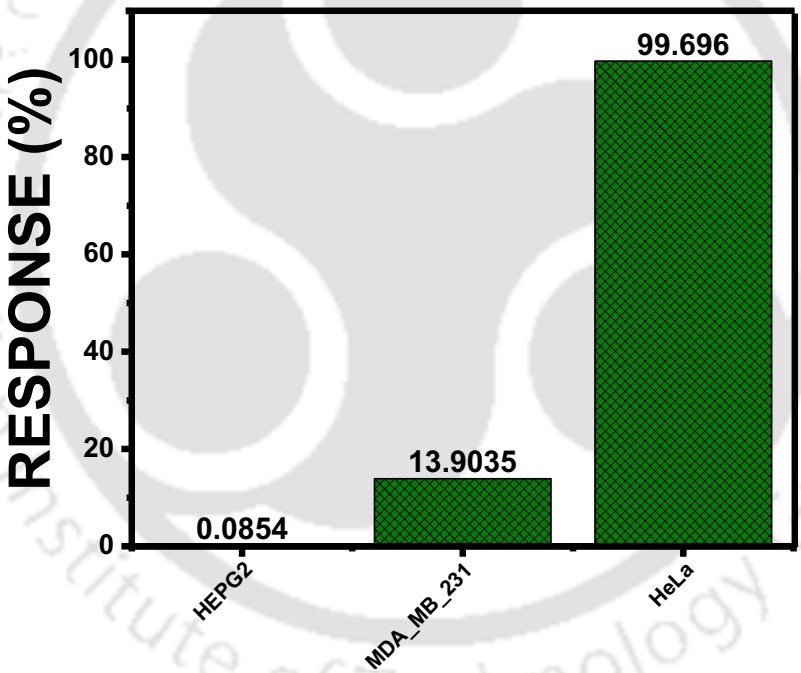

Figure 5.2. Selectivity Study of different cell lines.

The OECT and poly-hydroxyl derivatives used for coating are shown in Chapter 4. The electronic transfer characteristic is indicated at V_d = -0.2V and drain characteristics at different gate voltages are shown in Fig. 5.1. The measurements were done under positive gate bias which subsequently changes the channel conductance through injection of ions from the aqueous medium. This process, in turn, affects the conductivity of the PEDOT: PSS layer which is referred to as doping/de-doping of PEDOT: PSS. The transistor characteristic of the OECT is due to ions acting as charged carriers contributing to its high sensitivity. Therefore, these characteristics may result in a built-in amplification entity.

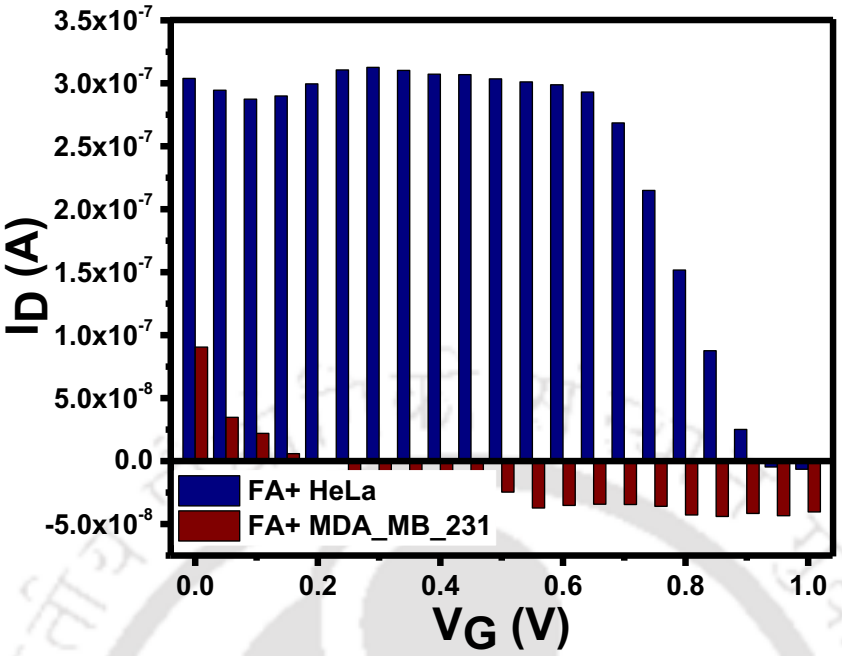

Figure 5.3. OECT-PHD/FA Hybrid Sensor Response to HeLa and MDA_MB_231 cell lines.

The functionalization of device surfaces is required. Various methods have been reported for surface functionalization. FA is a water-soluble vitamin of the B-complex group. Mammals are incapable of synthesizing FA and must obtain it from their dietary intake. The cell internalizes FA with the help of specialized molecules on the cell surface called FR. The FR has a high affinity towards FA. These molecules are responsible for the uptake of FA from the blood into the inside of the cell. The selective increase in the uptake of FA by malignant cells led to the idea that FA could be used as a targeting moiety. The high affinity between FR and FA makes them work as a lock and key technology with the cancer cell, which serves as an attractive property for tumour detection and therapy. Therefore, the selectivity of FA immobilized on the transistor surface will be able to catch FR-rich tumour cells in our system. Most cancer cells can express abundant FR on their surfaces. Thus, FR-rich HeLa cells were chosen as a model to construct a typical OECT sensor in this study.

OECTs conjugated with PHD mesoporous membrane were implored with FA immobilized on surfaces for electrochemical selectivity. This modified OECT with FA/PHD bed has been investigated for applications in electrochemical analysis and biosensor fields because PHD are hydrophobic, stable, and promising in nanotechnology applications. On the other hand, it can introduce functional groups, such as carboxylic (COO-) and OH- through

chemistry for further linking biomolecules. In this paper, FA were deposited on a PEDOT: PSS/PHD OECT surface, to covalently bond folic acid (FA) (to make PEDOT: PSS/PHD/FA). The basic idea of the measurement is that the cells on the OECT surface essentially hinder unrestricted current flow from the electrode into the bulk electrolyte and thereby increase the overall electronic potential when human cervical carcinoma (HeLa) cells attach on the surface of a PEDOT: PSS/PHD/FA OECT. This OECT can detect folate receptor (FR)-rich HeLa cells suspended in phosphate-buffered saline (PBS), with high sensitivity and selectivity using a 2614B Keithley Instruments without additional labelling. The PEDOT: PSS/PHD/FA layer-by-layer (LBL) deposited on the transistor surface was used to assemble the device. Negatively charged species would reduce the non-specific binding of cells by electrostatic repulsion due to the negative charge on the cell membrane. The amperometric measurements were carried out in HeLa cells suspended in DMEM by PEDOT: PSS/PHD/FA transistor. The change in current was recorded immediately with the immersion of cell suspensions for a variety of cancer cell lines. It can be seen that the concentration of 10^5 cells mL^{-1} HeLa cell can be detected using this method. The electrochemical signal was directly related to the number of cells attached to the surface of the modified OECT.

In particular, PEDOT: PSS thin films exhibit p-type semiconductors, where cell bonding induces a potential that penetrates the PEDOT: PSS/PHD/FA surface and changes its conductivity. These results indicate that HeLa cells were effectively captured by FA molecules immobilized on the FA-modified surface. The FA-modified slides were also incubated with HEPG2 and MDA_MB_231 cells, but only some cells were adsorbed on the surface, which suggests the excellent selectivity of the FA-modified transistor toward FR-rich cancer cells. The above measurements were carried out in HeLa cells suspended in PBS in the absence of other cells. The figure 5.2 shows that the FR-lack cells have little effect on the relative potential. Based on the above results, FA-modified transistors can selectively detect cancer cells from normal cells with high sensitivity, and stability. In this study the integration of OECTs as sensors to allow electrical monitoring of the surface changes has been preceded. Cells incorporated on the OECT can determine the electrical selectivity of the live cancer cell. The results clearly demonstrate that the OECT– FA sensors are capable of the real-time monitoring of cancer cell lines.

The OECT–folic acid-modified configuration was characterized by Keithley Instruments. The modification of the OECT with folic acid led to a conductivity change in the resultant signal. The human cervical cancer cells were attached to the modified electrode through the folic acid–folate receptor interaction. From the current measurements, the binding of the folate receptor from human cervical cancer cells to the OECT–folic acid configuration has been demonstrated because of lowered electron transfer resulting in a decrease in the measured current. From the control experiments, it has been confirmed that the OECT–folic acid configuration specifically recognized folate receptors.

5.3.2. FA AS BIOMARKER FOR THE REAL-TIME ELECTRICAL DETECTION OF HELA CELL LINE

We have tested the electrical responses of our devices to FA in real-time. All the following real-time electrical measurements were conducted at a constant bias voltage. The devices were kept in a 5ml DMEM at pH 7. We have used FA as a binding site to attach cells in DMEM and the device exhibited current readouts in real-time. After adding the HeLa cells in DMEM, the conductance of our device exhibits a noticeable gradual difference. On the other hand, the device shows less or no obvious conductance change when other cell lines like HepG2, and MDA_MB_231 were added respectively. This study clearly demonstrates that OECT-PHD/FA device can indeed show significant response specifically to HeLa in DMEM solutions (Fig. 5.2). This study could clearly demonstrate that the OECT–PHD/FA devices can function as a highly sensitive sensor for the detection of HeLa cell media. This shift can be attributed to the hydrogen bond effect of the OECT-PHD complex to the PEDOT: PSS/PHD/FA channel as a result of binding to HeLa. Therefore, the binding of HeLa to PHD/FA is equivalent to the hydrogen bond effect to OECT-PHD. This hydrogen bond effect explains the shifting of the current upon the introduction of HeLa and is consistent with the reduction of conductance in the transport branch of the OECT-PHD devices.

5.3.3. CANCER CELL DETECTION WITH OECT

According to the present fabricated device design, OECTs can be used for the analysis of living cancer cells by recording channel currents at the V_d of -0.2 V DMEM media. The change in the current response of HeLa cells indicates the attachment of more cells to the channel. To demonstrate the selectivity of the device (Fig. 5.3), we also tested other types of cell lines HEPG2 and MDA_MB_231 using the same OECTs. In general,

MDA_MB_231 cells are ER-negative breast cancer cells, while HeLA cells and HEPG2 cells are ER-positive cancer cells, which showed a much greater response to binding to surfaces by adsorption. Therefore, the OECT-based biosensor showed good selectivity towards overexpressed FA cells. These results are useful for analyzing certain cells.

5.3.4. SWELLING STUDY

PHD 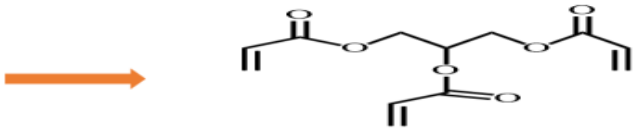

NAME	AFTER 5 MINS	AFTER 10 MINS
PHD (FILM)	11.41%	52.71%

NAME	AFTER 5 MINS	AFTER 10 MINS	AFTER 15 MINS
PHD (POWDER)	39%	60%	98.8%

Table 5.1. Swelling Study of PHD.

The membrane was weighed before swelling and the weight was recorded. The sample was then immersed in 200 ml PBS solution. At the same time, a stopwatch was started, which recorded the swelling time of the sample (the time of the sample immersed in the PBS solution). After the prescribed swelling time of 5 minutes, the sample was removed from the solution and surface water was quickly removed with filter paper. The sample was weighed on an electronic scale and the weight was marked for the next step of management. The swelling ability of PHD (Table 5.1) determines its hydrophilicity and strengthens it as a hydrogel. The swelling of PHD is due to the presence of carboxyl groups in the structure of the hydrogels. In addition, the swelling process can occur in three different steps: (a) diffusion of water molecules through the matrix, (b) relaxation of polymer chains through hydration, and (c) expansion of the polymer network upon relaxation. This process occurred when the PHD hydrogel was immersed in PBS, the hydrophilic polymer chains exerted osmotic pressure on the hydrogel, resulting in the swelling of the hydrogel matrix. Thus, easy transport of analytes can occur through this mesoporous PHD hydrogel.

Hydrogels were classified into two categories: the chemical gel was covalently cross-linked. Physical gel: Networks held together by molecular entanglement, ionic forces, hydrogen bonds or hydrophobic interactions. Here were cross-linked gels (physical interactions) that occur between different polymer chains. The swelling of hydrogels between their polymer chains in response to environmental changes such as temperature, pH, electric field, radiation, etc., is promising as smart materials with increasing interest in various biomedical, industrial and agricultural applications. The swelling properties of the hydrogel were very important and very dependent on the chemical structure of the gel. The hydrophilicity of the network resulted from the presence of chemical residues such as hydroxyl (-OH), carboxyl (-COOH), amide (-CONH-), primary amide ($-CONH_2$), sulfonic acid ($-SO_3H$). and others can be found in the polymer body. However, by mixing or polymerizing hydrophilic and hydrophobic polymers, it was also possible to produce hydrogels with a significant proportion of hydrophobic polymer. Under these conditions, hydrogels can retain water and are suitable for drug diffusion, many hydrogel-based networks have been developed and are being prepared as smart drug carriers. Complex textures were created thanks to hydrogen bonding. Mixtures of two or more polymers can form a polymer composite. It was well known that composites could be made with superior properties that the constituent materials might not have. The interfacial properties influenced the properties and performance of these compounds. One of the most attractive features was their dielectric properties, which could be widely varied by choosing the shape, size and conductivity of the polymer of the filling ingredients; most of the interesting properties of polymers were complex motions in their molecular matrix. The polymer interfaces act as charge carriers. Therefore, it has become necessary to show the effect of interfaces on the transport, storage and generation of charge carriers in polymer systems. Thus, in covalently cross-linked hydrogels composed of OH functional groups in different proportions, it was observed that the maximum swelling occurs due to the free -COOH functional groups of acrylic acid. These groups increased the swelling capacity significantly than other hydrogels. [45]

5.3.5. FLUORESCENCE CELL IMAGER BIO-RAD ZOE

Fluorescence microscopy between HeLa and MDA_MB_231 cells (Figures 5.4 and 5.5) showed a strong fluorescence signal in HeLa cells, while the signal observed in MDA_MB_231 cells was negligible, confirming the ability of this FA to discriminate between FR-a positive and FR-a negative cell lines as well as those with features like

similar properties and morphology which is promising for future cancer diagnostics. The electrochemical system can provide a very sensitive signal for cells attachment, and the electrochemical data can also provide the parameters of cell capture and immobilization. In order to further confirm the fact that the current change has really resulted from HeLa cells capture and immobilization, the selective capture of HeLa cells on the FA-modified PEDOT: PSS/PHD surface was further confirmed by fluorescent microscopy. A large number of cells could be observed on the surface of FA-coated slides which were incubated with HeLa cells. HeLa and MDA_MB_231 cells were incubated for 12 h.

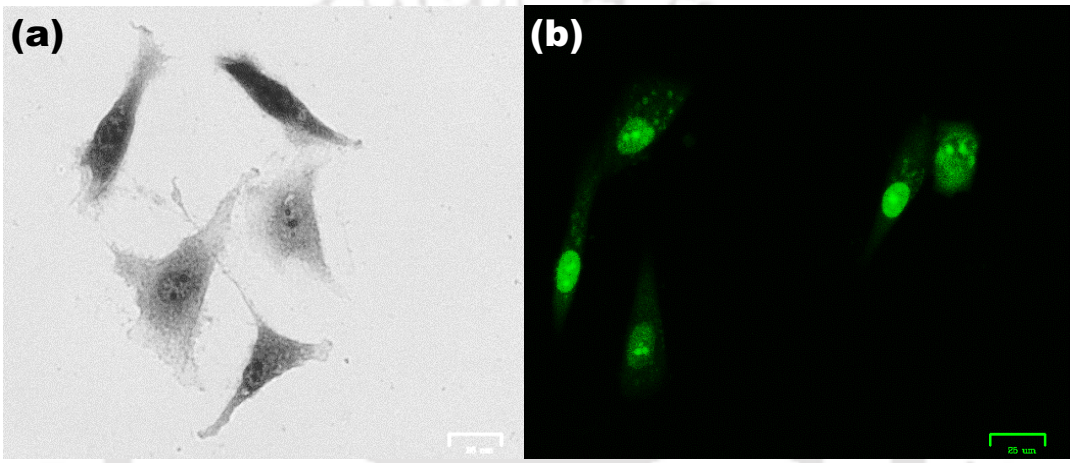

Figure 5.4. Fluorescence Imaging of MDA_MB_231. a) Before the addition of ammonia (Bright field); b) After the addition of ammonia (Green Field).

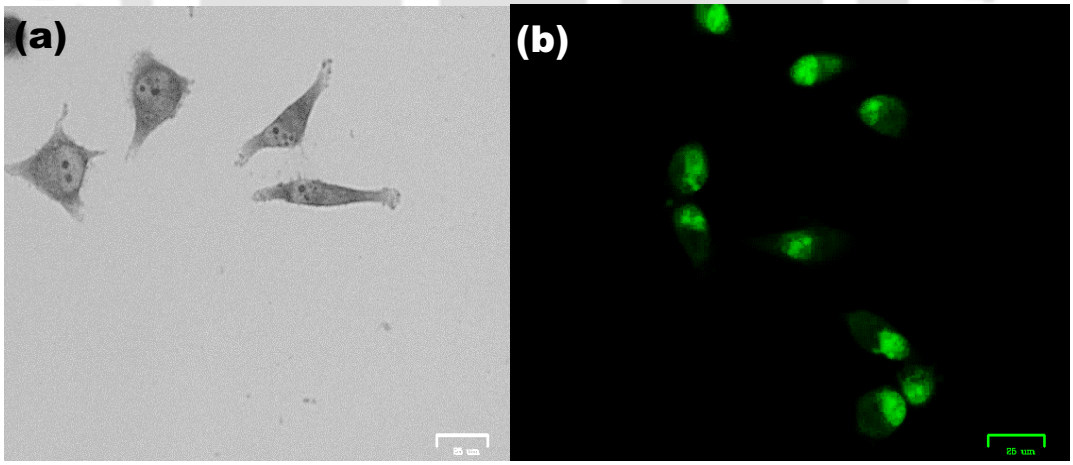

Figure 5.5. Fluorescence Imaging of HeLa. a) Before the addition of ammonia (Bright field); b) After the addition of ammonia (Green Field).

5.4. CONCLUSION

Folate receptor-targeting constructs have been developed against FRa-expressing tumours, which have their own advantages and limitations. Several technologies have been

investigated in this area, these strategies and platforms are also applicable to FRb-expressing tumours (since folic acid effectively binds both FRa and FRb) and represent an exciting emerging field. In addition to PET, CT, SPECT and fluorescence imaging; Transistor PoCs (point-of-care diagnostics) have recently emerged as an attractive option due to the relatively simple nature of the biotechnology. Therefore, the interaction between folic acid immobilized on the PEDOT: PSS/PHD layer and its overexpressed receptor on the cancer cell membrane without additional labelling is used to detect cancer cells containing folate receptors using electrochemical transistor technology. The results were confirmed by comparison with the acridine orange cell viability assay. The results show that cell-based electrochemical detection, which is fast and easy to perform, enables cell identification and viability. This OECT method can provide a simple way to study cell viability, cell growth, and the effects of anticancer drugs on cancer cells. In addition, we confirm the potential of PHD as a hydrogel to transport molecules. Polymer hydrogel has received increased attention in many application fields, including the medical field; can carry and release drugs. Therefore, the modified OECT described here opens new possibilities for future applications in the diagnosis of early cancers in which cells overexpress folate receptors. Future drug development and toxicology testing may benefit significantly from more predictive and multiparametric in vitro models. Despite recent advances in microfluidics and, more recently, organ-on-a-chip technology, there is still a high demand for real-time monitoring systems that can be easily managed. In addition, multiparameter monitoring is important to improve the prognostic quality of data used to inform subsequent clinical trials.

5.5. REFERENCES

1. K. Brindle, *Nat Rev Cancer*, 2008, 8, 94–107.
2. T. Mosmann, *Journal of Immunological Methods*, 1983, 65, 1–2, 55-63.
3. L. Ruei-Min, H. Yu-Chyi, L. I-Ju, L. Chi-Chiu, T. Han-Zen, L. Hsin-Jung & W. Han-Chung, *J Biomed Sci,* 2020, 27, 1.
4. L. Zhong, Y. Li, L. Xiong, W. Wang, M. Wu, T. Yuan, W. Yang, C. Tian, Z. Miao, T. Wang & S. Yang, *Sig Transduct Target Ther*, 2021, 6, 201.
5. I. Giaever, C. Keese, *Nature*, 1993, 366, 591–592.
6. I. Giaever, C. Keese, *Proceedings of the National Academy of Sciences of the United States of America,* 1991, 88(17), 7896-7900.

7. R. Wang, J. Di, J. Ma, Z. Ma, *Electrochimica Acta*, 2012, 61, 179-184.
8. L. Yi-Ting, C. Yeh-Shiu, L. Jun-Chih, H. Yu-Han, L. Chun-Min, *Sensors and Actuators B: Chemical*, 2019, 288, 707-715.
9. H.S. Magar, R.Y.A. Hassan, A. Mulchandani, *Sensors*, 2021, 21, 6578.
10. H. P. Schwan, *Ann. N. Y. Acad. Sci*, 1965, 125, 2, 344-354.
11. H. P. Schwan, *Ann. N. Y. Acad. Sci*, 1968, 148, 1, 191-209.
12. J.-Z. Bao, C. C. Davis and R. E. Schmukler, *IEEE Transactions on Biomedical Engineering*, 1993, 40, 4, 364-378.
13. G. L. Zwicke, G. A. Mansoori, C. J. Jeffery, *Nano Rev.*, 2012, 3.
14. K. Cho, X. Wang, S. Nie, Z. Chen, D. Shin, *Clin Cancer Res,* 2008, 14,1310-6.
15. G. Kim, S. Nie, D. Shin, *Mol Cancer Ther*., 2006, 5, 1909–11.
16. P. Rubin, G. Casarett, *Clin Radiol.*, 1966, 17, 346–55.
17. J. F. Kukowska-Latallo, K. A. Candido, Z. Cao, S. S Nigavekar, I. J. Majoros, T. P. Thomas, L. P. Balogh, M. K. Khan, J. R. Baker Jr, *Cancer Res.*, 2005, 65(12), 5317-24.
18. H. Yoo, T. Park, *J Control Release*, 2004, 100, 247–56.
19. P. Garin-Chesa, I. Campbell, P. E. Saigo, J. L. Lewis, L. J. Old, W. J. Rettig, *Am J Pathol*., 1993, 142, 557–67.
20. C. Muller, R. Schibli, *J Nucl Med*., 2011, 52, 1–4.
21. K. Se-Lim, J. Hwan-Jeong, K. Eun-Mi, L. Chang-Moon, K. Tae-Hyoung, and S. Myung-Hee, *J Korean Med Sci*., 2007, 22(3), 405-411.
22. E. Basal, G. Z. Eghbali-Fatourechi, K. R. Kalli, L. C. Hartmann, K. M. Goodman, E. L. Goode, B. A. Kamen, P. S. Low, K. L. Knutson, *PLOS ONE*, 2009, 4(7), e6292.
23. M. Fernandez, F. Javaid and V. Chudasama, *Chem. Sci.*, 2018, 9, 790–810.
24. D. Richard, P. Leprohon, J. Drummelsmith, and M. Ouellette, *The Journal Of Biological Chemistry*, 2004, 279, 52, 54494 –54501.
25. Y. Young-Su, *IMMUNE NETWORK*, 2016, 16, 6, 337-343.
26. A. B. Chinen, C. M. Guan, J. R. Ferrer, S. N. Barnaby, T. J. Merkel, C. A. Mirkin, *Chem Rev*., 2015, 115(19), 10530-74.
27. H. Kobayashi, M. Ogawa, R. Alford, P. L. Choyke, Y. Urano, *Chem Rev.*, 2010, 110(5), 2620-40.
28. E. R. Zarrella, M. Coulter, A. W. Welsh, D. E. Carvajal, K. A. Schalper, M. Harigopal, D. L. Rimm & V. M. Neumeister, *Lab Invest*, 2016, 96, 1016–1025.
29. Y. Zheng, H. Karimi-Maleh, L. Fu, *Chemosensors*, 2022, 10, 194.

30. Q. Ning, S. Feng, Y. Cheng, T. Li, D. Cui, K. Wang, *Mikrochim Acta.*, 2022 , 189(8), 310.
31. R. Geetha Bai, K. Muthoosamy, R. Tuvikene, H. Nay Ming, *Nanomaterials,* 2021, 11, 1272.
32. J. Lius, Y. Qin, D. Li, T. Wang, Y. Liu, J. Wang, E. Wang, *Biosensors and Bioelectronics*, 2013, 41, 436-441.
33. J. J. Castillo, W. E. Svendsen, N. Rozlosnik, P. Escobar, F. Martíneza and J. Castillo-León, *Analyst*, 2013,138, 1026-1031.
34. J. H. Kim, Y. J. Suh, D. Park, H. Yim, H. Kim, H. J. Kim, D. S. Yoon, K. S. Hwang, *Biomed Eng Lett*., 2021, 11(4), 309-334.
35. A. Bonanni, M. Pumera and Y Miyahara, *Phys. Chem. Chem. Phys*., 2011,13, 4980-4986.
36. Á. Terán-Alcocer, F. Bravo-Plascencia, C. Cevallos-Morillo, A. Palma-Cando, *Nanomaterials (Basel)*, 2021, 11(1), 252.
37. J.A. Ledermann, S. Canevari, T. Thigpen, *Annals of Oncology*, 2015, 26, 10, 2034-2043.
38. A. R. Poh, M. Ernst, *Front Oncol.*, 2018, 8, 49.
39. S. P. Hussain, C. C. Harris, *Int. J. Cancer*, 2007, 121,2373–2380.
40. R. Islam,1, H. T. L. Luu and S. Kuss, *J. Electrochem. Soc*., 2020, 167, 045501.
41. J. G. Manjunatha, *Heliyon*, 2018, 4(11), e00986.
42. D. Baron, E. LaBelle, D. Coursolle, J. A. Gralnick, D. R. Bond, *J Biol Chem*., 2009, 284(42), 28865-73.
43. T. Sun, B. D. A. Levin, J. J. L. Guzman, A. Enders, D. A. Muller, L. T. Angenent & J. Lehmann, *Nature Communications*, 2017, 8, 14873.
44. M. Velický, D. F. Bradley, A. J. Cooper, E. W. Hill, I. A. Kinloch, A. Mishchenko, K. S. Novoselov, H. V. Patten, P. S. Toth, A. T. Valota, S. D. Worrall, and R. A. W. Dryfe, *ACS Nano*, 2014, 8, 10, 10089–10100.
45. I. A. Latif, H. M. Abdullah, M. H. Saleem, *American Journal of Polymer Science*, 2016, 6(2), 50-57.

Chapter – 6

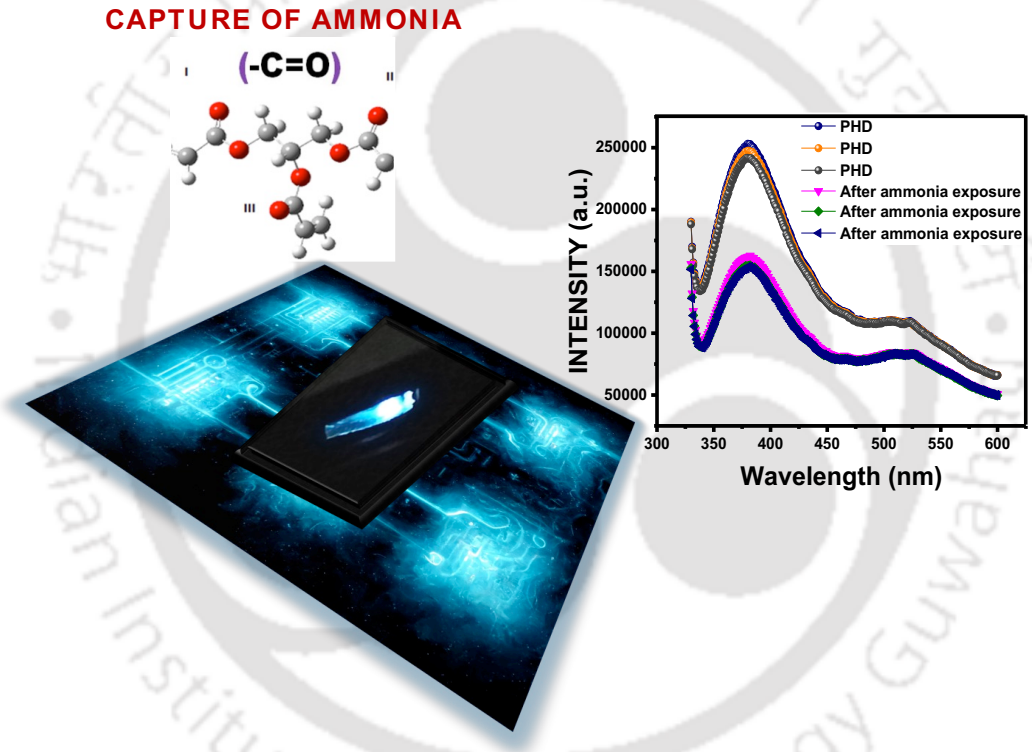
CAPTURE OF AMMONIA
(-C=O)
PHD
PHD
PHD
After ammonia exposure
After ammonia exposure
After ammonia exposure
INTENSITY (a.u.)
250000
200000
150000
100000
50000
300
350
400
450
500
550
600
Wavelength (nm)

ABSTRACT

Ammonia, used as a reactive form of nitrogen in agricultural processes, can have negative effects on human health and the environment, including skin/eye irritation and damage to sensitive ecosystems. It is known that industrialization and population growth, together with more intensive agricultural practices, have led to a stronger accumulation of ammonia in the environment. As such, on-site monitoring of ammonia concentrations is beneficial to human health. These monitoring methods must be sensitive at low doses, resistant to corrosion and, most importantly, more cost-effective than the established but inhibitory methods. In this paper, we describe the fabrication of a sensitive two-electrode UV amplification system to detect ammonia in its gaseous form at room temperature.

6.1 INTRODUCTION

Ammonia (NH_3) emissions are a growing problem worldwide due to their toxic and reactive nature. Although atmospheric emissions of NH_3 have decreased slightly in recent years, many agro-industries make the Indo-Gangetic plains one of the largest emitters of ammonia in the world.[1] Exposure to NH_3 has serious consequences for human health. Inhalation, ingestion or direct contact with NH_3 causes many side effects such as inflammation, tissue damage and many other scars due to its reaction with water and the formation of ammonium ions.[2] Due to its pungent smell, NH_3 is detectable between 5-53 ppm and causes extreme irritation above 80 ppm concentration.[3] Extensive research has led to the development of several ammonia detection systems. They are based on (but not limited to) colourimetric or fluorometric methods, gas or liquid chromatography-based methods, and electrochemical or enzyme-based methods. However, each method has advantages or disadvantages in terms of sensitivity, selectivity, ease of preparation, production costs, efficiency and stability compared directly to the others.[4]

One example of an ammonia detection system is the use of silver nanoparticles. UV exposure to silver nitrate solution enables the synthesis of silver nanoparticles. The colourimetric change mediated by these silver nanoparticles results in the detection of ammonia in solution in the range of 1-100 ppm. Thus, the availability of such detection methods makes it possible to measure ammonia in solutions such as water. However, the manufacturing and synthesis of such silver nanoparticle-based ammonia sensors are not environmentally friendly and pose a threat to the ecosystem.[5,6,7] Therefore, there is an urgent need to design less hazardous and more sensitive ammonia sensors. In this study, we have established a UV-based two-electrode ammonia detection system that is stable at room temperature. In the current state, ammonia can be detected in its gaseous form. The current trace is detectable in the controlled system in the absence of ultraviolet radiation. In the presence of UV, the amplitude of the current decreases. The existence of ammonia induces a drop in current intensity. Such reduction is further enhanced in the presence of UV. This enables sensitive detection of ammonia. Therefore, we report a UV-based design of an ammonia sensor that is sensitive, scalable, cost-effective, reusable and eco-friendly.

6.2. EXPERIMENTAL SECTION

6.2.1 MATERIALS AND METHODS

PEDOT: PSS, Acrylic acid and 30% Ammonia solution was purchased from Sigma-Aldrich. Glycerol was purchased from Merck and p-toluene sulfonic acid from Loba Chemie. CV measurements were carried out using a CH instruments Model 700D series. The thickness of the deposited films was optimized using a profilometer (Dektat-150).

6.2.2. SENSOR DESIGN AND CONSTRUCTION

As discussed in Chapter 2, 1cm X 2 cm sensor dimensions were fabricated and placed in a beaker.

6.2.3. ELECTRICAL CHARACTERIZATION AND MEASUREMENTS

All the electrical characterizations of the devices were carried out under ambient conditions at room temperature using a Keithley2614B. The two aluminium electrodes served as positive and negative terminal. The analyte and ammonia solutions were confined in a 10 mL beaker and mixed with electrolyte prior to testing.

6.3.RESULTS AND DISCUSSION

6.3.1. ELECTRICAL MEASUREMENTS

A two-terminal device was fabricated with a poly-hydroxyl derivative used for coating. The electronic transfer characteristic indicated at UV on/off is shown in Figure 6.1a. The measurements were done inside a black box under UV on state subsequently changes the channel conductance and current changes. Again, after exposure to ammonia the current further shifts (Figure 6.2b).

This system is found to be highly sensitive towards ammonia, i.e., it forms an ammonia-sensitive layer. Hence, the presence of a small concentration of ammonia is selectively detected. It is found that the electron transfer curve shifts significantly upon the addition of different concentrations of ammonia. Various analytes, such as diethylamine, propylamine, ethanolamine, triethylamine, pyridine and cyclohexylamine have been tested with this device system.

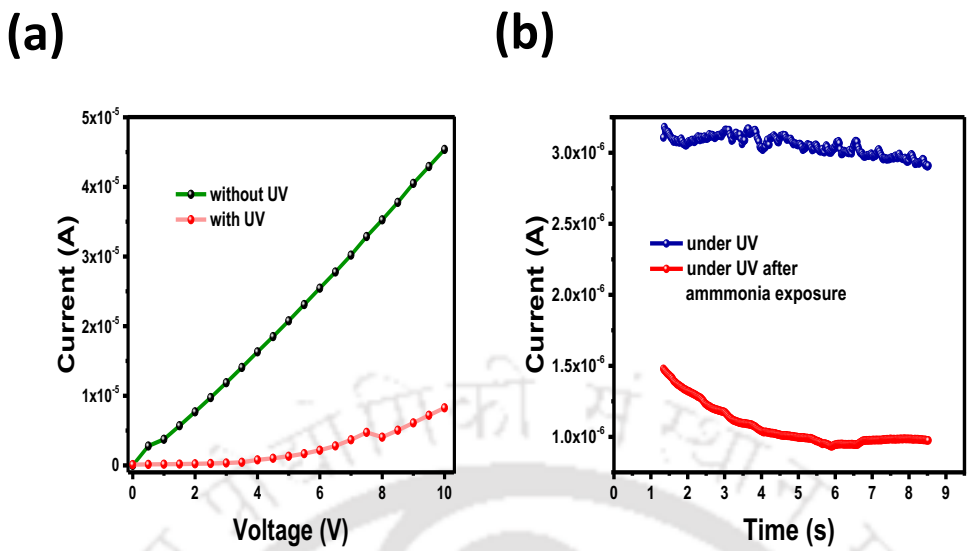

Figure 6.1. Device characteristics. (a) Current Output without and with UV. (b) Current Output under UV after ammonia exposure.

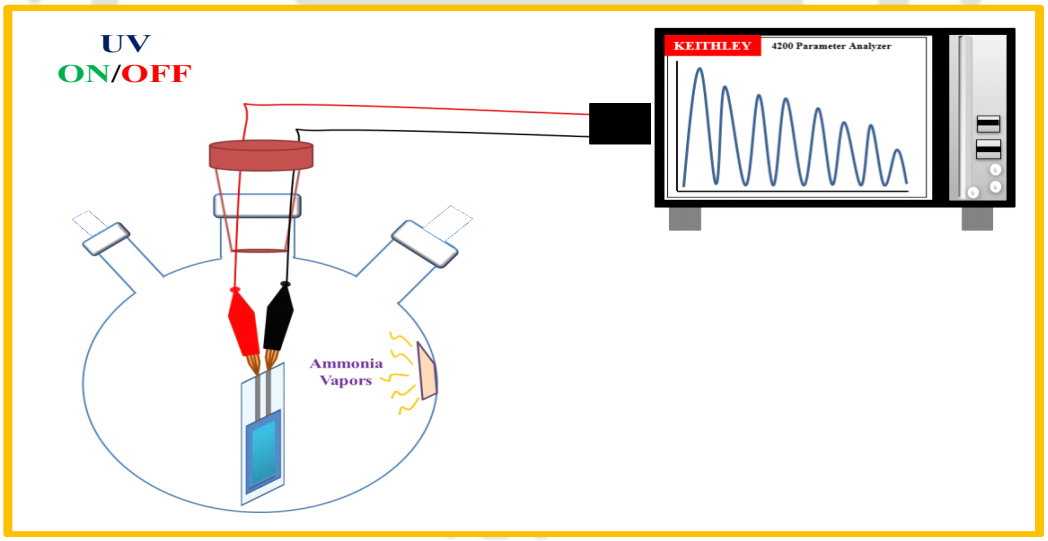

Figure 6.2. Device Setup under UV off and illumination.

6.3.2. SENSING MECHANISM

Two terminal sensing device is based on a base layer of PEDOT: PSS polymer with a polyhydroxyl layer on top of it. In normal ambient conditions of 298K and 1 bar pressure, the I-V Characteristics of the two-terminal device are shown in Figure 6.1. On further analysis, it is evident that there is a change in current values when the device is exposed to

NH_3(g). The reduction in current is due to the elevation in resistance values of the device due to ionic interactions between NH_3(g) with polyhydroxyl (PHD) layer based on dipolar interactions between polar ammonia gas and polar carboxy part (-COO-) of polyhydroxyl layer of the sensor.

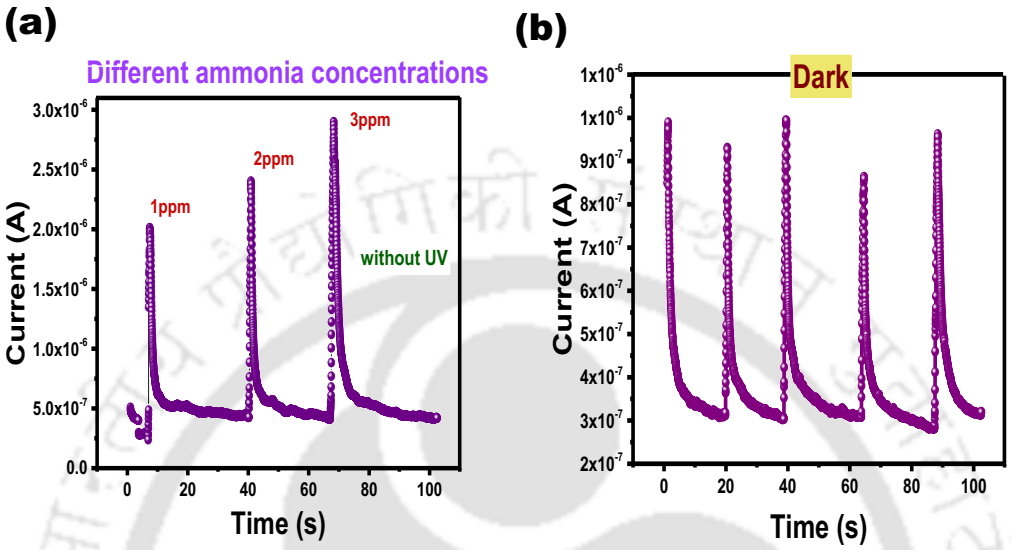

Figure 6.3. Sensor Response to ammonia. (a) Current Output with different ammonia concentrations. (b) Current Output under dark after ammonia exposure showing reusability of device.

When ammonia gas NH_3(g) interacts with the PHD layer it is absorbed due to many ionic interactions mainly in terms of H- bonds formed between the polycarboxy (-COO-) part of PHD and ammonia vapours. This absorbtion of ammonia molecules leads to depletion in electron density at PEDOT: PSS showing p-type material properties. Further, current values are seen with increasing ambient concentration of ammonia vapours (NH_3(g)) which clearly indicates the increasing absorbtion of ammonia vapours on the sensing PHD layer and in turn making the PEDOT: PSS Layer (Fig. 6.3a). The reusability of the device has been explored as seen in figure 6.3b. As seen in the Figure 6.3b, upon exposure to ammonia and removal of ammonia the current values increase and drop respectively. We can clearly deduce that sensor current varies inversely with increasing ambient ammonia vapour concentration; which is clearly signifying the p-type semiconducting behaviour of the sensor. This property is further analysed with other reducing analytes like diethylamine, propylamine, ethanolamine, triethylamine, pyridine and cyclohexylamine (Fig. 6.4). Results obtained clearly indicate that the sensor behaves as a p-type semiconducting material in the presence of almost all reducing analytes and the maximum selectivity of the sensor for ammonia vapours is clearly seen.

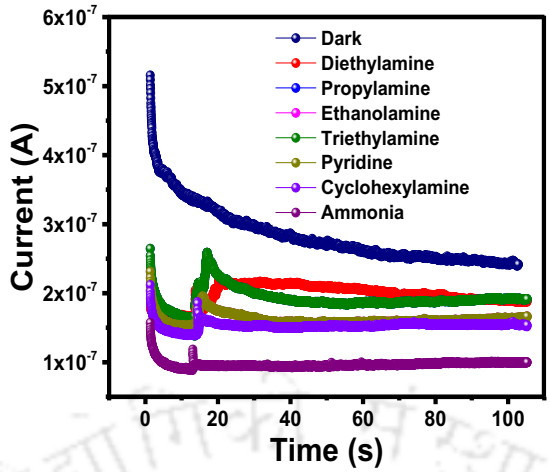

Figure 6.4. Current Output with different analytes under dark.

The device is highly sensitive and selective towards NH_3(g) vapours can be explained on the basis of the maximum interaction of NH_3(g) with the PHD layer. Among all the gaseous analytes, NH_3(g) has maximum potential for H-bonds which is around 6 H-bonds per molecule of ammonia. In all other cases, the association between vapours and PHD is somewhat weaker due to fewer H- bonds formed per molecule, making the device most selective for ammonia detection. Furthermore, the gas sensing capability of our device is purely based upon the interaction of absorbed gas with the PEDOT: PSS base layer making it a p-type semiconducting material. These interaction changes the resistance or conductance profile of the conduction band which is evident in variation in the I-V characteristic of the device.

6.3.3. EFFECT OF UV RADIATION

Ultra-violet radiations are highly energetic which leads to homolytic bond cleavage of covalent bonds present in organic molecules of the sensing layer producing various free radicals in the process. Irradiation of UV rays makes the sensing surface more oxidising due to a high number of free radicals generated in homolytic bond cleavage which in turn increases the absorbtion of reducing analytes over it. Due to the more concentrated absorbtion of gas over the PHD sensing layer, a further change in current is seen in the I-V characteristic of the sensor. It is evident that the device is highly sensitive and selective towards NH_3(g).

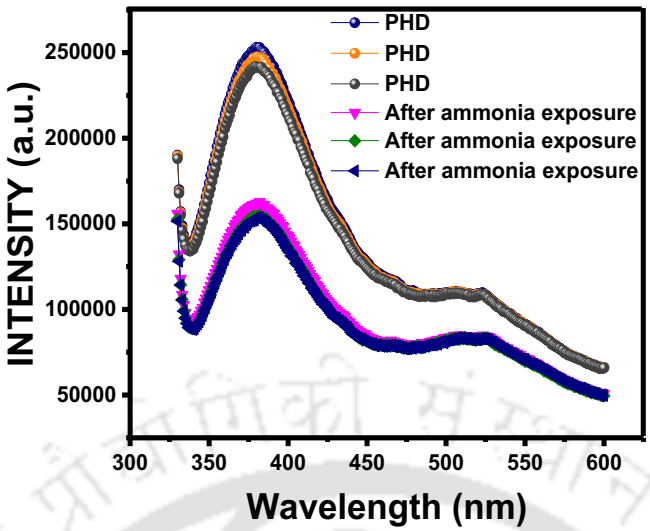

Figure 6.5. Photoluminescence Characteristics of PHD layer upon exposure to ammonia.

In Photo-luminescence (PL) analysis of the sensing layer, it is evident that the sensing layer is highly fluorescent with high intensity of photons obtained at lower wavelengths as shown in Figure 6.5. The higher intensity is fairly visible in terms of very bright light obtained during PL analysis. High intensity vs wavelength ratio iterates a high photo-sensitivity and photo-luminescence sensing layer of the device. The intensity of photo-luminescence decreases when the sensing layer is exposed to gaseous analytes due to increasing absorbtion of gaseous analytes over the sensing layer.

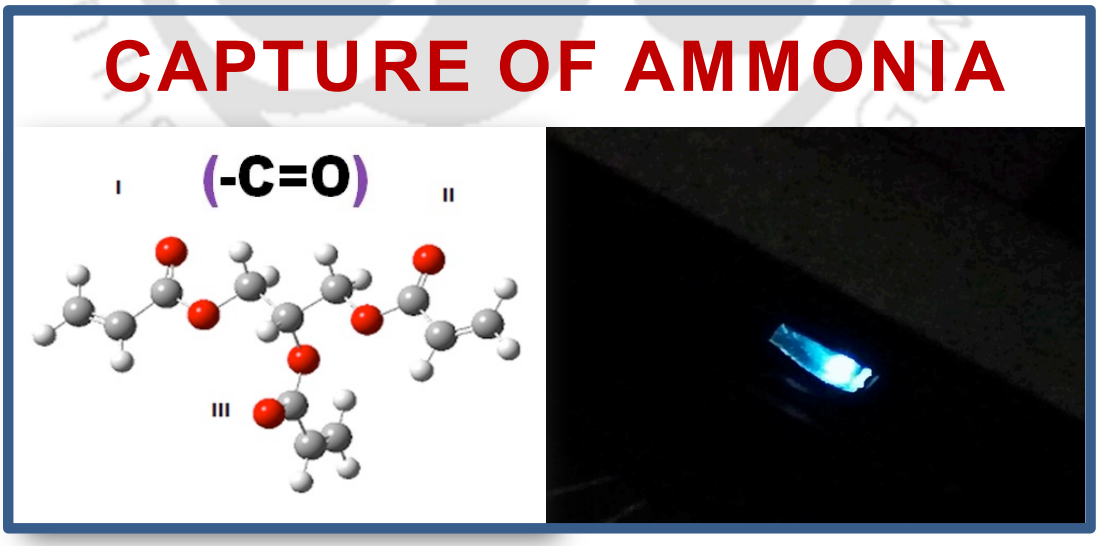

Figure 6.6. Sensor Characteristics upon exposure to ammonia.

Under excitation, the electron density increases in this region. After the addition of ammonia, it attaches to the (-C=O) region and accumulates by drawing all the electron

density towards this region (Fig. 6.6). Therefore, more electrostatic potential is observed in this region rather than in other regions.

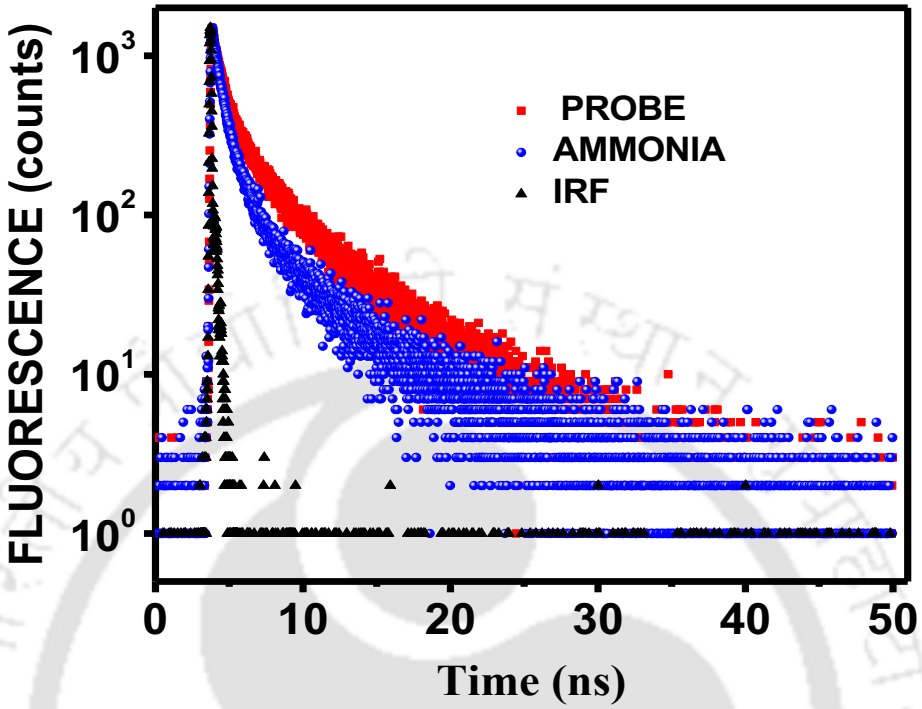

Figure 6.7. Time-Resolved Photo-luminescence (TRPL) study of PHD upon ammonia exposure.

In Time-Resolved Photo-luminescence (TRPL) analysis of the sensing layer, the plots between the number of photons emitted with time elapsed are obtained. Sensing layer exhibit stable photo-luminescence with a decay half-life period ($t_{1/2}$) of 2.5ns. Furthermore, the photo-luminescence half-life time ($t_{1/2}$) further increases when the sensing layer is exposed to different gaseous analytes indicating the improving stability of the sensor layer. TRPL variation of raw sensor and sensor exposed to NH_3(g) is obtained as in Figure 6.7.

6.4. CONCLUSION

In this work, a two-terminal device with a polyhydroxyl derivative has been developed and ammonia sensing has been achieved under a UV on/off state. We demonstrate that the device has excellent current characteristics and can be operated with voltages as low as 1V or less. The poly-hydroxyl film is optimal in at room temperature due to its crosslinked homogenous texture. The proposed device is highly sensitive and selective towards ammonia both under UV on/off state. PL and TRPL analysis of the sensing layer

of the device evidently showcase the photo-luminescence with high intensity (brightness) and prolonged stability. The reusability study of the device proved another important aspect of our device. Thus, new possibilities and findings could be further explored using such materials in different configurations.

6.5. REFERENCES

1. J. Kuttippurath, A. Singh, S. P. Dash, N. Mallick, C. Clerbaux, M. Van Damme, H. Varikoden, *Science of the Total Environment*, 2020, *740*, 139986.

2. R. P. Padappayil & J. Borger, *Ammonia toxicity,* 2021, StatPearls [Internet].

3. *In Acute Exposure Guideline Levels for Selected Airborne Chemicals: Volume 6*. 2008, National Academies Press (US).

4. T. N. Annisa, S. H. Jung, M. Gupta, J. Y. Bae, J. M. Park, & H. I. Lee, *ACS applied materials & interfaces*, 2020, 12(9), 11055-11062.

5. T. Ritthichai & V. Pimpan, *Journal of King Saud University-Science*, 2019, 31(2), 277-284.

6. S. T. Dubas & V. Pimpan, *Talanta*, 2008, 76(1), 29-33.

7. E. Detsri, J. Popanyasak, N. Laomaneenopparat, & K. Warngbun, In *Advanced Materials Research,* 2015, 1105, 225-230.

8. F. Wang, G. He, B. Zhang, M. Chen, X. Chen, C. Zhang, H. He, *ACS Catal*., 2019, 9, 1437−1445.

9. F. Wang, J. Ma, G. He, M. Chen, C. Zhang, H. He, *ACS Catal.*, 2018, 8, 2670−2682.

10. X. Zhu, C. Jin, X.-S. Li, J.-L. Liu, Z.-G. Sun, C. Shi, X. Li, A.-M. Zhu, *ACS Catal.* 2017, 7, 6514−6524.

11. S. Song, C. Lu, X. Wu, S. Jiang, C. Sun, Z. Le, *Appl. Catal. B*, 2018, 227, 145−152.

12. O. Debono, V. Hequet, L. Le Coq, N. Locoge, F. Thevenet, *Appl. Catal. B*, 2017, 218, 359−369.

13. V. Hequet, C. Raillard, O. Debono, F. Debono, N. Locoge, L.´ Le Coq, *Appl. Catal. B*, 2018, 226, 473−486.

14. J. Ma, H. He, F. Liu, *Appl. Catal. B*, 2015, 179, 21−28.

15. J. Ma, H. Wu, Y. Liu, H. He, *J. Phys. Chem. C*, 2014, 118, 7434−7441.

16. S. Yamazoe, T. Okumura, Y. Hitomi, T. Shishido, T. Tanaka, *J. Phys. Chem. C*, 2007, 111, 11077−11085.

17. S. Yamazoe, K. Teramura, Y. Hitomi, T. Shishido, T. Tanaka, *J. Phys. Chem. C*, 2007, 111, 14189−14197.

18. S. Heylen, S. Smet, K. G. M. Laurier, J. Hofkens, M. B. J. Roeffaers, J. A. Martens, *Catal. Sci. Technol*., 2012, 2, 1802−1805.

19. M. Chen, J. Ma, B. Zhang, G. He, Y. Li, C. Zhang, H. He, *Appl. Catal. B*, 2017, 207, 397−403.

20. M. Chen, J. Ma, B. Zhang, F. Wang, Y. Li, C. Zhang, H. He, *Appl. Catal. B*, 2018, 223, 209−215.

21. R. Asahi, T. Morikawa, H. Irie, T. Ohwaki, Chem. Rev. 2014, 114, 9824−9852.

22. G. Liu, H. G. Yang, J. Pan, Y. Q. Yang, G. Q. Lu, H.- M. Cheng, *Chem. Rev*., 2014, 114, 9559−9612.

23. J. Low, B. Cheng, J. Yu, *Appl. Surf. Sci.,* 2017, 392, 658−686.

24. H. Xu, S. Ouyang, L. Liu, P. Reunchan, N. Umezawa, J. Ye, *J. Mater. Chem. A*, 2014, 2, 12642−12661.

25. M. Ceotto, L. Lo Presti, G. Cappelletti, D. Meroni, F. Spadavecchia, R. Zecca, M. Leoni, P. Scardi, C. L. Bianchi, S. Ardizzone, *J. Phys. Chem. C*, 2012, 116, 1764−1771.

26. H. Zhang, W. Wang, H. Zhao, L. Zhao, L.-Y. Gan, L.- H. Guo, *ACS Catal*., 2018, 8, 9399− 9407.

27. P. Unwiset, A. Makdee, K. C. Chanapattharapol, P. Kidkhunthod, *J. Phys. Chem. Solids*, 2018, 120, 231−240.

28. H. Li, H. Shang, X. Cao, Z. Yang, Z. Ai, L. Zhang, *Environ. Sci. Technol*., 2018, 52, 8659− 8665.

29. M. Zhang, J. Xu, R. Zong, Y. Zhu, *Appl. Catal. B*, 2014, 147, 229−235.

30. L. Huang, L. Li, W. Dong, Y. Liu, H. Hou, *Environ. Sci. Technol*., 2008, 42, 8070−8075.

31. Y. Wang, X. Zhao, D. Cao, Y. Wang, Y. Zhu, *Appl. Catal. B*, 2017, 211, 79−88.

32. W. Yang, Y. Zhu, F. You, L. Yan, Y. Ma, C. Lu, P. Gao, Q. Hao, W. Li, *Appl. Catal. B*, 2018, 233, 184−193.

33. Y. Ji, Y. Luo, *J. Phys. Chem. C*, 2014, 118, 6359−6364.

34. S. Yamazoe, T. Okumura, T. Tanaka, *Catal. Today*, 2007, 120, 220−225.

35. M. A. Kebede, N. K. Scharko, L. E. Appelt, J. D. Raff, *J. Phys. Chem. Lett*., 2013, 4, 2618−2623.

Chapter – 7

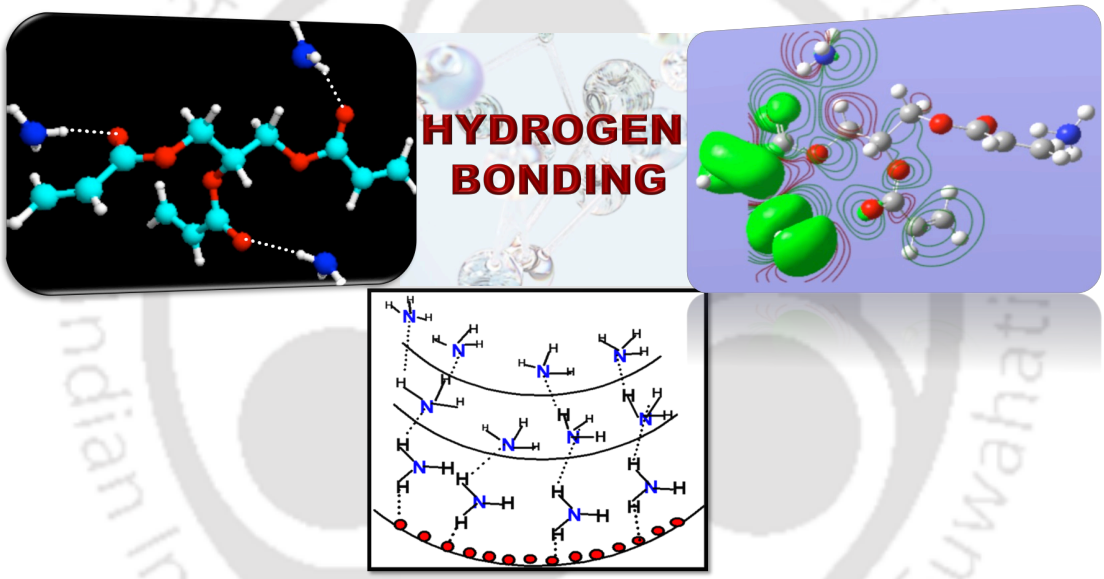

ABSTRACT

Theoretical studies have been carried out by using DFT and TD-DFT methods to understand the sensing mechanism of Polyhydroxyl Derivative (PHD) towards ammonia (NH_3). This article reports on the study of PHD for ammonia sensing through hydrogen bonding which leads to the sensitivity of NH_3. In this case induced hydrogen bond interaction has been found and subsequent condensation is also contributed in this process. The computed hydrogen bond strength (HBS) values are large enough for undergoing chemisorption process. However, association of more ammonia molecules is possible through interaction between induced PHD-NH_3 of polymer with incoming NH_3. It may work as selective non-conducting layer since the band gap is -6.12 ev. This work is focused on the mechanistic study on the sensitivity of PHD for NH_3 sensing. The geometries and electronic properties of PHD-n NH_3(n=1-3) are evaluated for the constructed models. The H-bonds usually forms between –C=O groups and NH_3 .The electronic properties such as ionization potentials(IP), Electron affinity (EA), HOMO-LUMO gap and λ_{max} support the sensing mechanism. From the electrostatic potential of PHD, the highest negative potential is observed around –C=O chromophores which are found to be the favorable sites for interaction with NH_3. The band gaps before and after associations with NH_3 are found significantly different for both the ground and excited states. Also, reduction of band gaps as well as increase of LUMO energies on associations of NH_3 is noticeable.

7.1. INTRODUCTION

The aspects of gas sensing devices are vast and the techniques used in several problems are crucial depending on the nature of the problem. In general, the importance of polymer-based sensors has been highlighted in many literatures particularly in the field of disease detection at the early stage.[1-10] Many of the techniques hardly indicate in-depth information about the mechanism of sequential detection during the progress of the diseases in the bio-system where several types of proteins or amino acids are liberated from time to time. The strategy of detecting small quantities of disease-related molecules like amino acid, peptides, proteins, nucleic acid fragments and also NH_3 liberated as small quantities in the bio-system is a challenging area. So, polymer-based materials may be useful for some of these systems. In addition, the relevance of NH_3 contamination in the air can be focused on as one of the main environmental issues because it is one of the toxic volatile molecules. It is used in industries such as dye, fertilizer, plastic, petrochemical, textiles, pesticides etc. and also it is a common reagent in routine chemical experiments in the laboratory. [11-13] The applications of polymer-based electronic devices have been attempted in many studies. Likewise, various polymers have been developed for specific applications to ammonia or amino acid sensing devices.[14-20] In-depth mechanism-based study of such an application has not been yet explored and probably it undergoes various mechanisms such as electron transfer, proton transfer and any other mediation by donor-acceptor type of interactions. In this paper, we intend to study the properties of a PHD for understanding the mechanism of sensing NH_3. The structure of PHD shown in Fig. 1 has 6 donor sites at –C=O and-C-O-C -groups which are susceptible to NH_3 molecules capable of forming hydrogen bonds. So, the hydrogen bonding ability may be examined by using quantum mechanical (DFT) studies which enable estimating the hydrogen bonding strength between PHD and NH_3. Also, the importance of the electron density profile and HOMO-LUMO gap may be useful to illustrate any electronic effect involved in this device.

As such the aim of the research in such areas is to design a sensitive as well as a selective sensor with stability at room temperature. There are several sensors such as semiconductors (metal oxide), metal oxide semiconductors, field effect transistors, surface acoustic wave and conducting polymer.[20-25] If we analyze the sensor properties like stability, sensitivity and quick response mechanism, conducting polymers (CPs) are much superior to others. There are several polymers i.e., polyaniline (PANI), polypyrrole (ppy),

poly (o-phenylene diamine), PPD and poly (3, 4-ethylene dioxythiophene) (PEDOT) etc. useful for their applications as biosensors and gas sensors.[25-32] However, PHD has been used experimentally and shows excellent response towards NH_3 molecules at room temperature.[33] Several experimental reports on CP-based sensors for the detection of NH_3, especially at room temperature are found. Experimentally, PHD shows the ability to sense NH_3 sensing of this conducting polymer has not been reported. Hence, we intend to investigate the NH_3 sensing mechanism of PHD and the result may provide certain information to further design of sensors and other related molecules.

7.2. COMPUTATIONAL DETAILS

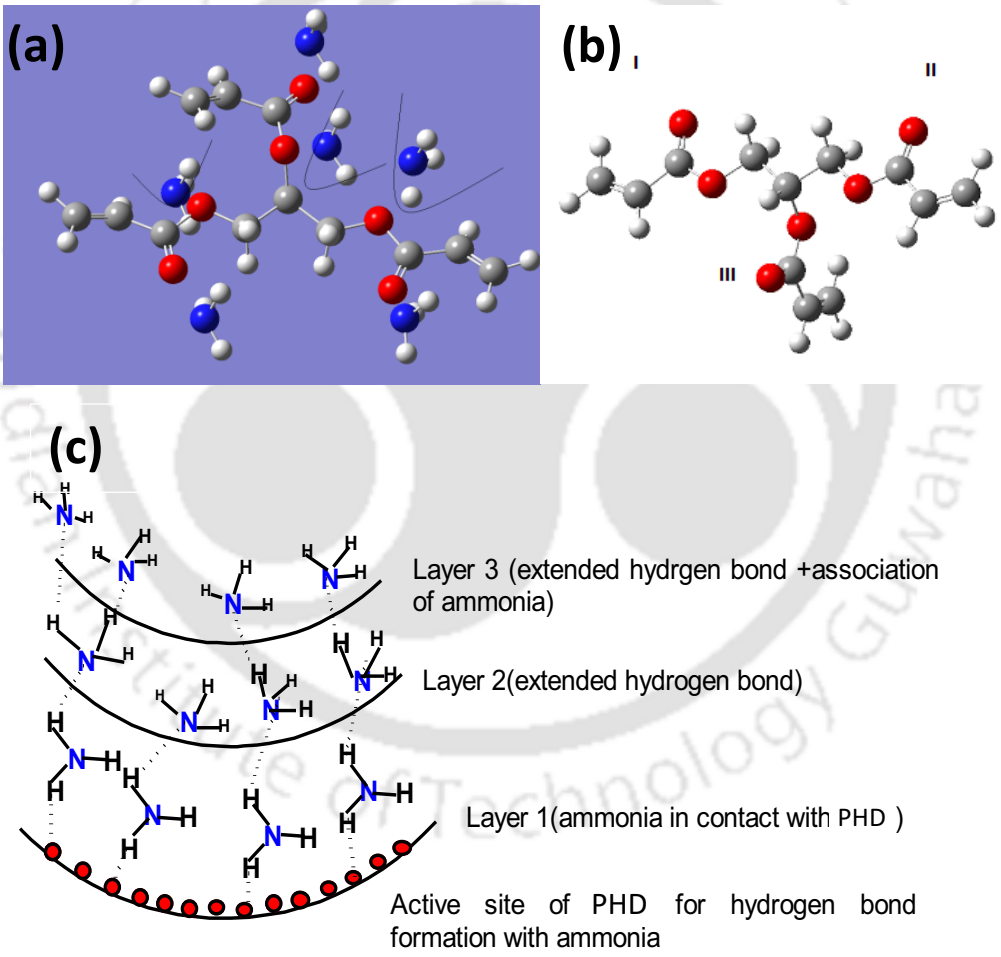

Figure 7.1. (a) Possibility of accumulating 6 ammonia molecules, but the three regions marked are not forming H Bonds. (b) Susceptible regions of hydrogen bond formation (I, II, III). (c) Ammonia sensing model through absorption/ condensation.

The structure of PHD shown in Fig. 1a has six donor sites at –C=O and –C-O-C groups which are susceptible to NH_3 molecules for forming hydrogen bonds. In this aspect, the capability of trapping NH_3 molecules through hydrogen bonding may be examined by using quantum mechanical studies. This will enable us to estimate the hydrogen bonding strength between PHD and NH_3, the electrostatic potential profile and the HOMO-LUMO gap which are important to illustrate any electronic effect in the sensing mechanism. The geometries of PHD and their complexes with NH_3 are completely optimized at DFT-B3LYP++G(d,p) without considering any symmetry constraints. The H-bonding strength (HBS) of the PHD is computed from the completely optimized geometries of the complexes which are the difference between the energies of the supermolecule PHD-nNH_3(n is the number of NH_3) and PHD. The geometries of PHD-nNH_3 and PHD were also completely optimized geometries before calculating HBS.

HBS calculated from the following equation,

$$\mathbf{HBS = E(PHD\text{-}NH_3) - (E(PHD)+E(NH_3))}$$

where, E(PHD-NH_3) = Energy of supermolecule

$$\mathbf{E(PHD) = Energy\ of\ PHD\ and\ E(NH_3) = Energy\ of\ NH_3}$$

The DFT method has been used in this study because of its popularity and accuracy in predicting molecular properties, particularly hydrogen bonding and adsorption of molecules.[10] Different models of NH_3 association are taken. For the excited state calculation, the TD-DFT method with 6-31G(d,p) was used. The HBS of these complexes of PHD and NH_3 are further calculated at the B3LYP/6-31G(d,p) for comparison with excited state calculations with this basis set. All calculations were carried out on Gaussian 09 Programme suite and Gaussview was used for constructing the model geometries and visualization of results.[34] Similarly, the HOMO-LUMO gaps are also computed for all the systems. The other descriptors of reactivity are electrophilicity(ε), chemical potential(μ), electronegativity (χ), and hardness (η).

These values are also calculated in this study:

$$\mu = -\frac{(I+A)}{2},\ \eta = \frac{I-A}{2},\ \chi = \frac{I+A}{2},\ \varepsilon = \frac{\mu}{2}$$

The values of ionization energies I and electron affinity A are taken from the HOMO and LUMO values. From these values, the reactivity of the –C=O group can be illustrated.

7.3. RESULTS AND DISCUSSION

7.3.1. FEATURES OF HYDROGEN BONDING BETWEEN PHD AND AMMONIA

The three donor sites, the –C=O group of PHD are prone to forming hydrogen bonds with NH_3 but not with the other three –C-O-C- groups (Fig. 7.1b). Hence the sensitivity may be understood from the capability of trapping NH_3 molecules within three regions I, II and III (Fig. 7.1b). It is essential to examine the geometrical parameters of PHD after interaction with NH_3. Geometry optimization of PHD- NH_3(n=1,2,3) were carried out with DFT(B3LYP)/6-31G(d,p) level of theory, and the H-bonding energies (HBS) and distances with –C=O groups are given in Tables 7.1 and 7.2. The corresponding optimized structures are shown in Figures 7.2 (a-d) and 7.3 (a, b). The H-bond lengths are almost the same for all these three H-bonds and –C=O..H H-bond distances are shown in Table 7.2. These slight differences in the bond lengths arise due to the unsymmetrical configuration of –C=O groups of PHD. The changes in the remaining geometrical parameters due to H bond formation are insignificant. So, the hydrogen bonding strength is considered as the sensing of PHD (doped) for NH_3 (guest). In addition to this, in the close proximity of PHD-NH_3 complexation as shown in Figure 7.2, the hydrogen bonding may be extended in several layers of NH_3 due to the difference in electronegativity of N of NH_3 (partial negative) and N(NH_3) of subsequent layers which may further induce other incoming NH_3 molecules to facilitate the formation of extended H-bonds. The geometries of complexes bearing two extended H bonds are also completely optimized and the H-bond lengths are shown in Table 7.2. Two configurations are obtained in these extended geometries of PHD-2NH_3, and accordingly, the geometries are optimized with the same method. In the case of the NH_3 sensor, the unique affinity of this analyte towards the sensor involves the H-bond. The interaction ability of NH_3 towards PHD by theoretical calculation may be used to elucidate the strength of H- bonding or for undergoing either chemisorption or physisorption. From the equilibrium geometry, the H bond of analyte attached to PHD is <2.2Å which is quite sufficient to form strong H-bonds and as such the first NH_3 is likely to be chemisorbed which may subsequently be followed by physisorption. The bonding between the first molecule of NH_3 with active sites is shown to be 2.06 Å, which is predominantly attributed to chemisorbed through H-bond. The equilibrium geometry of interaction of first H bonding with NH_3 at the surface specifically attached to -C=O group in the ratio of 1:1,1:2 and 1:3 respectively shown in Figs. 7.2 (a-d), and 7.3 (a,b) for the extended interaction model with NH_3. The calculated interaction

energies based on the number of hydrogen bonds as well as the most effective sites of interaction are well elucidated from these calculations (Table 7.1). The most favourable site of H-bond formation leading to chemisorption has been shown. The H-bond distances in 1:2 and 1:3 are slightly longer than in the 1:1 combination and the orientation of NH_3 in these systems (Table 7. 2).

Table 7.1. Computed electronic energies and hydrogen bond energies with B3LYP/6-31++G(d,p).

Systems	Total energies (a.u)	H-bond energies kcal/mol
NH_3	-56.56346	---------
NH_3-NH_3	-113.13298	-3.80
PHD	-917.06931	---------
PHD-NH_3	-973.63339	-0.39
PHD-NH_3($2NH_3$ extended)	-1030.11927	**-48.29**
PHD-NH_3(3 extended)	-1086.77919	-12.24
PHD-$3NH_3$ at specific sites	-1086.77685	-10.77
PHD-$2NH_3$ at specific sites, position 1	-1030.20541	-5.76
PHD-$2NH_3$ at specific sites, position 2	-1030.20696	-6.73

The HBS depends on the electronegativity of the –C=O group (partial negative end) for interacting with H (partial positive end) of NH_3. Usually, the HBS is less than an ion-dipole type of interaction. The values of HBS for PHD-$1NH_3$ are given in Table 7.4. One N-H bond length increases on subsequent H-bonding and also –C=O bond length increases. The HBS values depend on the number of H-bonds between PHD and NH_3, hence the highest (-ve) value is found in PHD-$3NH_3$. The order of HBS is of the order of the complexes PHD-$3NH_3$>PHD-$2NH_3$>PHD-NH_3(for specific H bonding at –C=O). Similarly, the HBS of extended PHD-$2NH_3$ complexation is shown in Table 7.4, we observed a significant difference from PHD-$2NH_3$. This observation may contribute to the

development of an H-bond network (layers) with weak interaction resulting in the efficient sensing ability of PHD (Fig. 7.1c).

7.3.2. ELECTRONIC PROPERTIES AND EXCITATION ENERGIES

The electronic properties such as HOMO-LUMO and the excitation energies are calculated at the B3LYP level of theory with 6-31G(d,p) and 6-31++G (d,p) basis sets. For the excited state calculation, TD-B3LYP with 6-31G(d,p) basis sets were used. The excitation energies of PHD may give information on the sensing ability of this material. The excitation energies for PHD and PHD-nNH_3 (n=1-3) complexes are given in Table 7.3. We have used the TD-B3LYP method with 6-31G(d,p) because the excitation energies obtained with this calculation are reported to be reliable compared to other methods. Accordingly, the values of excitation energies of TD/B3LYP(6-31G(d,p)) are relatively small compared to the corresponding energies of HOMO to LUMO obtained from B3LYP/6-31G(d,p). The variation of excitation energies on complexation with NH_3 is also observed, which is due to the perturbation of HOMO and LUMO of PHD due to hydrogen bonding with NH_3. For PHD-NH_3, an increase of HOMO energy by 0.011 a.u. is found more than the isolated PHD, which means 0.011 a.u. is the measure of the sensing power of PHD for 1NH_3. Likewise, the increase of HOMO energy i.e., the reduction capability of PHD by NH_3 can be analyzed. On the other hand, an increase in HOMO is also observed, however, the decrease of LUMO is also observed. Hence the values of I.P, E.A and band gap of PHD-NH_3 complexes are calculated with B3LYP/6-31G(d,p). The negative value of I.P is the ionization potential of the complexes and Table 7.3 shows the decrease of I.P after complexation with NH_3. The I.P values of PHD-NH_3 is highest compared to the value of PHD-2NH_3 and PHD-3NH_3. Likewise, EA is the negative value of LUMO and the values of PHD-NH_3 are shown in Table 7.3. The decrease in EA of complexes from PHD is quite significant which indicates the interacting power of PHD with NH_3. It is essential to compare the nature of interactions between H of NH_3 with PHD, subsequently, the interaction energies (HBS) through the H-bond between –C=O group of PHD have been calculated (Tables 7.1 and 7.4). There are three -C=O groups in PHD which can form hydrogen bonds at the distances of 2.1Å, 2.09Å, 2.088 Å etc. (Table 7.2), however, the hydrogen bond lengths vary for PHD-1NH_3, PHD-2NH_3 and PHD-3NH_3. In this case, –C-O-C- oxygen is not shown to be the effective site for forming hydrogen bonds. The interaction energies of PHD with nNH_3 in the ratio of 1:1, 1:2 and 1:3 is shown in Table 7.1. The modes of interactions shown in Figs. 7.2 (a-d) and 7.3 (a, b) clearly indicate how

the HBS is involved in the stability of PHD-nNH_3 at the three –C=O specific sites. All these three -C=O sites have the ability to form hydrogen bonds without much variation in H-bond lengths. Hence, the effect of HBS has been shown in sensing ability and the interaction energies of these PHD-1NH_3, PHD-2NH_3 and PHD-3NH_3 are likely to form a stable complex and the values are -0.39 kcal/mol, -5.76 kcal/mol(position1), -6.73 kcal/mol (position 2) and -10.77 kcal/mol respectively.

Table 7.2. Computed H bond lengths of the specific models (at –C=O groups) and extended models (at –C=O with more than one NH_3 at one site).

Systems	H bond lengths of types in Å (10^{-10} m)				
	H-N..H(1)	H-N..H(2) (Association in extended NH_3 chain)	-C=O..H-N(1)	-C=O..H-N(2)	-C=O..H-N(3)
NH_3-NH_3	2.06	-------	-------	-------	-------
PHD-NH_3	2.19	-------	-------	-------	-------
PHD-NH_3 ($2NH_3$ chain) Position 1	2.18	2.23	-------	-------	-------
PHD-NH_3 ($2NH_3$ chain) Position 2	2.08	2.09	-------	-------	-------
PHD-3NH_3(chain)	2.06	2.93	2.19	-------	-------
PHD-3NH_3 at specific sites	-------	-------	2.083	2.132	2.099
PHD-2NH_3 at specific sites, position 1	-------	-------	2.04	2.40	-------
PHD-2NH_3 at specific sites, position 2	-------	-------	2.04	2.09	-------

Table 7.3. Computed ground (DFT/6-31G(d,p) and excited state energies (TD/DFT 6-31G(d,p), HOMO-LUMO gaps of PHD and PHD-nNH_3 at different states (n=1-3).

Systems	HOMO(IP) (a.u.)	LUMO(EA) (a.u.)	HOMO-LUMO gaps(a.u.)	Lowest excitation energy(eV)	Oscillation strengths (nm)
PHD (Ground state)	-0.25701 (0.25701)	0.00693 (-0.00693)	0.25008	-------	-------
PHD (Singlet)	-0.27784 (0.27784)	-0.05025 (0.05025)	0.22759	4.7378	261.69
PHD (Triplet)	-0.14787 (0.14787)	-0.04903 (0.04903)	0.09884	0.7802	1589.10
PHD-NH_3(Ground State)	-0.01500 (0.01500)	-0.26736 (0.26736)	0.25236	-------	-------
PHD-1 NH_3(Singlet)	-0.24634 (0.24634)	-0.00199 (0.00199)	0.24435	3.9413	314.57
PHD-1NH_3(Triplet)	-0.23206 (0.23206)	-0.03718 (0.03718)	0.19488	0.2674	4636.54
PHD-2 NH_3(Singlet)	-0.22800 (0.22800)	-0.00230 (0.00230)	0.22976	3.3644	368.52
PHD-2 NH_3 (Triplet)	-0.14173 (0.14173)	-0.05527 (0.05527)	0.08646	0.0983	12613.37
PHD-3 NH_3(Singlet)	-0.24834 (0.24834)	-0.00398 (0.00398)	0.24436	3.9300	315.48
PHD-3 NH_3 (Triplet)	-0.21649 (0.21649)	-0.00221 (0.00221)	-0.21428	0.5539	2238.21

Table 7.4. Computed electronic energies, thermodynamics parameters and hydrogen bond energies with B3LYP/6-31G(d,p).

Systems	Total energies (a.u)	Zero-point correction (Hartree/ Particle)	Thermal correction to Energy (a.u)	Thermal correction to Enthalpy (a.u)	Thermal correction to Gibbs Free Energy (a.u)	H-bond interaction energies (HBS) (a.u)
NH_3	-56.53131	0.03463	0.03798	0.03925	0.01630	-------
NH_3-NH_3	-113.07066	0.07049	0.07446	0.07541	0.04542	-0.00804 (-5.05)
PHD	-916.71545	0.25003	0.26449	0.26543	0.20719	-------
PHD-NH_3	-973.26505	0.28592	0.30892	0.30986	0.22826	-0.01829 (-11.48)
PHD-NH_3($2NH_3$ extended)	-1029.80535	0.32301	0.34988	0.35083	0.25835	-0.0273 (-17.13)
PHD-NH_3(3 extended)	-1086.36542	0.36275	0.39135	0.39230	0.29976	-0.05600 (-35.14)
PHD-$3NH_3$ at specific sites	-1086.35350	0.36024	0.38958	0.39053	0.29596	-0.04409 (-27.67)
PHD-$2NH_3$ at specific sites, position 1	-1029.81158	0.32369	0.34975	0.35070	0.26311	-0.03353 (-21.04)
PHD-$2NH_3$ at specific sites, position 2	-1029.80970	0.32387	0.35009	0.35069	0.26311	-0.03155 (-19.80)

***Bracketed values are in kcal /mol**

The incoming 2 NH_3 can form H bonds in two different configurations and the HBS values are slightly different. The interaction with more NH_3 molecules may take place due to the formation of chain/extended H-bonds between induced polar NH_3 molecules (Figs. 7.2(a-d) & 7.3(a, b)). But we have examined the sensitivity for detecting NH_3. Considering the aggregation of NH_3 molecules it is possible to form a network of H bonds between PHD-NH_3 directly and among induced NH_3 molecules leading to condensation of NH_3 within PHD. Hence it may be useful for explaining the stability and sensitivity of NH_3 detection. To explain the concept of cavity condensation, it may be easier to establish from the intermolecular interaction between PHD and NH_3 through hydrogen bonds. The complex nature of the effect of H-bonding in PHD-NH_3 supermolecule can be interpreted to get the correct description of extended H-bonds NH_3 molecules. This may result in subsequent H bonding effects exerted by the PHD-NH_3 complex on the other nearby NH_3 molecules through long-range polar interactions. Thus, the direct hydrogen bonding between PHD and NH_3 as well as extended long-range interaction between polarized PHD-NH_3 complex and NH_3 molecules through several H-bonds may contribute to forming H-bonded clusters of NH_3 molecules around the polarized PHD-NH_3 supermolecule. The distribution of NH_3 molecules around PHD-NH_3 can be picturised as where condensation with many incoming NH_3 molecules form a cluster system as PHD-NH_3-NH_3… etc. (Fig. 7.1c). The layer of adsorption shown in Fig. 7.1c has been modelled as chain interaction of NH_3 with PHD. Understanding the process of condensation may be useful to explain the sensing mechanism. The mechanistic investigation into this process may be performed from the intermolecular interaction of PHD-NH_3 and condensation may be modelled as the PHD-NH_3-NH_3-NH_3 system (Fig. 7.3(a,b)). Using this concept, the intermolecular interaction of PHD-NH_3 and another NH_3 molecule is expected during NH_3 detection which is assumed to be through the interaction of polarized NH_3 in PHD-NH_3 with the incoming NH_3 molecule. This PHD-NH_3 supermolecule (blended) may possess the excellent capability of attracting more NH_3 molecules around it, we have reported interaction energies (HBS) of PHD-NH_3, PHD-NH_3-NH_3 and PHD-NH_3-NH_3-NH_3. The values of the interaction energies are provided in Table 7.1 and the geometrical features are shown in Figures 7.2(a-d) and 7.3(a,b). We have also computed NH_3-NH_3 association with PHD-NH_3-NH_3 association and the types of H-bonds and HBS are shown in Tables 7.1 & 7.4 to support this assumption. The value for extended interactions is larger (negative) than the specific interaction. The interaction of PHD-NH_3 is strong

enough to form the cluster of NH_3 within PHD (Table 7.1). As such NH_3 molecules do form stable clusters, the existence of NH_3-NH_3 interaction at the optimum distance between them has been tested. Thereafter, we observe effective NH_3 aggregation as an extended H-bonding network PHD-NH_3-NH_3-NH_3 system and also reveal the instability of extended NH_3 molecules within PHD and favouring NH_3-NH_3 association, hence HBS values are large (-ve) i.e., -48.29kcal/mol. So, this elucidates the concept of blended PHD with one NH_3 molecule that may assist the polarization of attached NH_3 molecule for attracting incoming NH_3 molecules facilitating cavity condensation. This particular polymer is a useful template unique for NH_3 sensing. As a consequence, it has the potential for developing other blended PHD for further application to other systems.

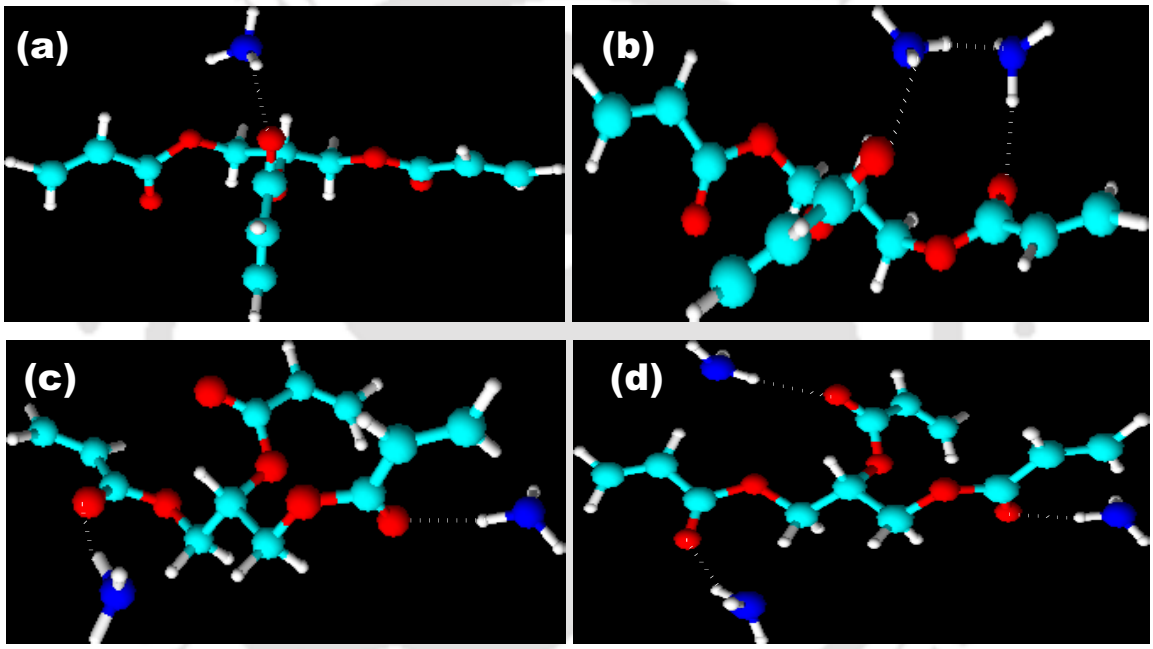

Figure 7.2. Optimized structures of (a) PHD- 1ammonia; (b) PHD-2Ammonia (Position 1); (c) PHD-2Ammonia (Position 2); (d) PHD-3Ammonia at specific sites.

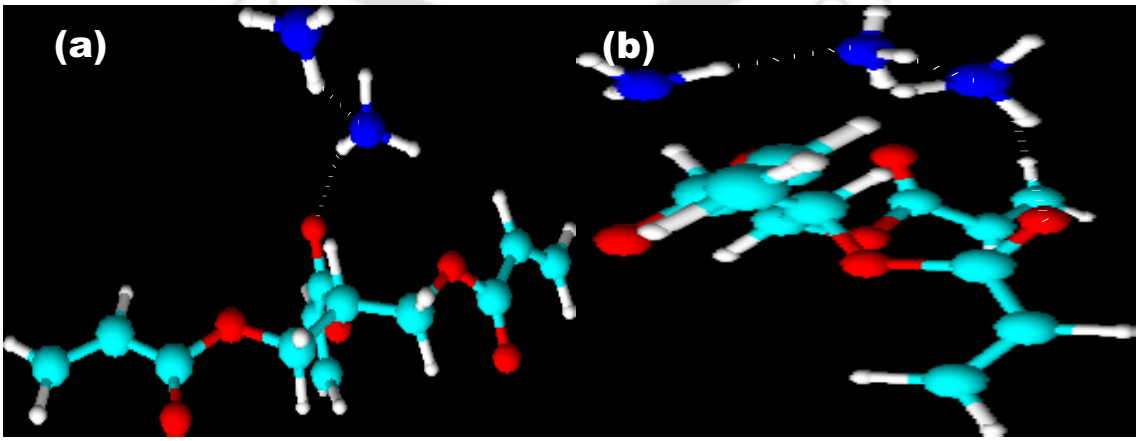

Figure 7.3. Optimized structures of (a) PHD-2Ammonia extended interaction; (b) PHD-3Ammonia extended interaction.

Table 7.5. Computed effect of solvent polarity on PHD with dielectric continuum model.

Solvents	Polarized Solute-Solvent (kcal/mol)	Cavitation energy (kcal/mol)	Dispersion energy (kcal/mol)	Repulsion energy (kcal/mol)	Total non-electrostatic (kcal/mol)
Water	-23.11	39.20	-23.07	1.47	17.60
Acetone	-20.96	28.42	-20.30	1.22	9.34
Methanol	**-21.75**	27.99	-19.86	1.22	9.35
Ethanol	**-20.96**	28.42	-20.30	1.22	9.34
DMSO	**-21.66**	36.62	-23.58	1.43	14.48

Since, the newly fabricated PHD-based NH_3 sensor intrinsically depends on the H bond between PHD-NH_3, the blended PHD-NH_3 is particularly involved in inducing incoming NH_3 molecules through polarization. It is in fact related to the sensing property of PHD for NH_3 and further application to similar molecules through H-bond as well as condensation rather than any other thermochemical properties and intermolecular hydrogen bonding strengths are calculated in Tables 7.1 and 7.4. We can find out the strength of the hydrogen bonds in extended hydrogen bonding structures up to three NH_3 molecules. The decrease of hydrogen bonding strength at this site indicates how the cavity condensation process is possible in this system. On the other hand, a comparison of the thermophysical properties free energy change, entropy, vibrational energy and enthalpy for the hydrogen bonding directly interacted at the specific site of PHD and also for the extended hydrogen bonding up to three NH_3 are shown in Table 7.4. We have observed distinct variations of these values and the decrease of vibrational energies indicates less stable hydrogen bonding of these extended NH_3 molecules. The effect of surrounding solvent should be considered while dealing with the basic interaction in a supermolecule i.e., the effect of solvent on PHD prior to PHD and NH_3 association, since the processes of molecular association may interfere with solvent molecules. The such solvent effect may

be examined by using the solvent dielectric field on PHD. In particular, the magnitude of solvent effects on PHD while sensing NH_3. Hence the sensitivity of PHD towards solvents has been checked with various solvent dielectrics, small variation has been observed (Table 7.5). Also, the reactivity descriptors such as ε, μ, χ, and η are usually examined to understand the molecular interaction. Also, the reactivity descriptors such as ε, μ, χ and η are usually examined to understand the molecular interaction. The computed reactivity parameters are shown in Table 7.6, and the electron–donor ability of PHD is also indicated from these values.

7.3.3. 3D ELECTROSTATIC POTENTIAL (EPS) AND HOMO-LUMO GAPS

Electron lability of monomer PHD can be related to the energy gap of Frontier orbitals i.e. HOMO-LUMO. The optimized structure of monomer PHD with B3LYP/6-31++G(d,p) was taken for calculating HOMO and LUMO. The HOMO-LUMO gap is found to be -6.12 eV, but the value is large for a typical electronic conductive material. According to the electronic property of several groups in PHD, i.e. -C=C-, -C-O-C-and –C=O groups of PHD, the nπ* and ππ* electronic transitions are possible, but such transitions occur on excitation. It is essential to analyze the electrostatic potential around the 3D structure of monomer PHD to depict the most electronegative region. The completely optimized PHD with B3LYP/6-31G(d,p) method was used for calculating electrostatic potential. The structure of PHD may be examined in three subunits I, II and III. The configuration of subunit I and II maintain along the same axial plane whereas unit III lie along the perpendicular of this plane. The acrylate groups are bonded to primary carbon centres in subunit I and II, whereas in subunit III the acrylate group is attached to the tertiary carbon centre through the -C- bond.

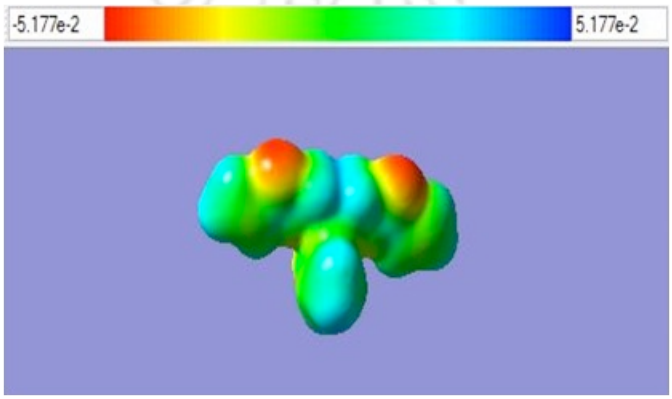

Figure 7.4. Electrostatic potential showing negative potential at regions of -C=O groups.

So, the nature of electrostatic potential around this monomer PHD may indicate distinguishable variation in electron density. We have computed the EPS profile in the 3D structure of monomer PHD, more negative values are found around –C=O of these three regions (Figure 7.4) and less negative or positive values are found around the rest of the regions. The maximum negative value in regions I and II is approximately $-4.31X10^{-2}$ a.u. whereas the value for region III is $-4.58X10^{-2}$ a.u. So, region III may be more perceptive for NH_3 than regions I and II. Sensitivity toward NH_3 may be influenced by these regions for this material. The electronic behaviour of sensing analytes through adsorption (chemisorption/physisorption) on the surface may be clarified from the structure and fundamental background of the predictable sites of bonding. In the case of the NH_3 sensor, the unique affinity towards PHD is through H bonds. In fact, it is possible to construct the model of adsorption from the nature of bonding.

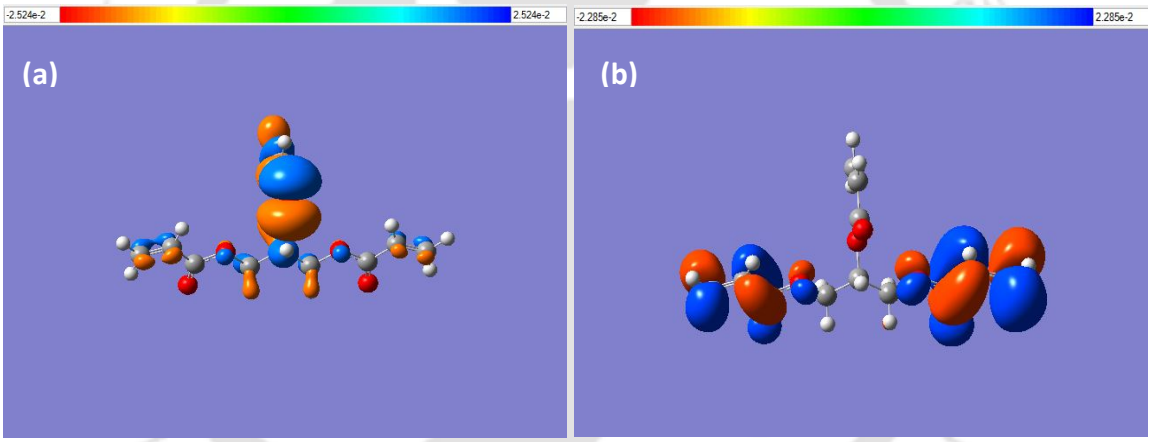

(Orbital energy, HOMO=-0.2923 a.u) (Orbital energy, LUMO=-0.0668 a.u)

(HOMO-LUMO gap = -0.226 a.u. = -0.226X27.1 eV = -6.1246 eV)

Figure 7.5. Gaussian Model. (a)HOMO of PHD. (b) LUMO of PHD.

Theoretical properties are often used to explain the chemistry of adsorption on materials.[10] On the other hand, the molecular and chemical structure are also some of the characteristic properties of physio chemically controlled mechanism of adsorption usually found in the design of several biosensors, and in the approach of tunable chemical properties of polymer incorporated sensors. Most of the polarizable H atoms are known for their ability to form hydrogen bonds with donor atoms, such as NH_3, amide and carboxylate anions etc. In such cases, the internal properties of several groups in polymer involved in the subsequent interaction with the available molecular sites can determine the chemical properties of the material and its applicability. The electronic structure

calculations, the HOMO- LUMO gaps and chemical reactivity are considered useful parameters for engineering other related sensor materials. Here, we are focusing on the electronic transition from the listing of HOMO and LUMO, which in turn define the electrophilic and nucleophilic attraction of the molecule, although the chemical reactivity can be understood from the HOMO-LUMO gap. The analysis of these parameters can be useful to understand insight into the sensing mechanism. The polarization of NH_3 molecules due to hydrogen bonding at certain active sites in the cavity is understood from Figs. 7.3 (a,b), and chain hydrogen bonds built up due to the induced hydrogen bond of the first NH_3 molecule rigidly attached at the –C=O site. The resultant polarization of the incoming NH_3 molecule subsequently decreases and weaker bonding between NH_3 molecules is expected among extended NH_3 molecules, unlike the rigidly bonded first NH_3 molecule.

Thus, polar NH_3-induced H-bonds are considered the characteristic feature associated with NH_3 sensing. In view of these repetitive interactions among NH_3 molecules, it is highlighted that (a) rigid hydrogen bonding and (b) cavity condensation of the NH_3 molecules due to weak interaction of the incoming NH_3 molecules, when repulsive forces due to overcrowding of NH_3 dominates the H bonding interaction and also association among NH_3 molecules except the rigid NH_3 molecule has been observed. Such features are explained in Figs. 7.2 (a-d), 7.3 (a,b) and the bond lengths and interaction energies of H bonds are shown in Tables 7.1 & 7.4. The computed values of HOMO and LUMO energies are used to understand the reactivity of these –C=O groups and the values are given in Table 7.3 along with the HOMO-LUMO gaps. The values of HOMO and LUMO are -0.2923 a.u and -0.0668 a.u, HOMO-LUMO gap is -6.12ev (Figures 7.5 (a,b)). These values signify the electron-donating ability of this material, the energy gap is also reasonably small unlike any other CP having π electron systems, which explains the importance of the H bond efficiently by electron donor property of –C=O groups in the sensing mechanism.

7.3.4. Theoretically predicted IR spectra and UV Spectra of PHD and PHD-nNH_3(1-3)

Theoretically, we have calculated the vibration frequency of N-H, after and before interaction with PHD. The N-H frequency in the calculated value increases (redshift) is between 99-105 cm^{-1}. The IR stretching frequency is calculated from the optimized

geometry of the PHD and PHD: NH_3 molecules using frequency calculation with B3LYP/6-31G(d,p) route in the Gaussian Programme code 09(34). Such variation of frequency indicates strong hydrogen bonding in PHD-NH_3.

Table 7.6. Computed descriptors of reactivity electrophilicity (ε), chemical potential (μ), electronegativity (χ), hardness (η), Ionization energy (I) and electron affinity (A) with DFT/6-31G++(d,p) for PHD.

Descriptors	Respective values (a.u)	HOMO, LUMO and HOMO-LUMO gap
μ	-0.17955	HOMO= -0.29230 a.u
η	0.11275	LUMO= -0.06680 a.u
ε	0.08977	HOMO-LUMO gap=0.22550 a.u
χ	0.17955	-------
I	0.29230	-------
A	0.06680	-------

Hydrogen bonding between the –C=O group of PHD and NH_3 results in an increase of –C=O as well as H—N- bond lengths and the vibration frequency for these bonds will decrease. It can be demonstrated from the change in IR stretching frequencies of –C=O(PHD) and H-N-(NH_3) (Figs. 7.6 (a-c)). So, the formation of hydrogen bonds may weakly polarize the NH_3 molecule which can facilitate the accumulation of more NH_3 molecules inside the pores of the material and thereby undergo further condensation of NH_3 molecules. Thus, both hydrogen bonding in PHD-NH_3 and NH_3 condensation are responsible for sensing and the possibility of reversibility in the process indicates that it can be reusable.

The gas phase calculations obtain the UV spectra of PHD and PHD-NH_3. The effect of solvent dielectrics on PHD has been studied while the solvent effect on this molecule is negligible with a small variation of solvation energies (Table 7.5). Hence, the gas phase spectral features of these systems are analyzed. The spectra after hydrogen bond formation with PHD show towards the longer wavelength (red shift) if this is indeed the case of nπ* and ππ*excitations of –C=O group within hydrogen-bonded structures.

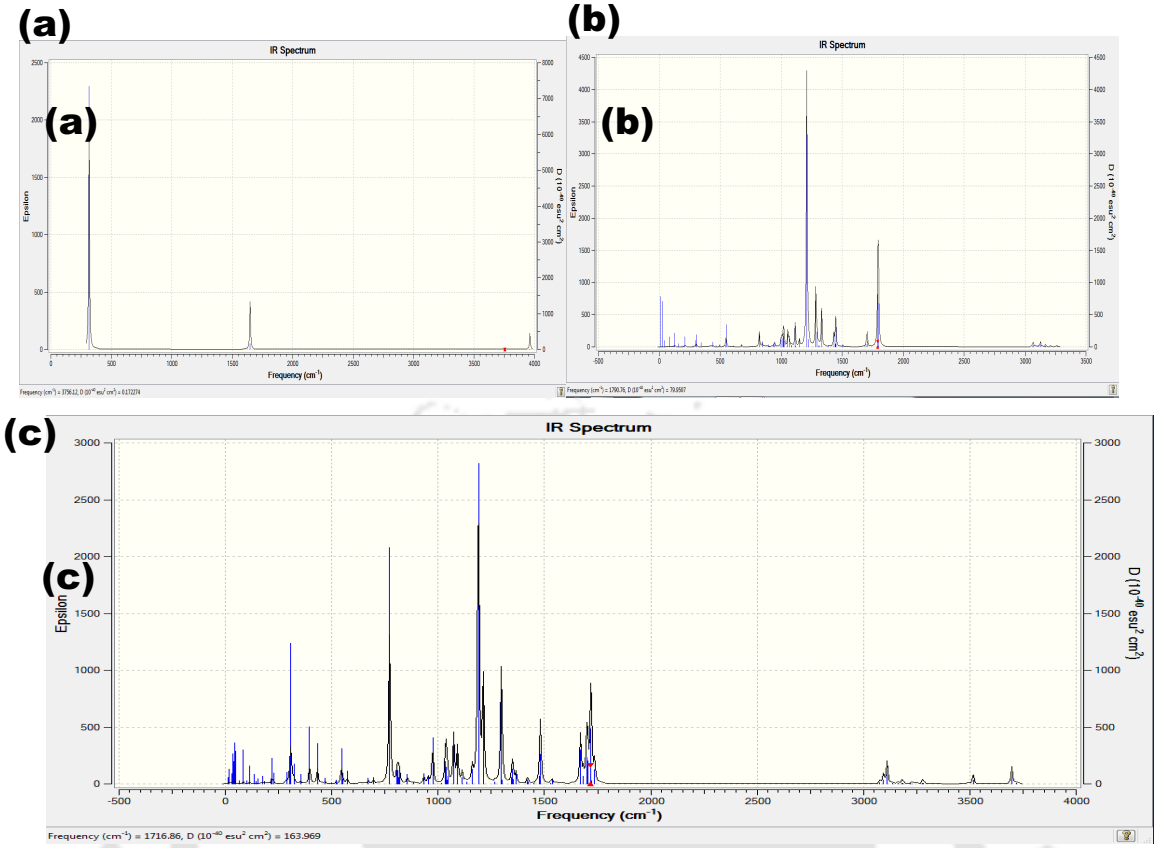

Figure 7.6. (a) Theoretical calculation of IR spectra of Ammonia. (b) IR spectra of PHD. (c) IR spectra of PHD-NH_3.

The UV peaks observed in PHD-NH_3 indicate the λ_{max} of PHD and NH_3, the peaks of PHD-NH_3, PHD-2NH_3 and PHD-3NH_3 show some differences. The λ_{max} values of PHD and NH_3 are also calculated for comparison with the values of PHD-NH_3 complexes. The difference of λ_{max} of PHD on complexation with NH_3 is shown in Figs. 7.7 (a-h) (red shift), which in fact is because of the nπ^* transition of the –C=O group on interaction with NH_3. Indirectly the red-shifted λ_{max} values correspond to the sensing of PHD for NH_3 through electron donation from the lone pair of electrons of O to NH_3. The excitation energies of the singlet and triplet states are largely different, which indicates the stability due to higher multiplicity. Hence the sensing ability of PHD for NH_3 is well demonstrated from the electronic properties of these complexes. This of course follows for all PHD-NH_3 aggregated systems.

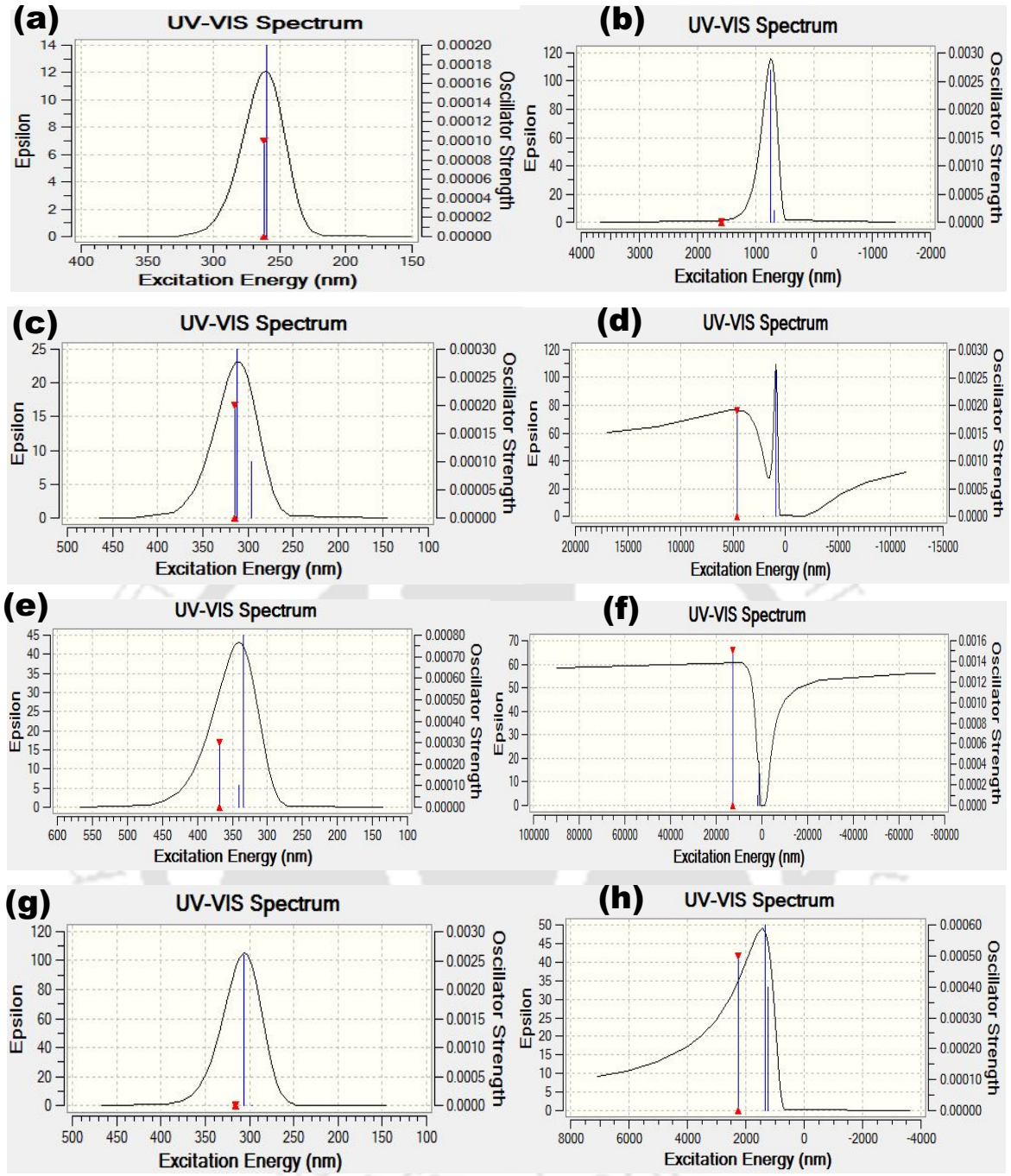

Figure 7.7. Theoretical calculations of (a) UV spectra of singlet PHD(λ_{max}=261); (b) UV spectra of triplet PHD(λ_{max}=1589); (c) UV spectra of singlet PHD-1NH_3(λ_{max}=314); (d)UV spectra of triplet PHD-1NH_3(λ_{max}=4636 nm); (e)UV spectra of singlet PHD-2NH_3(λ_{max}=368 nm); (f) UV spectra of triplet PHD-2NH_3(λ_{max}=12613 nm); (g) UV spectra of singlet PHD-3NH_3(λ_{max}=315 nm); (h)UV spectra of triplet PHD-3NH_3(λ_{max}=2238 nm).

7.4. CONCLUSION

In this work, a Polyhydroxyl derivative platform has been developed and ammonia sensing has been achieved. This work shows the characteristic mechanism of ammonia sensing with blended PHD. The results show induced hydrogen bond by PHD-NH_3 for effective hydrogen bonding, cavity condensation and also reusability of this non-conductive device. We have investigated with DFT calculation at B3LYP/6-31++G(d,p) and 6-31G(d,p) for the ground state, TDB3LYP/6-31G(d,p) level of theory for the excited state studies. The PHD –NH_3 complexes have been examined to understand the sensing mechanism. In these systems, the strength of the non-covalent hydrogen bond between PHD and NH_3 depends on the nature of the association of these molecules. The perturbations of HOMO, LUMO and band gaps are also analyzed. The red shifts in UV-VIS spectra for the NH_3 aggregated PHD are also used to justify the sensing ability of PHD.

7.5. REFERENCES

1. A. Shahmoradi, A. Hosseini, A. Akbarinejad and N. Alizadeh, *Anal. Chem.*, 2021, 93, 17, 6706–6714**.**

2. S. Pandey and K. K. Nanda, *ACS Sens.,* 2016, 1, 55–62.

3. J. Liu, N. Cui, Qi Xu, Z. Wang, L. Gu and W. Dou, *ECS J. Solid State Sci. Technol*., 2021, 10, 027007.

4. B.G. Ghule, N. M Shinde, S.D. Raut, S.F Shaikh, A. M Al-Enizi, K.H. Kim, R. S Mane, *J Colloid Interface Sci.*, 2021, 589, 401-410.

5. D. J. Carlsson and D. M. Wiles, *Encyclopedia of Polymer Science and Engineering*, 2nd ed., John Wiley & Sons, Inc., New York, 1986, 4, pp 631–696.

6. M. Nedjar, A. Béroual, A. Boubakeur, *Journal of Applied Polymer Science*, 2006, 102(5), 4728 - 4733.

7. E. M. Sadek, S. L. Abd-El-Messieh, A. Khalil, N. A. Fatthallah, A. I. A Eid, K. M. El-Ashry and A.M.Motawie, *Journal of Applied Chemistry*, 2014, 7, 37-45.

8. J. Fraysse, T. Olinga, J. Planes, A. Pron, M. Nechtshein, *Synthetic Metals*, 101(1999), 722-723.

9. P. Banerjee and B. M. Mandal, *Synthetic Metals*, 1995, 74, 3, 257-261.

10. X. Sun, T. Ma, D. Yin, B. Tan, F. Yang, M. Liu, P. Gao, S. Zhang, Y. Wang and Y. He, ECS *J. Solid State Sci. Technol.*, 2021, 10, 024003.

11. P. Yang, D. Lv, W. Shen, T. Wu, Y. Yang, Y. Zhao, R. Tan, and W. Song, *Mater. Lett.*, 2020, 271, 127798.

12. B. Timmer, W. Olthuis, and A. V. D. Berg, *Sens. Actuators B Chem*., 2005, 107, 2, 666 -667.

13. S. N. Behera, M. Sharma, V. P. Aneja, and R. Balasubramanian, *Environ. Sci. Pollut. Res*., 2013, 20, 8092 -8131.

14. J. H. Sung, J. Y. Shin, H. J. Choi & M. S. Jhon, *Journal of Materials Science*, 2005, 40, 4951–4953.

15. M.A. Ratner and D.F. Shriver, *Chem. Rev.* 1988, 88, 1, 109–124.

16. V. S. Kolosnitsyn, G. P. Dukhanin, S. A. Dumler and I. A. Novakov, *Russian Journal of Applied Chemistry*, 2005, 78, 1–18.

17. R. Sathyamoorthy, S. Velumani, A. Subbarayan, K. Natarajan,P. J. Sebastian, *J. New. Mat. for Electrochem. Systems*, 2005, 8(2), 121-125.

18. M. J. Reddy, J S. Kumar, U.V. S Rao, P. Chu, *Solid State Ionics*, 2006, 177(3-4), 253-256.

19. A. Kumar, P. Y. Hsieh, M. O. Shaikh, R. K. R. Kumar, and C. H. Chuang, *Micromachines (Basel)*, 2022, 13(2), 197.

20. I. R. Agool, K. J. Kadhim and A. Hashim, *Int. J. of Plast. Technol*, 2017, 21, 397–403.

21. J. Lee, E. J. Park, J. Choi, J. Hong, S. E. Shim, *Synthetic Metals*, 2010, 160, 7–8, 566-574.

22. P.B. Bhargav, V.M. Mohan, A.K. Sharma, V.V.R.N. Rao, *Curr Appl Phys*, 2009, 9(1), 165–171.

23. N.V. Stanciu, F. Stan, I. L. Sandu, C. Fetecau, A. M. Turcanu, *Polymers*, 2021,13(2), 187.

24. M. Son, Y. Pak, S. S. Chee, F. M. Auxilia, K. Kim, B. K. Lee, S. Lee, S. K. Kang, C. Lee, J. S. Lee, K. K. Kim, Y. H. Jang, B. H. Lee, G. Y. Jung and M. H. Ham, *Nano Research*, 2018, 11(7), 3529–3536.

25. M. Sadiq, M.Moeen, M. M. Raza, T. Murtaza, M. Zulfequar and J. Ali, *Journal of Electronic Materials*, 2021, 50, 403–418.

26. M. S. Cho, H.J. Choi, K.Y. Kim, W.S. Ahn, *Macromol. Rapid Commun*., 2002, 23, 713-716.

27. B.H. Kim, J.H. Jung, S. H. Hong, J. Joo, A.J. Epstein, K. Mizoguchi, J.W. Kim, H.J. Choi, *Macromolecules*, 2002, 35, 1419 –1423.

28. S. Arya, M. Riyas, A. Sharma, B. Singh, P. Mahajan, P. Bandhoria, S. Khan, and V. Bharti, *Appl. Phys. A*, 2018, 124, 1-7.

29. Y. Li, H. Ban, M. Jiao and M. Yang, *RSC Adv*., 2016, 6, 74944-74956

30. J. Yin, X. Xia, L. Xiang, Y. Qiao and X. Zhao, *Smart Mater. and Struct.*, 2009, 18, 095007 (11pp).

31. S. Tohidi, M. Parhizkar, H. Bidadi, and R. M. Rezaei, *Nanontech*., 2020, 31, 415501.

32. C. Zhu, U. Cakmak, O. Sheikhnejad, X. Cheng, X. Zhang, Y. Xu, S. Gao, H. Zhao, L. Huo, and Z. Major, *Nanotech*., 2019, 30(25).

33. I. Medhi and P.K.Iyer, *Sens. Diagn*., 2022, Advance Article.

34.(a) Gaussian 09W, M. J. Frisch, G. W. Trucks, H. B. Schlegel, G. E. Scuseria, M. A. Robb, J. R. Cheeseman, G. Scalmani, V. Barone, G. A. Petersson, H. Nakatsuji, X. Li, M. Caricato, A. Marenich, J. Bloino, B. G. Janesko, R. Gomperts, B. Mennucci, H. P. Hratchian, J. V. Ortiz, A. F. Izmaylov, J. L. Sonnenberg, D. Williams-Young, F. Ding, F. Lipparini, F. Egidi, J. Goings, B. Peng, A. Petrone, T. Henderson, D. Ranasinghe, V. G. Zakrzewski, J. Gao, N. Rega, G. Zheng, W. Liang, M. Hada, M. Ehara, K. Toyota, R. Fukuda, J. Hasegawa, M. Ishida, T. Nakajima, Y. Honda, O. Kitao, H. Nakai, T. Vreven, K. Throssell, J. A. Montgomery, Jr., J. E. Peralta, F. Ogliaro, M. Bearpark, J. J. Heyd, E. Brothers, K. N. Kudin, V. N. Staroverov, T. Keith, R. Kobayashi, J. Normand, K. Raghavachari, A. Rendell, J. C. Burant, S. S. Iyengar, J. Tomasi, M. Cossi, J. M. Millam, M. Klene, C. Adamo, R. Cammi, J. W. Ochterski, R. L. Martin, K. Morokuma, O. Farkas, J. B. Foresman, and D. J. Fox, Gaussian, Inc., Wallingford CT, 2016.

(b) Gauss View 5.0, GAUSSIAN Inc., Pittsburgh.

Thesis Overview & Future Prospect

THESIS OVERVIEW

OECTs were first demonstrated by White et al. in a device where the conductivity of the semiconducting polymer polypyrrole film was modulated by applying a gate voltage to the liquid electrolyte. Organic electrochemical transistors (OECTs) are thin-film transistors that have shown great promise in a variety of applications such as biosensing, logic circuits, and neuromorphic models. The device properties of OECTs are determined by the interaction between ionic and electronic charge carriers. This interaction distinguishes OECTs from conventional transistor technologies and requires the development of device models for the unique behaviour of OECTs.

In recent years, research into new and more efficient NH_3 gas sensors using nanostructured materials has received much attention due to various applications such as environmental monitoring, industrial process monitoring, automotive exhaust gas detection and medical diagnosis. Room temperature operation, low detection limit and fast response time are highly desirable in many gas detector applications. OECTs based on poly(3,4-ethylenedioxythiophene) doped with polystyrene sulfonate (PEDOT: PSS) can be integrated into microfluidic systems used in logic circuits. Such integration facilitates the detection of biomolecules such as glucose, deoxyribonucleic acid (DNA), neurotransmitters, and certain other biomarkers. These devices follow an ion-to-electron conversion mechanism that allows easy biology and electronics coupling. Thus, these devices have the advantage of detecting large changes in electron flow even with a relatively small ion slip. Here, we have adopted a polyhydroxyl layer (PHD) to design a PEDOT: PSS-based OECT to investigate its ability to improve transistor efficiency. In addition to ammonia selectivity, the PHD layer also ensures device stability, protects the transistor in an aqueous environment and ensures operation at room temperature. We confirmed the existence of strong hydrogen bonds, N-H stretching and cavity condensation. All these remarkable features, together with the mesoporous nature of the PHD film, contribute to the remarkable response of the PHD-OECT-processed solution to ammonia at very low (<1 V) operating voltages.

Chapter 1 commences with a brief discussion on the need for advanced medical care, an introduction to Bioelectronics that involves fundamental aspects, background and a summary of OECT.

Chapter 2 demonstrates the conceptualization of a hybrid OECT, fabrication, incorporation of a new hybrid film and its influence to detect ammonia. This chapter also discusses the sensing pathway, thereby, touching on some detailed mechanisms.

Chapter 3 demonstrates the Clinical Application of our hybrid OECT for Chronic Liver Diseases. This chapter provides a mechanistic approach to sensing ammonia through basic fundamental concepts.

Chapter 4 provides a fresh perspective on detecting cancerous cells with our hybrid OECT. This chapter demonstrates the use of Ammonia as a Diagnostic Tool for the selective detection of Hepatocellular Carcinoma under physiological conditions.

Chapter 5 discusses the presence of Folate Receptors in Cancerous Cells. Using Folic Acid as Biomarker another selective approach targeting Cervical Cancer (CC) cells was showcased.

Chapter 6 demonstrates an engineered device which can be photo-stimulated and can be optically excited. These photophysical studies provide considerable insights to open a new way for future design and development of multifunctional sensing.

Chapter 7 provides theoretical insights and computational corroboration for room temperature ammonia sensing. Theoretical values confirm the influence of functional groups, porous networks, chemisorption and hydrogen bonding along with mechanistic aspects leading to sensitive detection.

The thesis concludes with a brief discussion on the future prospect of the development of new materials and the application of engineered hybrid OECT as Diagnostic medical electronics.

FUTURE PROSPECT

The incidence of chronic diseases such as diabetes, cancer and other infectious diseases is increasing due to sedentary lifestyles and other factors. Health authorities in various countries are also focusing on increasing diagnostic and treatment rates through awareness programs. As the prevalence and awareness of such diseases increase among the population, so does the number of patients requiring diagnostic procedures and tests. The increase in chronic diseases and the treatment of patients suffering from these diseases put enormous pressure on the health systems of various countries. This has greatly increased the financial burden of treating these diseases worldwide. The total costs of a patient's hospitalization are significantly higher, and a longer hospitalization leads to a greater financial burden. Due to the outbreak of the COVID-19 pandemic and the increasing healthcare of the population, the demand for these devices has increased in the market. According to independent research conducted in the United States, about 21.0% of the country's adult population owned a fitness tracker in 2019.

The launch of improved models with new features and reduced prices by market players has also increased the customer base of the devices. This provides a huge growth opportunity for new entrants and established players to focus on this segment and launch new mobile devices to meet the growing demand for these devices. Due to the growing financial burden and the growing number of residents over 60, the population's preference for home health services is decreasing. In addition, as key players and healthcare institutions make increasing efforts to develop and commercialize new and easy-to-use medical devices, such as portable and wearable devices to treat chronic diseases, the adoption of home healthcare services in developed countries is growing rapidly.

Conferences | Seminars | Publications | Book-Chapters

CONFERENCES/SEMINARS ATTENDED

- Poster Presentation – Organic Electrochemical Transistor- 4th International Conference on Advanced Nanomaterials and Nanotechnology, (ICANN-2015) held at IIT Guwahati.
- Research Conclave, an amalgamation of Academia, Industry & Startups held at IIT Guwahati, March 16th – 19th, 2017.
- National Workshop on MEMS/NEMS and Theranostics Devices (NWNTD), from March 21st – 23rd, 2017, at IIT Guwahati, Assam, India.
- 5th International Conference on Advanced Nanomaterials and Nanotechnology, (ICANN-2017) held at IIT Guwahati, Guwahati, during Dec 18th -21st, 2017.
- Research Conclave, an amalgamation of Academia, Industry & Startups held at IIT Guwahati, March 8th-11th, 2018.
- Presented a poster and was awarded the **Departmental Best Poster award (FIRST PRIZE)** in Research Conclave 2019 organised by the Academic Affairs Board, Indian Institute of Technology Guwahati, India from 14th – 17th March 2019.
- 6th International Conference on Advanced Nanomaterials and Nanotechnology (ICANN-2019) held at IIT Guwahati, Guwahati, during Dec 18th -21st, 2019.
- Participated in National Workshop on NEMS/MEMS and Theranostics Devices 2019 organised by Centre for Nanotechnology, Indian Institute of Technology Guwahati, India from Feb 21, 2019 -Feb 23, 2019.
- National Workshop on Municipal Solid Waste and its impact- organized by Assam Science and Technology University under the Collaborative Research Scheme of TEQIP III project on 3rd- 4th September 2020.
- Potential of Bio-Energy in North-East India-Organized by Assam Science and Technology University Guwahati held on 08th September 2020.
- Research Scholars Skill Development Workshop organized by the Indian National Young Academy of Sciences (INYAS), 19th – 20th September 2020.

- 6th National Workshop on NEMS/MEMS and Theranostics Devices NWNTD Fri, Dec 4, 2020- organized by Centre for Nanotechnology, Indian Institute of Technology Guwahati.

- 30th Annual Meeting of MRSJ- organized by Materials Research Society of Japan, 9th – 11th December 2020.
- Weekend Webinar Series – Windows of Opportunity in Science and Technology, Organised by the Indian Young Academy of Sciences (INYAS), April – May 2021 comprising the following weekend webinars –
    - 3rd April 2021 – Higher Education opportunities after BE/BTech.
    - 10th April 2021 – The 'S' in STEM: Relevance and Opportunities.
    - 17th April 2021 – Roadmap to a stress free research journey.
    - 24th April 2021 – Basic Sciences: To pursue or Not to.
    - 01st May 2021 – Sustainability: What we need vs what we think we need.
    - 15th May 2021 – Radiation Physics: Opportunity in Medical Devices.
- Advancing your drug development with metabolomics: bolster your 'omics data and gain critical insights- organized by ACS Publications August 11, 2021.
- RSC- IIT Desktop Seminar with Journal of Materials Chemistry A- organized by Journal of Materials Chemistry A and IIT Guwahati. 27 October 2021 15:00 - 28 October 2021.
    - Driving the development of bio-based polymers with molecular simulation- organized by Chemistry World Apr 13, 2022.
    - Fingerprinting recycled thermoplastic resins for process optimisation - organized by Chemistry World Jun 15, 2022.
    - Broadband benchtop NMR spectroscopy: it's more than just protons- organized by Chemistry World Jun 29, 2022.
- Engineering of Multi-Cellular Insulin Secreting Tissues for Diabetes Cell Replacement Therapy- organized by Terasaki Institute Sep 21, 2022.
- Leveraging Novel Modalities for Oncology Therapies- organized by ACS Publications October 26, 2022.

- Accelerate your Chemical Research with the help of Modern Tools-November 3, 2022 organized by ACS Publications.
- Innovations in Measurement Science - organized by ACS Publications March 2023.
- Driving the development of bio-based polymers with molecular simulation- organized by Chemistry World held on 13th April 2023.
- Info Sessions IITG-TIC- organized by IIM Bangalore and IIT Guwahati.
- Seminars organized by MIT live webcasts.

PUBLICATIONS/ BOOK CHAPTER

1. An engineered organic electrochemical transistor (OECT) platform with a high ammonia-sensitive mesoporous membrane **(Published), Sens. Diagn., 2022,1, 1176-1184. (Selected for Inside Cover Art) https://doi.org/10.1039/D2SD00099G; Indrani Medhi**, Prof. Parameswar Krishnan Iyer.
2. Theoretical Insights and Computational Analysis in Understanding the Role of Hydrogen Bonding in a Polyhydroxyl Derivative for ammonia sensing **(Communicated); Indrani Medhi**, Prof. Parameswar Krishnan Iyer
3. Photo-electronic room temperature detection of Ammonia using reusable luminescent porous networks **(Communicated); Indrani Medhi**, Nehal Zehra, Prof. Parameswar Krishnan Iyer
4. Clinical Ammonia detection as a potential biomarker for chronic liver disease (**To be Communicated**); **Indrani Medhi**, Upashi Goswami, Prof. S. S. Ghosh, Prof. Parameswar Krishnan Iyer
5. Ammonia as Early Diagnostic Tool via elevated metabolite in Cancer Microenvironment (**To be Communicated); Indrani Medhi**, Upashi Goswami, Debashree Debasmita, Prof. S. S. Ghosh, Prof. Parameswar Krishnan Iyer
6. Polyhydroxyl Derivative (PHD) conjugated folic acid as an efficient Biomedical Platform for identifying folate-receptor cancer cells (**To be Communicated); Indrani Medhi**, Upashi Goswami, Debashree Debasmita, Prof. S. S. Ghosh, Prof. Parameswar Krishnan Iyer

BOOK CHAPTER

- Subrata Mondal, Rahul Narasimhan, Ramesh B. Yathirajula, **Indrani Medhi**, Lidong Li, Shu Wang, Parameswar K. Iyer; Chapter 2 - Emerging technology for point-of-care diagnostics: Recent developments; Advanced Nanomaterials for Point of Care Diagnosis and Therapy 2022, Pages 15-42 ISBN 978-0-323-85725-3 Copyright © 2022 Elsevier Inc. All rights reserved.

Indrani Medhi

Indrani Medhi was born to Prof. Okhil Kumar Medhi and Prof. Chitrani Medhi, a notable family in Indian Academia, on 1988 at Guwahati, Assam, India. The family environment motivated Indrani to pursue her quest for excellence in science and research from a very young age. Indrani obtained her Bachelor of Technology (B.Tech.) degree in Biomedical Engineering from Sathyabama Institute of Science & Technology, Chennai in 2012. Later on, she pursued higher research in the field of Bioengineering & Biomedical Devices and obtained a Master of Technology (M.Tech.) in Biomedical Engineering from SRM University/Harvard-MIT Health Sciences and Technology (HST) in 2014. She was selected for the prestigious Semester Abroad Program at Harvard-MIT Health Science & Technology, Massachusetts, USA. She has been trained in Prof. Ali Khademhoesseini's Lab, who comes in one of the top Material Scientists in the World. Her Hands-on-training as a Research Associate at Harvard-MIT Health Science & Technology, Massachusetts, USA led to her publication in a reputed peer-reviewed journal and a book chapter.

Currently, Indrani is working as an Experienced Doctoral Researcher at the Centre of Nanotechnology, IIT Guwahati with a demonstrated history of working in Biomedical Research. Indrani has more than 10 Years of Rich research experience in the area of Biomedical devices, Bio-sensors, and Theranostic device fabrication with hands-on training from Harvard-MIT Health Science & Technology, Massachusetts, USA. Apart from avid learner and researcher in the field, Indrani has skilled in Technical Writing, Microscopy, Organic Electronics, Sensor Fabrication, Electrospinning, Material Technology, Tissue Regeneration and Tissue Culture Engineering.

Laboratory Skills

Electrochemical Station, Fluorescence Microscopy, Soft Lithography, UV Lithography, PDMS Molding, Basic Microfluidics, Keithley Instruments, Thermal Deposition (Glove Box), Universal Testing Machine (UTM), Material Printing System (MPS), 3D Bioprinting, Cryofreezing, Cryosectioning, Dynamic Light Scattering (DLS).

Technical Skills

MATLAB, Simulink, LabVIEW, COMSOL, SolidWorks, AutoCAD, ImageJ, Gaussian, Chemdraw, Origin, Adobe Illustrator, Microsoft Office, Coreldraw, Paint, Canva

Research Expertise

Hydrogel, Wound Healing, Biomaterials, Regenerative Medicine, Scaffold Development, 3D Cell Culture, Electrospinning, Biomimetics, Organic Electronics.